OPERATION AND CONTROL OF THE MICROGRID WITH MULTIPLE DISTRIBUTED ENERGY RESOURCES

Thesis

Submitted in partial fulfillment of the requirements for the degree of

DOCTOR OF PHILOSOPHY

by

SIDDARAJ
165121EE16P02

DEPARTMENT OF ELECTRICAL AND ELECTRONICS ENGINEERING,

NATIONAL INSTITUTE OF TECHNOLOGY

KARNATAKA, SURATHKAL, MANGALORE -575025

January 2024

DECLARATION

by the Ph.D. Research Scholar

I hereby declare that the Research Thesis entitled **OPERATION AND CONTROL OF THE MICROGRID WITH MULTIPLE DISTRIBUTED ENERGY RESOURCES** which is being submitted to the National Institute of Technology Karnataka, Surathkal in partial fulfillment of the requirements for the award of the **Doctor of Philosophy** in **Electrical and Electronics Engineering** is a bonafide report of the research work carried out by me. The material contained in this Research Thesis has not been submitted to any University or Institution for the award of any degree.

SIDDARAJ
(Reg. No: 165121EE16P02)
Department of Electrical and Electronics Engineering

Place: NITK-Surathkal
Date:

CERTIFICATE

This is to certify that the research thesis entitled **OPERATION AND CONTROL OF THE MICROGRID WITH MULTIPLE DISTRIBUTED ENERGY RESOURCES** submitted by **Siddaraj** (Register Number: **165121EE16P02**) as the record of the research work carried out by him, is accepted as the research thesis submission in partial fulfilment of the requirements for the award of the degree of **Doctor of Philosophy**.

Dr. Udaykumar R Yaragatti
Professor (HAG)
Department of Electrical and Electronics Engineering
National Institute of Technology Karnataka, Surathkal.

Dr. Nagendrappa H
Associate Professor
Department of Electrical and Electronics Engineering
National Institute of Technology Karnataka, Surathkal.

Dr. Dattatraya Narayan Gaonkar
Professor, Head and Chairman - DRPC
Department of Electrical and Electronics Engineering
National Institute of Technology Karnataka, Surathkal.

Acknowledgements

I would like to express sincere gratitude to my guides Dr. Udaykumar R Y, Professor, Dr. Nagendrappa H, Assistant Professor, Department of Electrical and Electronics Engineering, for giving me an opportunity to work under their guidance which is invaluable. Their unflinching support, suggestions, and directions have helped in the smooth progress of the Ph.D. work. They have been a constant source of inspiration in all possible ways for the successful completion of my research work.

I am extremely grateful to our beloved HOD Dr. D. N. Gaonkar, Department of Electrical and Electronics Engineering, National Institute of Technology Karnataka, Surathkal for his encouragement and for providing me with sufficient computational facilities to complete the research work. I express my heartfelt thanks to Prof. C. S. Adiga, Head Dept. of EEE, MIT Manipal for his support. I express my heartfelt thanks to all the teaching and non-teaching staff of the Department of Electrical and Electronics Engineering of NITK Surathkal and MIT Manipal for their full cooperation and assistance.

I would also like to express my deepest gratitude to the research progress assessment committee members, Dr. Krishnan C M C, Assistant Professor, Department of Electrical and Electronics Engineering and Dr. M Aruna, Associate Professor, Department of Mining Engineering, for their valuable guidance, suggestions, and support throughout my research work.

It’s my pleasure to thank my father, my mother, my wife, and my sisters for the support, encouragement and love they gave me. They are the ones who kept me in high spirits all the time.

I would like to thank my friends Praveen Kumar, Vikash Kumar, Swathi T, Om Prakash Kumar, Sudhindra Prabhu, Lokesh, Chethan, Santhosh Kumar, and all others who helped me directly and indirectly.

SIDDARAJ

ABSTRACT

Human activities contribute to the problem of global warming. Consequently, all nations are striving to lower their carbon releases. The world's economy is in breakdown because of several factors, including the diminishing supply of fossil fuels and an associated price increase. Governments on each continent are making united efforts to develop healthier energy sources and reduce pollution. Solar electricity, also known as photovoltaic technology, is the fastest-growing electricity generation ways and it is the most significant renewable energy source that generates power. The primary goal of this research is to study the interaction between a microgrid's photovoltaic and battery storage systems with power electronic interface and the loads, as well as to investigate methods for tracking the solar panel's maximum power point (MPP) and for managing power efficiently among each source.

This research presents a microgrid that provisions energy using solar photovoltaics (PV) and batteries. The proposed microgrids address issues associated with electrification and systems/loads that rely on utility power and are affected by power outages. Utilizing non-conventional resources and battery storage to power remote areas and eliminate power disruptions is one solution to these problems. Nevertheless, multifunctional microgrids are being developed to ensure that loads continue to receive power in the event of utility grid outages. Grid dynamic inverters and isolated operations inverters are additional configurations that can be utilized effectively in a coordinated manner.

Microgrids generate and distribute electricity using renewable energy sources such as windmills, solar arrays, and smaller hydroelectric facilities. The system's dispatch ability must be sufficient to produce electricity when consumers require it. However, photovoltaic energy cannot be utilized after sunset. Maximum power point tracking (MPPT) is typically carried out by power converters and is associated with the PV panels and DC link capacitor of the voltage source converter (VSC). To enhance the efficacy of the PV module, MPPT must provide improved performance in a wide range of environmental conditions. In this thesis, precise models of PV systems with MPPT methods such as P&O, PSO-Sliding, PSO-ANN and PSO-ANFIS are proposed. Another source is the necessity of energy storage devices for the dispatch ability of the

microgrid. Battery Energy Storage (BES) provides power to the areas even when PV power and utility are unavailable, making it a crucial component for the microgrid's dispatch ability. The PV array incorporated with the BES is responsible for consumer demand. When operating in islanding mode, the microgrid assumes responsibility to provide voltage to the load along with frequency stability by the voltage source converter (VSC) controller during a power grid outage using a proposed droop control. To retrieve the utility, an alternative working mode is employed. In grid following mode, the voltage-frequency is controlled by the grid. As a power conditioner, the VSC supplies active and reactive power to applications.

This research aims to develop techniques for regulating and deploying PV-BES systems with grid. The suggested microgrids are tested in a MATLAB environment to validate the topology, control methodologies, and simulation model. This study concentrates predominantly on grid-interactive PV-BES microgrids, which can continue to provide power to customers in the absence of both the utility grid and PV production. This work develops a configuration of PV-BES microgrids to address the issue of distribution network power outages. PV microgrids with two stages consist of a boost converter for maximal power point tracking and a grid interactive VSC in the second stage. In PV-BES microgrid systems, the bidirectional inverter is utilized for battery charging and discharging. To enhance the dynamic performance of the PV and BES microgrid and to facilitate the injection of active power into the utility grid, a PV feed-forward (PVFF) loop is implemented in the grid-interactive mode for current control. Consequently, the selection of microgrid variants is determined by consumer requirements. Remote areas regularly experience power disruptions. Effective, isolated with intelligent control mechanisms are developed for grid-interactive PV-BES microgrids to continue to provide uninterrupted power to end users during utility grid outages and PV array power variation.

TABLE OF CONTENTS

LIST OF FIGURES

LIST OF TABLES

LIST OF ABBREVIATIONS

AC	Alternating Current
ANFIS	Artificial Neural Fuzzy Interference System
ANN	Artificial Neural Network
BES	Battery Energy Storage
BESS	Battery Energy Storage System
DC	Direct Current
DER	Distributed Energy Resource
DG	Distributed Generation
DS	Distributed Storage
DSTATCOM	Distribution Static Compensator
EMS	Energy Management System
FLC	Fuzzy Logic Control
INC	Incremental Conductance
I-V	Current Voltage Characteristics
kvar	Kilo volts ampere reactive
kW	Kilo Watts
MG	Microgrid
MPP	Maximum Power Point
MPPT	Maximum Power Point Tracking
MSE	Mean Square Error
P&O	Perturb and Observe
PCC	Point of Common Coupling
PF	Power Factor
PI	Proportional Integral
PLL	Phase Locked Loop
PMS	Power Management System
POI	Point of Interconnection
P-Q	Active and Reactive Power

PSO	Particle Swarm Optimization
PV	Photovoltaic
P-V	Power Voltage Characteristics
PVFF	PV Feed-Forward
PWM	Pulse Width Modulation
RES	Renewable Energy Sources
SMC	Sliding Mode Controller
SOC	State of Charge
SPWM	Sinusoidal Pulse Width Modulation
STC	Standard Test Condition
VSC	Voltage Source Converter

NOMENCLATURE

Symbol	Meaning
I_{ph}	Solar cell current (A)
R_s	Resistance series (Ω)
R_p	Resistance parallel (Ω)
G_a	Irradiance (W/m^2)
T	Cell temperature (K)
I_d	Diode current (A)
I	PV output current (A)
V	PV output voltage (V)
Voc	Voltage at open circuit (V)
Isc	Current at short-circuit (A)
P_{mp}	The maximum power point (W)
V_{mp}	Maximum power point voltage (V)
I_{mp}	Maximum power point current (A)
I_o	Reverse saturation current of diode (A)
q	Elementary electron charge (1.602x10^{-19} C)
V_d	Diode voltage (V)
a	Diode ideality constant
k	Boltzmann constant 1.381x10^{-23} (J/K)
$I_{sc}(T_1)$	Current at T_1 temperature
T_1	Cell temperature at STC
G_{nom}	Irradiance at STC
N_s	Number of series cells
K_i	Current temperature coefficient
Δ_T	Change in Temperature
dV/dI	I-V curve slope at the V_{oc}
D_m	Duty cycle of the switch
f_s	Switching Frequency
V_{om}	Maximum of the dc component of the output voltage

ΔIL_{ripple}	Ripple current of the inductor
I_{om}	Output current at maximum output power
V_{pv_mpp}	PV output voltage at maximum power point
V_{load}	Output voltage of the boost converter
ΔV_{load}	Output ripple voltage
X_i	Present position of each particle
V_i	Velocity of the search space
i	Optimization vector
k	Number of iterations
w	Inertia weight factor of the velocity
c_1	Cognitive coefficient of each of the particles
c_2	Social coefficient of each of the particles
r_1, r_2	Randomized velocity values of the search space between 0 and the maximal velocity.
W_i	Normalized firing strength from Layer 3
p_i, q_i, r_i	Linear parameters of the ANFIS network
K_p, K_i	Proportional and integral gain of the PI controller
x_j	Input training node
w_{ij}	Input, hidden, and layer connection weights
bj	Bias of the hidden and output layer nodes
n	Total number of input signals
m	Total number of input signals
$Y_{j(i)}$	The actual output
$T_{j(i)}$	The desired output
i_L	Inductor current
V_{pv}	PV array voltage
V_o	PV output voltage
V_L	Inductor voltage
u	Switch function (0 or 1)
V_{LL}	Line-line RMS voltage on the inverter side
L_f	Filter inductance

I_{ac}	Maximum possible RMS value of the ac load current
m_a	Modulation index of the inverter
k_{pvpv}, k_{ivpv}	Gains of the PV voltage loop PI controller
k_{pipv}, k_{iipv}	Current controller PI gains
V_{BAT}	Battery voltage (V)
V_o	Battery constant voltage (V)
K	Polarization constant (V/Ah)
Q	Battery capacity (Ah)
i_t	Actual battery charge (Ah)
R	Internal resistance (Ω)
i	Battery current (A)
i^*	Filtered current (A)
A	Exponential zone amplitude (V)
B	Exponential zone time constant inverse (Ah)

Chapter 1

INTRODUCTION

1.1 OVERVIEW

Microgrids (MGs) based on renewable energy sources are gaining popularity due to their benefits such as regulating electric power consumption, improved reliability, flexibility, lower capacity changes etc. (Ashwin et al. 2018; Mahmood & Jiang, 2018a; Philip et al. 2016a). By producing electricity during peak load demand hours, renewable energy sources (RES) minimize overall prices while also being environmentally friendly. It also provides power to customer loads during a utility outage. Power converters (mostly grid-linked voltage-source converters) play a substantial role to control the energy flow and manage the energy in the microgrid (Dayal et al. 2013a; Pan et al. 2015a). Distributed energy resources (DERs) and storage linking with the microgrid are challenging also for disconnecting from the distribution network. While in standalone mode, the controller needs to maintain the voltage across the load and frequency. However, certain methods are implemented to guarantee the highest possible level of reliable energy and microgrid management, as some research and manufacturing facilities and hospitals could not even afford to lose electrical power because these facilities are so important and have such a high demand for continuous electrical power.

Among all renewable energy sources, photovoltaic (PV) electricity generation is the most potent solution under varying atmospheric conditions. In a distributed network the PV system of a smart grid has great promise and is an appropriate technology. The bulk of installations involves connecting the PV array to the power grid using DC to AC converters. In addition to producing electricity, PV systems may actively inject power into the utility grid, filter the electricity, and balance the currents in the grid. However, the fundamental problem of stability in the current distribution network is raised by the significant penetration of distributed renewable energy sources

(DERs). The development of the microgrid, which also offers uninterruptible supply to the loads and high-quality power injection to the grid even with variable loads, alleviates stability concerns. Despite these advantages, the microgrid raises several questions, including how it will function and be controlled, how it will handle transitions, and how it will meet the load demand sharing.

The photovoltaic (PV) - battery energy storage (BES) powered microgrid operating in grid-connected and islanded modes may thus be a potential option to avoid data loss, financial transaction losses, and other essential services during a utility power outage (Adhikari & Li, 2014; Fernández-Guillamón et al. 2019; Tang et al. 2022; Teodorescu et al. 2010). Furthermore, since PV arrays have a high initial cost, it is important to maximize output from the built plant within the restrictions of available capacity. Several researchers have proposed maximum power point tracking (MPPT) techniques to maximize the output of a PV array (Chakraborty et al. 2020; Rezkallah et al. 2018). The literature also offers a comparison of many MPPT approaches, highlighting the advantages and disadvantages of each (Philip et al. 2016b; Sarvi & Azadian, 2022).

A typical microgrid consists of distributed energy resources (DERs), a battery management system, integrated three-phase variable loads, and the main grid, all of which are coupled at a single point of common coupling (PCC). The PCC is now seeing a surge in unbalanced loads, which makes the islanding and synchronization method more challenging. The current technology necessitates a reliable and stable grid synchronization system with improved power quality in the presence of grid distortion (Harirchi et al. 2015a; C. Li et al. 2014a). Whether connected to the grid or islanding, the microgrids should be able to effortlessly shift to deliver continuous energy to adjacent loads. Although islanding only lasts for a brief amount of time, it offers reliability by retaining constant voltage, frequency, with powering to the load (Bisht et al. 2018; Oviedo et al. 2018a). With the progress of the utility grid, a reliable synchronization technique is necessary for several industrial and power applications (Safa et al. 2018). In addition, the microgrid's controlled battery storage unit is an essential component that supplies power to the local load even when the utility is disconnected (Kumar et al. 2020; Thirugnanam et al. 2018). Energy management

systems (EMSs) are essential for properly matching net power production to demand. In general, RES-integrated microgrids deliver additional active energy to the principal utility via grid integration. Much research has lately been conducted on a variety of systems for managing energy and transferring energy in grid-connected and standalone modes (Gupta et al. 2018; Karimi et al. 2017).

Power quality issues are a problem nowadays due to the widespread usage of electronic devices such as information technology (IT) devices (Balcells et al. 2016), uninterrupted power supplies (UPSs), fluorescent bulbs, light-emitting diodes (LEDs), etc. Such equipment impact the power quality of the distribution network, modifies the form of the load current, and increases distribution losses (Dong et al. 2018a; Gowtham & Shankar, 2018). Many studies have proposed alternative solutions to address power quality issues, including passive filters, active filters, and distribution static compensators (DSTATCOM) (Mishra et al. 2023; B. Singh & Arya, 2013).

In this research work, the setup of standalone, grid-interactive, and smooth transfer between the modes of a solar PV-BES-based microgrid has been investigated. The seamless transfer refers to a dual-mode microgrid that can go from grid connected to islanded mode and vice versa. The suggested solution not only supplies the grid and loads with the power collected from the solar PV array. Also, the same converters can enhance the distribution network's power quality (Saxena et al. 2017a, 2018). The concept, integration, and management of three-phase systems are performed, and their behaviour is investigated using simulation results (Shen & Khaligh, 2015).

1.2 PV-BES MICROGRID SYSTEM CLASSIFICATION

The categorization of several PV-BES microgrids in grid and standalone modes is shown in Figure 1.1 and Figure 1.2. A single-stage, double-stage, or multiple-stage PV-BES microgrid is possible. Moreover, the category of converters (current-source converters, voltage-source converters, and multilevel converters) operated to integrate active power into the utility. Also, may be used as power-voltage-based microgrids. The storage connection is used to categorize microgrids in autonomous and grid-tied modes, maybe as direct or through a bidirectional converter, power stages (single and two stages), and the number of supply phases (single phase, three phases). For

delivering combined 1-ϕ and 3-ϕ loads, the 3-ϕ microgrids are further divided into 3-ϕ, 3-wire and 3- ϕ, 4-wire.

1.3 CURRENT PV-BES MICROGRID SYSTEMS

The functioning of PV-BES microgrids among both grid-connected and island modes is described in many publications (Sangwongwanich et al. 2016; Shi et al. 2016a). Researchers have studied islanded microgrids that can handle both balanced and unbalanced nonlinear loads, (Biswas et al. 2017; Thang et al. 2015). The literature has discussed single-stage grid-connected PV systems (see, for example, (Lal & Singh, 2017)). The literature reports (Zhang et al. 2018) single-phase utility linked-up topologies in depth. Moreover, numerous single-phase PV inverters connected to the utility and interconnected in series are discussed in (Mirhosseini et al. 2015). (Rajeev & Agarwal, 2020) reviewed the ride-through possibilities of PV systems during grid interruptions. PV-BES microgrid systems are capable of maximizing power extraction, reactive power, and harmonics correction, as described in (Mahmood & Jiang, 2018b; Vahedi et al. 2016). It can be turned to isolated mode during a blackout of utility. To provide these capabilities in a PV-BES microgrid, a current controller, voltage controller, islanding, and mode transition mechanism are required. The grid-connected mode takes advantage of the current controller, which also has possibilities for improving power quality. If the utility grid goes down, the PV-BES microgrid operates in an isolated mode to provide power to loads (Krithiga & Gounden, 2014). Hence, to supply reliable power it's crucial to keep an eye on power outages and rectify them as soon as they occur. Also, many researchers have discussed the various aspects of grid-integrated PV-BES microgrids. This article goes into several controls for grid-connected and standalone modes of PV-BES microgrid systems. A bidirectional converter may be controlled using cascaded proportional and integral (PI) control, the microgrid can be switched from current control to voltage control mode using mode transfer control in standalone mode, and current control can be used to improve power quality. Several control strategies are used to separate the fundamental or in-phase and the quadrature-phase components of load currents.

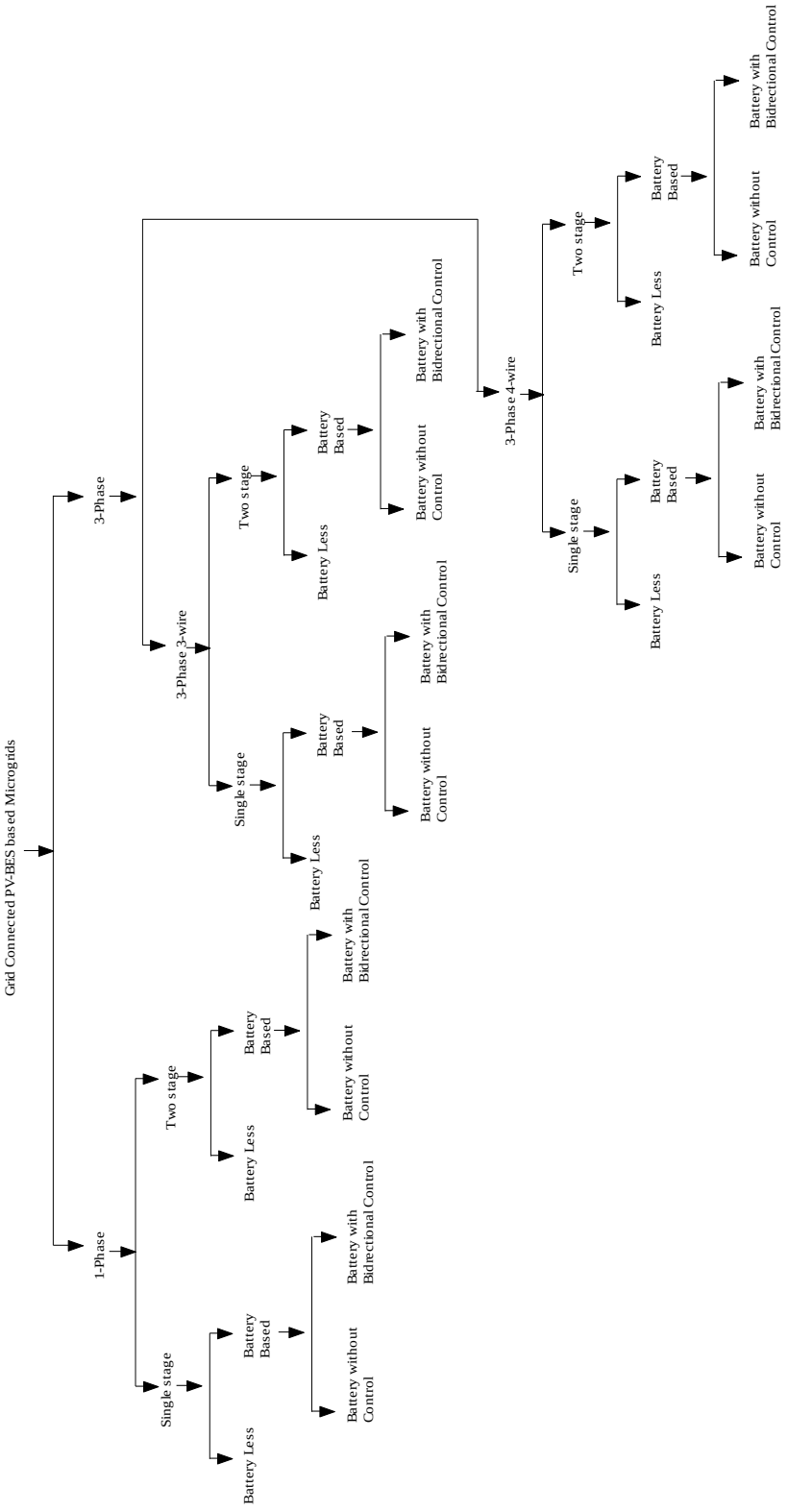

Figure 1.1: Grid-connected classification of PV-BES microgrid systems.

(Sangwongwanich et al. 2016; Shi et al. 2016a)

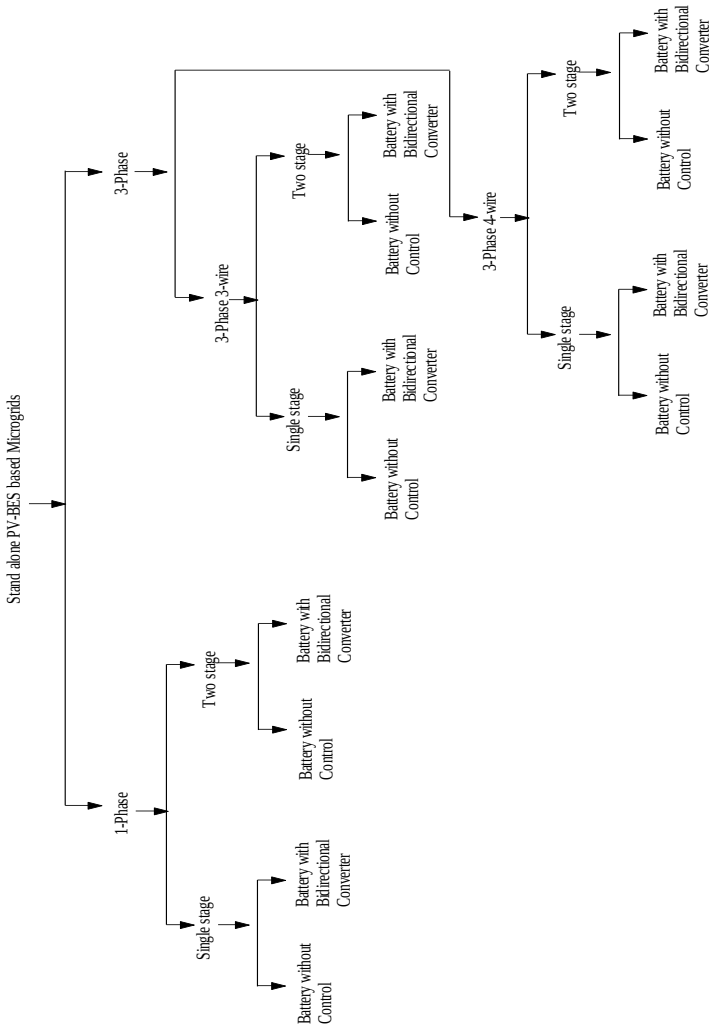

Figure 1.2: Isolated mode classification of PV-BES microgrid systems.
(Sangwongwanich et al. 2016; Shi et al. 2016a)

1.4 THE SYSTEM ARCHITECTURE

A test microgrid consisting of two inverters and a utility is shown in Figure 1.3. The following are the main parts of the microgrid under consideration: Solar PV, Battery Energy Storage system, grid, filters and load. For the study, MATLAB/SIMULINK is used to simulate a two-inverter, 3-ϕ, grid-based test microgrid. A distribution line of the grid is connected to the PV system and BESS inverters. The PCC is where loads are connected. For one inverter, the input is a PV system followed by a boost converter. For the other inverter, the input is a battery

energy storage system. The detailed discussion is done in chapters 3 and 4. In microgrid mode, the two inverters and the grid work together in a coordinated PQ and droop-controlled islanded mode to keep system frequency and bus voltages stable while making sure that generation and load are balanced (merabet et al. 2017).

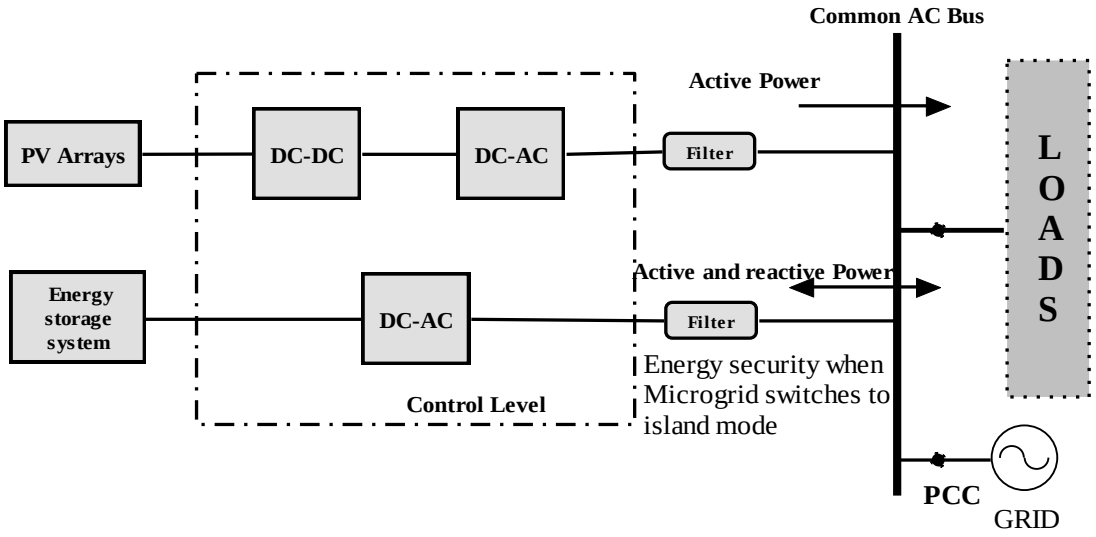

Figure 1.3: Block diagram of a test microgrid.

1.5 RESEARCH MOTIVATION

Few factors have a greater impact on the utilisation of renewable energy sources than the enormous disparity between generation and increasing demand, concerns regarding the environment, and economic constraints. The deregulation of the power industry and the numerous environmental, economic, and technological advantages of DER systems prompted the acceptance of renewable source-storage-based power utilisation. The solar and energy storage resources are adapted extensively as the PV resource is available abundantly and storage is used during emergency periods. Renewable energy sources depend on nature and their output fluctuates, which poses many challenges for the system operation. To enhance the efficacy of the PV module, MPPT must provide improved performance in a wide range of environmental conditions. The energy storage system is utilised to minimise the fluctuations. Control mechanisms for PV-battery systems need to be capable of stabilising bus voltages and controlling power transfers with flexibility. PV-battery-based hybrid microgrids must have an integrated control and power management system for both grid-tied and

islanded modes. Regulating the voltage-frequency consistently, controlling the voltage-power of all units flexibly, and automatically matching the power injection in the system under varying operating conditions, despite disturbances from changing modes, variations in irradiance and temperature, and changes in loads, are vital. As a result of the integrated PV grid, there will be less of an impact on the environment. Utilising energy storage devices that can be activated when demand is high, and generation is less can alleviate power fluctuations, the transients, and deprived load-following performance. Microgrids fueled by solar photovoltaic panels and batteries offer numerous advantages, such as environmental benevolence, efficiency, durability, and power quality.

1.6 IDENTIFIED RESEARCH GAPS

In this thesis, a 3-ϕ grid interactive microgrid based on a PV array and battery storage has been investigated. The control of the converter has been made more robust so that it can inject the extract PV power into the utility and provide additional stable operation during the off-grid and on-grid modes. In the daytime, when PV is available, it works as a power quality conditioner and injects extracted PV power into the utility. In the nighttime, it works as a power quality conditioner with the availability of the grid and under outage of the grid, the battery feeds the power to the grid using this converter. Based on the literature review presented, the following important research gaps have been identified:

- The literature depicts that the Maximum Power Point Tracking (MPPTs) prove to be unreliable when faced with the difficulties presented by unpredictable dynamic conditions and indicating a need for focused research on the development and optimization of on hybrid MPPT systems for PV systems.
- Most of the work reported in literature devoted to the combination of battery storage with Distributed Generation (DG) systems, with the primary focus being on cost and size optimization instead need to focus more sophisticated power-sharing control schemes for improved microgrid performance.

- The future literature needs to focus on improving techniques designed specifically for three-phase self-sufficient microgrids and systematically investigate the complexities of switching between grid-island-grid modes under various operational situations.

Based on these research gaps the research objectives are framed accordingly for the thesis work discussed in detail.

1.7 OBJECTIVES AND SCOPE OF WORK

To develop the main objectives of microgrid controllers for grid-connected and isolated power system with photovoltaic system and energy storage. The specific objectives are,

(i). To implement a 3-ϕ grid collaborative PV-based microgrid with efficient power sharing between the sources and also the various MPPT controls for the extraction of maximum power along with the quality power to load at different operating conditions.

(ii). To control and analyze the 3-ϕ, PV-BES microgrid systems to achieve better performance of power sharing among the sources by maintaining voltage and frequency within permissible limits under isolated mode also providing the quality power to load.

(iii). To implement the control requirement of a smooth transition between the mode of a 3-ϕ, PV-BES microgrid system and also to develop effective control techniques for BES systems to charge/discharge using bidirectional converters.

1.8 ORGANIZATION OF THE THESIS

In this section, the outline of the chapters with their detailed description are presented:

Chapter 1: This chapter elaborates on microgrids fueled by solar photovoltaic (PV) modules and battery energy storage (BES). In addition, it highlights cutting-edge research in areas pertinent to PV-BES microgrid systems. This section presents an overview of the challenges of seamless changeovers and power quality, as well as several options for addressing them. In addition, it describes the objectives and scope of the work and provides a summary of each chapter.

Chapter 2: In this chapter, an overview of the literature on PV-BES microgrid structures is presented. It includes grid-tied and autonomous PV-BES microgrid systems, as well as the capability to transition between the two. In addition, a review of the regulation of PV-BES in microgrids is presented. Based on the existing literature, the final section identifies prospective research topics.

Chapter 3: This chapter details the control and installation of 3-ϕ grid-interactive PV-based Various MPPT control for optimal energy extraction from microgrids without battery energy storage (BES). These PV-based microgrids interact with the grid, contributing available PV energy and with quality power at the point of common coupling (PCC). This chapter examines 3-ϕ grid interactive PV-based microgrids, including their configuration, control strategy, modelling, and performance evaluation in Matlab/Simulink.

Chapter 4: This chapter focuses on the implementation and control of 3-ϕ PV-BES systems with a smooth transition between utility and islanded modes. Using several types of MPPT controls, microgrid using a bi-directional converter-controlled BES. 3-ϕ PV-BES microgrids, including their circuit configuration, control strategy, modelling, and performance, are investigated in depth through MATLAB.

Chapter 5: The conclusions are drawn on the research findings presented in the earlier chapters. The scope for future work is also described.

Chapter 2

LITERATURE REVIEW

2.1 INTRODUCTION

Among all renewable energy sources, photovoltaic (PV) electricity generation is the most potent solution under varying atmospheric conditions. In a distributed network the PV system of a smart grid has great promise and is an appropriate technology. The bulk of installations involves connecting the PV array to the power grid using DC to AC converters. In addition to producing electricity, PV systems may actively inject power into the utility grid, filter the electricity, and balance the currents in the grid. However, the fundamental problem of stability in the current distribution network is raised by the significant penetration of distributed renewable energy sources (DERs). The development of the microgrid, which also offers uninterruptible supply to the loads and high-quality power injection to the grid even with variable loads, alleviates stability concerns. Despite these advantages, the microgrid raises several questions, including how it will function and be controlled, how it will handle transitions, and how it will meet the load demand sharing.

2.2 LITERATURE SURVEY

Recently, there has been a lot of interest in microgrids based on renewable energy and storage because of their independence, increased efficiency, ease of management, and compactness. Grid-integrated PV systems are overtaking standalone PV systems since the requirement for battery storage is no longer necessary. As a result, installing grid-integrated PV systems is easier than installing standalone ones. The extracted PV power may be utilised more effectively since there are no storage losses. The system must be shut down in the case of a power failure, stopping the supply of energy to the loads. A microgrid may, however, alternate between operating in the grid-tied and self-supporting modes depending on the state of the grid. It enables mode

change without turning off the supply to the loads. The VSC keeps supplying energy when the utility is cut off, and the control method shifts to standalone mode. As a result, it increases the microgrid's operational flexibility. This section surveys the research on microgrids that improve power quality by using solar panels and battery storage. Various types of standalone and grid interactive microgrids are also reviewed.

2.2.1 Review on Grid Interactive and Standalone Microgrid Systems with PV-BES

The price of a PV array is falling every day, and in years to come, it is anticipated to go much lower. As a result, grid support for PV energy is becoming more and more common (Shi et al. 2016b, 2016a). Furthermore, as grid integration does not rely on a storage system (batteries), it is also a cost-effective option. Without the use of either a smaller-scale or large-scale energy storage device, the grid integration transfers the PV power it generated to the utility. The installation of a battery bank or the use of a diesel generator as an emergency power source raises the cost and maintenance of island microgrids (Chen et al. 2013; Thang et al. 2015) compared to utility-interfaced systems (Campanhol et al. 2017). The batteries need regular maintenance and should be changed every 6 to 8 years depending on use. However, energy storage, including storage devices alongside photovoltaic (PV) systems, has attracted substantial interest and the need for energy for PV systems has expanded greatly to offer continuous power during grid interruption. Additionally, the PV array reduces the intermittent ness when energy storage is present and may transmit energy when it is needed. Additionally, (Mirhosseini et al. 2015) report on grid-supportive PV systems with various converter topologies. However, because of its ease of use and the broad range of operating frequencies, the voltage source converter (VSC) is still the converter of choice for microgrids. When the grid is present, grid-supportive PV systems are seen to be preferable after considering the problems with batteries. When PV energy is fed into a grid-integrated system, the grid serves as an energy hub.

The power management plan for the inflation reduction act (IRA) hybrid microgrid is provided in (Mahmood & Jiang, 2018b), which also covered the subject of autonomous power sharing. However, the power grid is not constantly operational in rural regions. Some industrial, research, and medical facilities cannot afford the loss of

electrical power due to the critical nature of these organisations and the great demand for continuous electrical power, so technologies have been included to guarantee the greatest level of ensure power as well as management of the microgrid. Therefore, a solar power (PV) - energy storage battery (BES) based microgrid with important crucial loads may be an effective way to prevent data loss, economic losses, and other vital services during outages of the utility grid. In addition, the microgrid with distributed energy and BES offers a considerable cost advantage with increased dependability since it can continue to deliver power to loads even if the utility goes out. Depending on how easily accessible the grid is, a microgrid may operate in either a grid-tied or independent mode (Krithiga & Gounden, 2014; Vahedi et al. 2016). However, the calculation of basic grid voltage, phase angle, and frequency play a vital role in grid voltage disturbances for the interface of these microgrids with the main utility grid. Here, a range of converter designs with combined grid-integrated and autonomous PV systems are analyzed. In reality, connecting the local DERs and storage and isolating them from the distribution network provides significant difficulties for microgrids. As a result, the microgrid must be capable of controlling utility integrated as well as islanded modes and transitions to any one mode without experiencing any transients. Current and voltage transients often happen during transition periods as a result of the transfer of modes, and frequency deviation happens as a result of a rapid change in the reference value that the controller produces.

The droop-based scheme is often used for the autonomous microgrid to control microgrid inverter when more than one DGs connected in parallel [pogaku et al.2007]. Implementing the droop scheme allows DG inverters to share the load proportionally by adjusting the voltage and frequency as a parameter of the total power. Besides, each inverter uses local measurements. Likewise, to improve the effectiveness of the droop-based voltage source inverter (VSI), a virtual impedance control based scheme has been also adopted (meng et al.2019). During islanded mode, the inverters should not overload. Inverters take the load change assurance by a proper control-based approach. The communication-based master-slave control method added to the microgrid, where DG sources are connected to a local bus or located nearby (Tayab et al.2017). Besides, communication-based control makes the system costly and not reliable. Droop based

approach, which uses local measurements by eliminating communication link, has been proposed (Guerrero et al.2011).

Domestic applications employ many power-converter based loads, which introduce harmonics into the power system (Bhoyar et al. 2014). This grid pollution results in appliances not operating properly, more losses, a heavier reactive power load on the system, and a worse power factor. To reduce such harmonics from the non-linear load current and the system, quick and precise control algorithms are discussed (Kampen et al. 2008). Several researchers (Dong et al. 2018b; Gray & Morsi, 2015b; Tareen et al. 2018) have proposed various adaptive solutions, including active filters, passive filters, and DSTATCOMs with their efficient control algorithms. For the system, the suggested methods lower the harmonics content of the grid current and maintain it below the value specified by the IEEE-519 standard. Moreover, it improves power factor, compensates for loads, and reduces harmonics. The PV inverter may also be utilised to improve power quality (Saxena et al. 2017b). PV array-fed microgrid systems decrease losses by integrating PV array power into the grid and improving power quality (A. K. Verma & Singh, 2018). PV arrays in microgrid systems that are powered by PV are nonlinear device that affects how the grid-tied VSC operates (Errouissi et al. 2016). Since the power production of the PV array varies over time, the operational point of a solar PV microgrid is not unique. Hence, a traditional controller for power converters must be developed to handle these uncomfortable tasks. For an accurate assessment of load current fundamentals and their weights, several retrofit solutions with control techniques for power sharing are reviewed in this section.

2.2.2 RECENT ADVANCEMENT OF MPPT ALGORITHMS A REVIEW

The electricity produced using the photovoltaic system must be extracted to improve the efficient use of the array under varying climatic circumstances. Numerous scholars have suggested various control strategies with comparative studies to achieve this objective (Esram & Chapman, 2007; Jedari Zare Zadeh & Fathi, 2017). Each of these control approaches offers advantages and disadvantages in terms of tracking effectiveness, quick response, additional hardware, and understandability. The PV array always runs in flexible and perfect conditions depending on the MPPT approaches. Typically, a power converter (Safari & Mekhilef, 2011; Shi et al. 2016a)is linked

intermediate between the PV array and inverter and is used to obtain the peak power from the PV array for monitoring the best array voltage determining to a certain irradiance. By raising the electrical output produced by the PV array and measuring maximum power, the PV array's efficiency is improved. However, in certain circumstances, the PV inverter carries out both tasks extracting the greatest amount of power maximal from the PV array and supplying any additional power to the utility. Since the suggested PV system is a single-stage system, both functions are carried out by a single converter, resulting in an economical PV system (Wu et al. 2007; Xiao et al. 2015). In(Killi & Samanta, 2015), the idea of an enhanced P & O (Perturb & Observe) method is presented under dynamic environmental changes and high perturbation frequency. (Sharma et al. 2014) presents a unique MPPT controller with quick tracking capabilities for assessing the peak power from the PV array.

However, MPPT is necessary under rapidly changing atmospheric circumstances to provide quick convergence with minimum switching loss. The perturb and observe (P & O) MPPT algorithm tracks the maximum power point by continually perturbing PV panel variables like voltage and power and measuring the variations between perturb variables before and after the perturbation (Manickam et al. 2016). In the P & O MPPT algorithm, the tipping point oscillates near the peak power point (Elgendy et al. 2015), with a greater perturbation speed described in. The implementation of MPPT methods is dependent on changes in voltage, current, and duty cycle. Additionally, the swift response has improved both the system's efficacy and efficiency of the MPPT approach. Additionally, the incremental conductance (INC) method, another common MPPT approach, is used to assess the solar plant's crest power (Elgendy et al. 2013; Kuo et al. 2001). A rapid convergence-based INC MPPT method for changeable atmospheric circumstances (Liu et al. 2008). Furthermore, the INC algorithm, which operates on the $dP_{pv}/dV_{pv} = 0$ hypotheses, does not see any disturbance in PV power. The trade-off between the change in power and tracking capacity is also present in the adoption of perturbation value. The INC approach maintains its precision and adaptability even when the weather is unpredictable. Nevertheless, it contains simulation and experimental complexities. However, the above-mentioned algorithms

are not efficient under varying solar irradiance and for the calculation of correct perturbation size.

Power converters are often used to carry out maximum power point tracking (MPPT), which is linked to the PV array and DC link capacitor of the voltage source converter (VSC). Many articles (Abo-Sennah et al. 2021; Craciunescu & Fara, 2023; Huynh & Dunnigan, 2016) compared various MPPT methods. Whereas MPPT is necessary to provide rapid convergence with low switching losses in rapidly changing atmospheric circumstances (Shi et al. 2016b). As a result, extracting the PV module's power output to get the output maximum from the PV module improves the module's efficiency. The article (Safari & Mekhilef, 2011) discusses an MPPT approach used to monitor the grid with no ripples. A quick convergence MPPT method under varying atmospheric circumstances has been reported (Wu et al. 2007). Modified MPPT Method (Xiao et al. 2015), Distributed MPPT methodology (Oliver et al. 2022), and MPPT algorithm for stand-alone PV systems (Sharma et al. 2014) are a few of the other well-known methods that have been reviewed in the literature. In (Elgendy et al. 2015; Manickam et al. 2016; Sera et al. 2013), the different methods of perturb & observe (P&O) algorithms are described, as well as an improvement of these algorithms that can handle large perturbation frequency and dynamic environments discussed. Moreover, P&O and INC-based algorithms are widely used because they are conceptually straightforward, practically easy to construct, and provide moderately better performance in a wide range of weather conditions. The detailed discussion on incremental conductance (IC), has been studied for the PV array for obtaining maximum power under different PV irradiance (Alaraj et al. 2022; Liu et al. 2008). Separate MPPT control (Ali et al. 2021), flexible multi-MPPT control (Wang et al. 2018), and a current-ripple-free MPPT algorithm (Pan et al. 2015b) were discussed.

Non-linear control methods have been the subject of much research for their potential to improve efficiency (Ahmad et al. 2020; Gonzalez Montoya et al. 2016; Ramos-Paja et al. 2022). One of the most reliable controllers for handling the PV system's nonlinear behaviour is sliding mode control (SMC), which was first described in (Slotine, 1984). The chattering phenomena in the control signal is a severe downside of the former when the uncertainties are sufficiently significant (Lamzouri et al. 2018).

This behaviour may be suppressed by including a boundary layer in the design of a Quasi-SMC (Slotine, 1984). In addition, a terminal sliding mode control (TSMC) is described as a robust controller for letting the PV system attain the MPP with high precision in a limited time(Saad et al. 2018), which is an improvement over the performance of a typical SMC controller.

To address the shortcomings of conventional MPPT algorithms in varying climates, modern MPPT trackers use intelligent fuzzy logic control (FLC) and artificial neural network (ANN) methodologies(Al-Gizi et al. 2017b). Fuzzy systems' derived rules and member functions both depend on probability to decide how the system will work. ANN techniques, on the other hand, depend on learned information and a multi-layered structure. The primary issue with this strategy is that there are no rules for establishing layer architecture. Furthermore, FLC and ANN are both comprehensive approaches to intelligence. An ANFIS technique is a rule base of inference that uses learning data to accelerate the calculations required for factual modeling while retaining high accuracy (Mir et al. 2018). Several collaborations of researchers have attempted to make PV-based industries more cost-effective while also increasing their control efficiency and reliability. Because of its simplified and adaptable design, the fuzzy logic based MPPT technique plays an essential role in resolving uncertainties and nonlinearity issues in the PV power system. The main challenges for FLC design are, however, the need for professional knowledge and the formulation of rule basis systems. Faster PV power tracking in dynamic environments is made possible by the ANN approach, which uses multilayered neurons rather than the traditional algorithms of MPPT approaches. However, to train this approach effectively, periodic huge amounts of data are needed to create an accurate MPPT. The hybrid algorithm, which is the result of integrating ANN and FLC, has appealing learning capabilities and provides learned membership for MPPT operation. It should also be mentioned that implementing MPPT algorithms necessitates the calculation of PV voltage and current. However, significant hardware complexity and noise computations led to the failure of several MPPT controllers. Here, a peak power tracker based on a hybrid adaptive neuro-fuzzy inference system (ANFIS) is used, gaining the benefits of a pair of algorithms (Abu-Rub et al. 2013). Designers have a difficult problem in training and updating

ANFIS requirements. Particle swarm optimization (PSO), the firefly algorithm, artificial bee colony (ABC), and ant colony optimization (ACO) are some of the more modern AI techniques used to handle optimization issues (Abu-Rub et al. 2013; Koad et al. 2017b; Windarko et al. 2016). Under circumstances characterized by consistent solar radiation, the FLC and ANN improve PV tracking performance. However, PSO gives an ideal solution in varying weather circumstances when several peaks are present, and it is extremely difficult to achieve the MPP as it includes a few factors that may be adjusted. Rapid and precise PV power monitoring under various operating circumstances is made possible by the PSO approach, which, in comparison to the previously described optimization methods, has a low sampling point, simplified mathematical analysis, straightforward hardware implementation, and inexpensive computing estimate. The PSO is easier to use and has a faster-enhanced convergence velocity (Priyadarshi et al. 2019) than gradient methods. In addition, there is no need to calculate starting parameters or set a minimum learning rate while using the PSO. With its high convergence speed, simplified build, and as well as simple implementation, PV tracking efficiency is maximized. This study provides a reliable, straightforward, and efficient method of implementing MPPT.

2.2.3 Control, Power Management, and Islanding-Synchronization in Grid-Interactive PV-BES Microgrids

For the analysis of microgrids, control techniques and power management schemes are the most essential requirements (Gupta et al. 2018; Karimi et al. 2017; Merabet et al. 2017). The described power management schemes of microgrid, share power in both the modes such as in grid-tied mode and an islanded mode. The exchange of energy in grid-interactive mode is achieved by connecting/disconnecting the utility grid from the PCC through the static transfer switch (STS), depending upon the utility parameters (utility voltage, frequency, and angle) and STS allows for exchanging of power in either way (import or export). Many researchers have addressed these issues in the literature (Neto et al. 2018; Pulcherio et al. 2018; Yi et al. 2018) and these technological issues in the microgrid have been solved by intelligent approaches.

In the study (Merabet et al., 2017) a wind-PV-battery system can operate reliably when a power management and control scheme is implemented. The control

algorithm to manage the reactive power was designed for a 1-ϕ inverter (Borowy & Salameh, 1996) and offers an alternative control strategy for a wind-PV-battery system that, as opposed to dynamic power balancing, optimises the proportions and charges of the PV-BES system. To calculate the power produced by the wind turbine and PV array, the proposed method requires 30 years of extensive historical data. Similarly, we discover a strategy to improve the wind-PV-battery configuration (Abbes et al. 2012). Both studies highlight size optimisation over specific control techniques for each power source (Borowy & Salameh, 1996). The authors of (Mahmood et al., 2014a) propose a droop-control-based power-sharing method for a PV-BES unit that permits power sharing among the battery- PV unit and another power source. The revised version published by (Mahmood et al. 2014b) considers varying power units. Although both of these systems are capable of effectively managing the power demand and output, their primary focus is on the power control of the PV-battery unit and other generating units. Furthermore, these techniques disregard the DC bus and loading systems. In (Guan et al. 2015), the authors describe a hierarchy-based controller for a PV-battery-hydropower structure that enables the hydropower generator to control the PCC voltage while the PV-battery unit manages active and reactive power. (Zia et al. 2022) present an analogous strategy for a diesel-PV-battery hybrid system. Neither of these controllers takes into consideration the voltage regulation in the absence of the hydropower or diesel generator. (Golsorkhi et al. 2017) present a decentralized approach for a single-island PV-battery system. In system topologies containing numerous PV and battery units, this method aims to solve load sharing. For a comparable approach for single-phase low-voltage islanded microgrids(Karimi, Oraee, Golsorkhi, et al. 2017). Many approaches neglect the grid-connected scenario in which the hybrid system exchanges electricity with the utility grid. For a grid-connected wind-PV-battery system, (Luna et al. 2017) proposes a supervisory control system that utilises data from the preceding 24 hours. In contrast to the system architecture employed in this study, the investigated system's topology consists of PV and a battery bank connected to the grid via distributed inverters. In (Brenna et al. 2018; Torreglosa et al. 2015), dynamic programming and neural networks are suggested for the power forecast of a PV-BESS system using day-ahead data. A mathematical method is proposed (Teng et al. 2013) for regulating battery storage in PV systems. Instead of

concentrating on specialised control algorithms, each of these four approaches prioritises the prediction of power production and demand, as well as the scheduling of power flow from PV or batteries. In addition, there are works that, rather than modifying controlling techniques, aim to improve power management by employing various converter topologies (Mishra et al. 2016; Zhu et al. 2015). The stabilisation of the DC link voltage, which is essential for the stable power supply of DC applications, is not taken into account by any of the studies examined.

Microgrids rely on battery energy storage (BES) to stabilise utility electricity and balance out fluctuations resulting from intermittent renewable sources such as solar panels (X. Li & Wang, 2021b; Thirugnanam et al. 2018). In addition to providing additional functions, such as load voltage and frequency regulation (Sun et al. 2011), a spinning reserve is used to feed loads when energy from renewable sources and utility power is unavailable. When the system is in utility-connected mode, its voltage and frequency adjust automatically to match those of the utility. In isolated mode, however, the voltage control determines the voltage and frequency of the loads. In this instance, the bidirectional buck-boost converter, charging and discharging are controlled. PI controllers keep the DC voltage stable when the microgrid is in utility-tied mode (Gadalla et al. 2018; Ota et al. 2016; Saxena, Hussain, et al. 2017; Saxena, Singh, et al. 2017b). In addition, the condition of the battery energy storage (BES) during charging and discharging is determined by the battery's state of charge (SOC) (Asakura & Akagi, 2009; Morstyn et al. 2016; Thirugnanam et al. 2018). When operating in standalone mode, PV array generation meets load demand while maintaining battery SOC. In addition, after the utility has recovered, the microgrid will resume operating in grid-tied mode, sending any excess power back to the grid.

The PV array generates more energy than the demand requires, the extra energy flows into the utility grid in grid-incorporated mode, with the quantity of energy infused depending on the BES's state of charge. In addition, the capacity requirement is fulfilled by the electrical grid if the PV power is inadequate. The maximum power point tracking (MPPT) algorithm of the PV array determines whether the array should be operating in MPPT or off-MPPT mode in an islanded mode based on the system's energy requirements and the power balance (Choi et al. 2018; Younus et al. 2017). If the PV

array system is sufficiently robust and the bidirectionally regulated SOC of BES is greater than the SOC maximum, the PV array will operate in non-MPPT mode, with derived power meeting load demand. If the PV array's generated power is insufficient, but the BESS's state-of-charge (SOC) is greater than the SOC min's lower limit, the DC link voltage will decrease and the BESS's reference current will become positive and begin discharging to power the emergency load. If the SOC of the BESS falls below the minimum threshold, load reduction is required to preserve the balance of power.

Microgrids with distributed energy resources (DERs) are the keystone to moving forward and increasing resiliency, efficiency, sustainability and strengthening the economy. The microgrids bring up new challenges to connecting the onsite DERs and storage and isolating them from the distribution network. Microgrids can operate either by connecting to a larger grid or independently, a process known as islanding. Although islanding only lasts for fleeting durations, it provides reliability by maintaining stable voltage and frequency and assuring that end-user loads always have access to energy.

When the utility is available, microgrids must be ready to connect to the main infrastructure. For this reason, dependable synchronisation algorithms are required for numerous power and industrial applications. As the number of unbalanced nonlinear loads at the point of common coupling (PCC) increases, the synchronisation process becomes progressively more challenging. For seamless transitions between grid-connected and islanded modes, scholars have developed a vast array of sophisticated control techniques. Enhanced phase-locked loop (EPLL) algorithms are prevalent and innovative. (Karimi-Ghartemani, 2014), limited cycle oscillator (Oviedo et al. 2018b), generalized delayed signal superposition (Lu et al. 2018) and the phase-locked loop (PLL) based control algorithm (Golestan et al. 2018; Oviedo et al. 2018b; Sangwongwanich et al. 2017). However, the performance of PLL normally deteriorates from wide frequency variation during phase jump (Karimi Ghartemani et al. 2012). This is because the loop evaluates the anticipated quantities continuously. In addition, during unanticipated grid recovery and interruption, PLL-based voltage angle and frequency calculations are susceptible to significant frequency fluctuations and phase variation.

The islanding and synchronization controller mechanism selects the operating mode and switches between them based on the grid's availability. While operating in grid-connected mode, the proposed multimode controllers achieve IEEE-519 compliance and maintain the power to loads in the event of a power loss. As the utility grid's operational circumstances change, the microgrid's control switches to the appropriate mode. To boost the detection pace and decrease the detection blind spot, researchers have reported multiple approaches (Harirchi et al. 2015b; Mondal & Illindala, 2018). Using synchronization methods, the anticipated phase angle, frequency, and magnitude of grid voltage are tracked. During the islanding, the control is changed from current control to voltage control. When intentional islanding is removed and the utility grid has been restored, the operation is reversed. As a result, based on the input data, the synchronisation mechanisms define the operational parameters. Synchronization with grid voltage is essential for PV-BES microgrid connections to the utility grid (X. Li, 2019; X. Li & Wang, 2021). The development for the implementation of sophisticated synchronization of grid techniques with a phase-locked loop (PLL), can latch to grid characteristics. PLLs are often employed to determine the phase difference between grid voltage (Bendrat et al. 2017; Dai et al. 2009). The output of a PLL may be locked in frequency and phase with the input signal owing to its sophisticated closed-loop feedback control. Several scholars (Y. Singh et al. 2018; Zeng & Shao, 2017) have also suggested alternative robust synchronization strategies. A grid transition approach is employed in this study; these methods are straightforward and rely on monitoring voltage magnitude, the frequency rate of change, and phase angle displacement between the grid and PCC voltages to restore to utility mode. The authors (Bei & Wang, 2016) present a method for synchronising the grid that is both effective and reliable, even when the grid is experiencing distortion and the power quality is poor. The authors (Thale & Agarwal, 2016) present a controller area network for synchronising grids. Nevertheless, (Golestan et al. 2016; Safa et al. 2018), an open loop synchronisation approach for the utility-tied converter is described, which requires less computation because it does not require complex sine and cosine functions. In (Bendrat et al. 2017) a new computation-efficient method is used to estimate utility and load voltage angles while also accounting for power quality concerns to synchronise DG under nonlinear loads at PCC.

2.3 SUMMARY

In this chapter, a detailed literature review has been given on standalone and grid interactive microgrids, intelligent MPPT control algorithms for photovoltaic systems and seamless transitions of quality power between the microgrids. Therefore, based on the literature review, it has been perceived that there is remarkable scope of work in grid-interactive microgrids based on PV array and battery storage with seamless transition. It has also been noted that a PV-battery-based microgrid for remote areas is distinct from a utility-tied PV system that synchronizes its output voltage, frequency, and phase with the distribution network's grid voltage waveform. The coming chapters in this thesis illustrate detailed research in these identified research areas.

Chapter 3

GRID-CONNECTED PHOTOVOLTAIC SYSTEM

3.1 INTRODUCTION

The power generated using photovoltaics is injected into the grid as shown in Figure 3.1. The type of converter interface utilised is determined by the topology of the PV system. It depends on the configuration, cost, and desired level of effectiveness. The configuration (Jain & Agarwal, 2007) of the one-stage power conversion using DC/AC inverter to interface the PV array to the grid is shown in Figure 3.1. The inverter is used to provide the voltage from PV, monitor the maximum power point (MPP) of the PV, and regulate the power injected into the grid.

Figure 3.1: One-stage DC/AC PV system.

The suggested two-stage architecture is shown in Figure 3.2. This architecture consists of DC/DC and DC/AC converters to link the PV array with the grid (Kjaer et al. 2005).

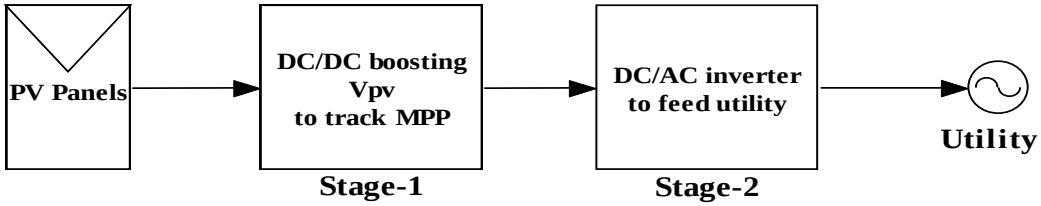

Figure 3.2: Two-stage DC-DC and DC-AC converter PV system structure.

This chapter's network topology study comprises a photovoltaic solar system associated to a voltage-boosting converter that focuses on raising the voltage across the load. A boost converter is coupled with a maximum power point controller to track the PV's MPP. This structure is seen in Figure 3.3. It makes it easier to analyze the efficiency of the MPPT technique and the PV's ability to produce the most electricity under varied temperature and radiation circumstances in order to fulfill demand.

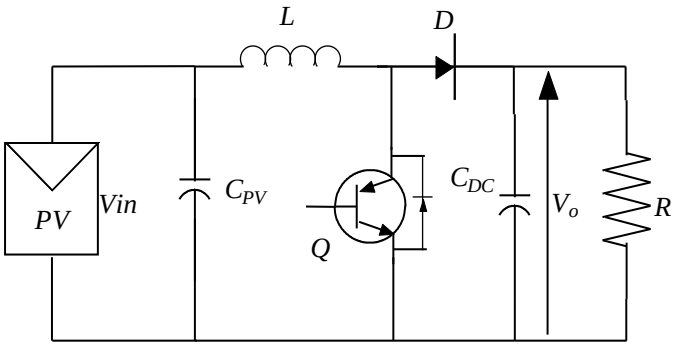

Figure 3.3: Boost converter-resistive load PV topology.

Figure 3.4 depicts a 3-ϕ photovoltaic system with a resistive load. The system's energy source is the solar array, and the DC-to-DC boost converter modifies the DC-link voltage, increases the PV voltage, and keeps an eye on the maximum power production. AC currents are supplied to the load via the DC/AC converter.

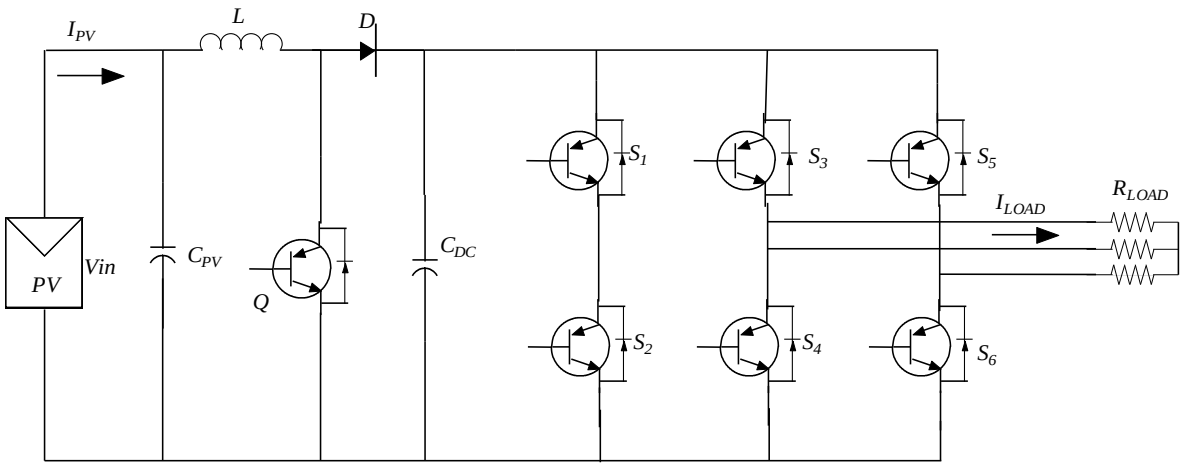

Figure 3.4: Two-stage PV system topology with R load

3.2 PV SYSTEM CONTROL METHODOLOGY

The control approach used by the PV-VSC is shown in Figure 3.5. The system consists of a boost converter with MPPT control to calculate the duty ratio to operate at the MPP point for a particular solar irradiation. The primary responsibilities of the inverter controller are to regulate the dc-link voltage and also to transmit the DG's active power into the grid through the converters. The current loop, dc-link voltage controller, and phase-locked loop (PLL) are the three primary command blocks that surround the inverter. The DC link outer voltage loop is fed by the measured dc-link voltage and the reference voltage, to get the reference current. This reference current and the measured current are given to the current control loop to get the reference voltage, which is given to the pulse generator to get the pulses for inverter switches. Phase Lock Loop (PLL) is used to synchronize the frequency and phase of DG with the main grid. The control methodology of each block is described below.

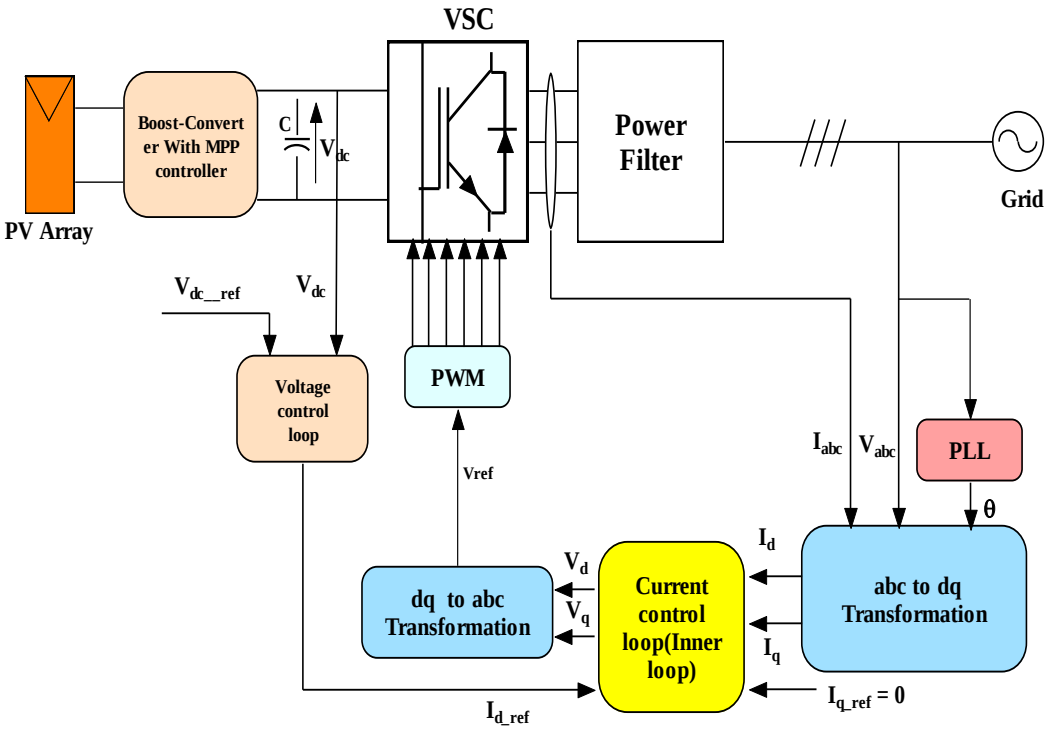

Figure 3.5: Controller block of 3-ϕ PV structure.

3.3 MODELING OF PHOTOVOLTAIC ARRAYS

3.3.1 PV Array I-V Characteristics

In Figures 3.6 and 3.7, the current-voltage (I-V) characteristics of the PV panel are displayed. The critical values of this nonlinear curve are dependent on both solar radiation and temperature. Figure 3.6 illustrates how the MPP and current increase when the irradiation increased while the voltage just minimally changes.

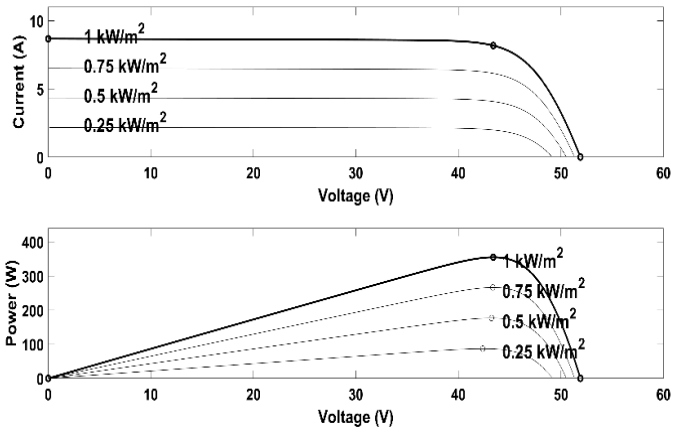

Figure 3.6: The I-V and P-V characteristics of a PV module in response to irradiance.

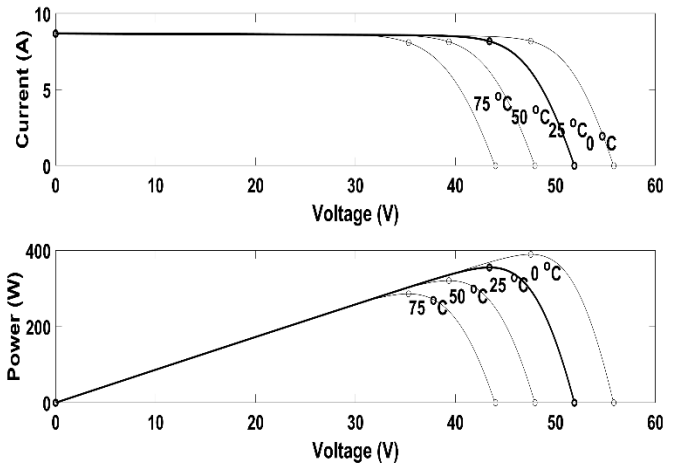

Figure 3.7: PV module I-V and P-V characteristics as a function of Temp.

The current varies less with temperature than voltage, as seen in Figure 3.7. As a result, there is a dynamic point on the I-V curve known as the Maximum power point MPP. As shown in Figure 3.7, the complete PV system must operate at maximum

output power. Since the maximal position is uncertain, we apply the search algorithms as techniques to keep the PV array operating at the MPP.

3.3.2 PV Cell Model

Solar energy may be transformed into useable power by use of a semiconductor p-n junction known as a PV cell (Villalva et al. 2009). It is necessary to analyze the effects of different components on the panels and use the manufacturer's requirements to develop a model of a solar cell. Cells that are linked in series or parallel make form a PV module. A PV array is made up of solar modules arranged in parallel and series. Consequently, the equivalent circuit of the PV cells is used to build mathematical models of PV arrays.

A typical PV cell is represented electrically by a single diode, series resistance Rs, and parallel resistance Rp, as illustrated in Figure 3.8.

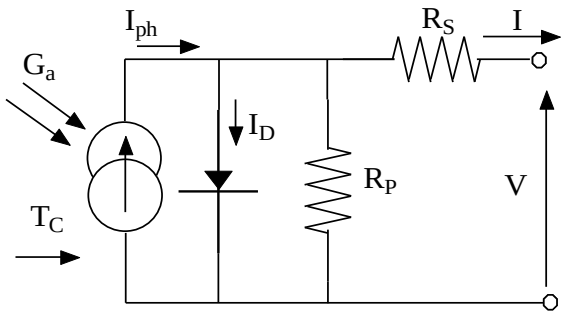

Figure 3.8: Single diode equivalent photovoltaic cell. (Villalva et al. 2009)

Another parameter provided by the solar module's manufacturer is necessary to model the PV cells (Sera et al. 2007). The electrical parameters stated on the datasheet are derived using standard test conditions (STC), which are defined as at 25^0C and 1000 W/m^2 irradiance. Table 3.1 shows the typical PV parameters.

The process begins with a model of a single solar cell, progresses to an individual PV module, and culminates in an analysis of a whole PV array. It can be seen in Figure 3.8 that the PV cell has an output current of

$$I = I_{ph} - I_d \tag{3.1}$$

where, I_{ph}: photon produced by the cell, I_d : diode current.

The diode current I_d is determined by the Shockley equation (Villalva et al. 2009),

$$I_d = I_o\left(\exp\left(\frac{qV_d}{akT}\right)-1\right) \tag{3.2}$$

where,
I_o: reverse saturation current of diode,

q: elementary electron charge ($1.602\text{x}10^{-19}$C),

V_d: diode voltage,

a is the diode ideality constant,

k: Boltzmann constant $1.381\text{x}10^{-23}$ (J/K),

T: temperature in kelvin (K),

The relation between voltage and current results from replacing the diode current.

$$I = I_{ph} - \underbrace{I_o\left(\exp\left(\frac{qV_d}{akT}\right)-1\right)}_{I_d} \tag{3.3}$$

where, V_d is the output voltage of the PV cell.

Using the equation above, the reverse saturation I_o is determined. Performing calculations at temperature T_1 while making the current I equal to zero (Gradella Villalva et al. 2009)

$$I_o(T_1) = \frac{I_{ph}(T_1)}{\left(\exp\left(\frac{qV}{akT}\right)-1\right)} \tag{3.4}$$

The short circuit current I_{sc} can be used to estimate the produced current by solar cells, I_{ph} (Tsai et al. 2008). At the various irradiances, the current produced can be estimated. The datasheet's temperature, standard current, and irradiance are utilized to calculate the current under various conditions.

$$I_{sc} \approx I_{ph} \tag{3.5}$$

$$I_{sc}(T_1) = \left(\frac{G}{G_{nom}}\right) I_{sc}(T_{1,nom}) \tag{3.6}$$

where,

$I_{sc}(T_1)$: short circuit current at T_1 temperature

T_1: cell temperature at STC

G_{nom}: irradiance at STC

After calculation, (Gradella Villalva et al. 2009)gives the equation,

$$I = I_{pv} - I_o\left(\exp\left(\frac{V + IR_S}{akT / q}\right) - 1\right) - \frac{(V + IR_S)}{R_p} \tag{3.7}$$

where, The V, voltage of the cell.

Multiplying the voltage across a PV module's series of cells yields the module's total output. Depending on the temperature T, the current at reverse saturation I_o changes. The following equation (Villalva et al. 2009) is used to compute it:

$$I_O = I_O(T_1)\left(\frac{T}{T_1}\right)^{\frac{3}{n}}\left(\exp\left(\frac{qV_q(T_1)}{ak\left(\frac{1}{T} - \frac{1}{T}\right)}\right)\right) \tag{3.8}$$

The resistance series R_s value is determined by dV/dI slope of the I-V curve at the no load i.e., open circuit voltage (Taufik et al. 2009). Given by, the equation Rs is,

$$R_S = -\frac{dV}{dI} - \frac{akT/q}{I_O \exp\left(\frac{qV_{OC}}{akT}\right)} \tag{3.9}$$

The aforementioned recursive equations are utilized to determine the model's currents (Taufik et al. 2009). Finding the current of a PV cell requires solving a recursive equation. Numerical solutions are chosen because they are easier to implement. The equation gives a more straightforward way to calculate series resistance by leaving out parallel resistance.

To complete the model, the currents are calculated using the corresponding recursive equations (Taufik et al. 2009). The current for a PV cell is determined using the recursive equation which is simpler to implement. In the equation, an efficient

method for calculating series resistance that eliminates the parallel resistance is introduced.

$$I_{n+1} = I_n - \frac{I_{ph} - I_n - I_O \exp\left(\frac{q(V + I_n R_S)}{akT} - 1\right)}{-1 - I_O\left(\frac{qR_S}{akT}\right)\exp\left(\frac{q(V + I_n R_S)}{akT}\right)} \tag{3.10}$$

3.3.3 Photovoltaic Module Modeling

The forthcoming model calculates the resistance series and parallel using a different technique. In this case, the PV module produces 355.012W of nominal maximum power and is constructed of 83 solar cells (silicon nitride multi-crystalline) connected in series. Table 3.1 provides the module's parameters, which are necessary to represent the PV array.

Table 3.1: PV Panel Parameters at 1000 W/m^2 and 25^0 C

Parameters	Nominal Value
Maximum Power (W) P_{MPP}	355.012
The voltage at maximum power point V_{mp} (V)	36.4
Current at maximum power point I_{mp} (A)	9.75
Open circuit voltage V_{oc} (V)	43.5
Short-circuit current I_{sc} (A)	10.34
Cells per module (N_{cell})	83
Temperature coefficient of V_{oc} (%/deg.C)	-0.304
Temperature coefficient of I_{sc} (%/deg.C)	0.017

In the literature, many photovoltaic models have been constructed (Chan & Phang, 1987). The model involves obtaining the PV module's curve characteristics from the datasheet. The curve known as the I-V curve is calculated using the following equation:

$$I = I_{pv} - I_O\left(\exp\left(\frac{q(V + IR_S)}{N_S kT\alpha}\right) - 1\right) - \frac{(V + IR_S)}{R_p} \tag{3.11}$$

where,

N_s: number of series cells

When N_s cells are linked in series in a module, the thermal voltage is defined as

$$V_t = \frac{N_S kT}{q} \tag{3.12}$$

The produced current I_{ph} is directly dependent on solar radiation and temperature.

$$I_{ph} = I_{ph,nom} + K_i \Delta_T \left(\frac{G}{G_{nom}} \right) \tag{3.13}$$

where,

K_i: current temperature coefficient

Δ_T: change in temperature

Saturation current I_o in a diode and its temperature dependence are both evident.

$$I_O = I_{O,n} \left(\frac{T}{T_1} \right)^3 \left(\exp\left(\frac{qE_g}{ak} \left(\frac{1}{T_{nom}} - \frac{1}{T} \right) \right) \right) \tag{3.14}$$

$$I_{O,n} = \frac{I_{sc,n}}{\exp\left(\frac{V_{oc,n}}{aV_{t,n}} \right) - 1} \tag{3.15}$$

The resistance series Rs value is determined by dV/dI slope of the I-V curve at the V_{oc}. Through differentiation, R_s become (Taufik et al. 2009),

$$R_S = -\frac{dI}{dV} - \frac{nkT/q}{I_O \exp\left(\frac{q(V + I.R_a)}{akT} \right)} \tag{3.16}$$

When the circuit is completely open, voltage V equals voltage V_{oc}, where I is set to 0 at this point. This is the series resistance:

$$R_S = -\frac{dV}{dI} - \frac{nkT/q}{I_O \exp\left(\frac{qV_{OC}}{akT} \right)} \tag{3.17}$$

In (Gow & Manning, 1999), the R_s, R_p are computed iteratively. The objective is to determine the suitable estimates of R_s, R_p which fit the P-V characteristics mathematically with the peak power at the MPP. The resistances R_s, R_p are set

automatically attained during an iteration is completed once the calculated P_{max} equals the estimated P_{max}.

The PV module as shown in Figure 3.9 depicts the circuit schematic. Equivalent resistors and the model's equation provide a regulated current source. Variation in the power consumed by the load influences the PV voltage.

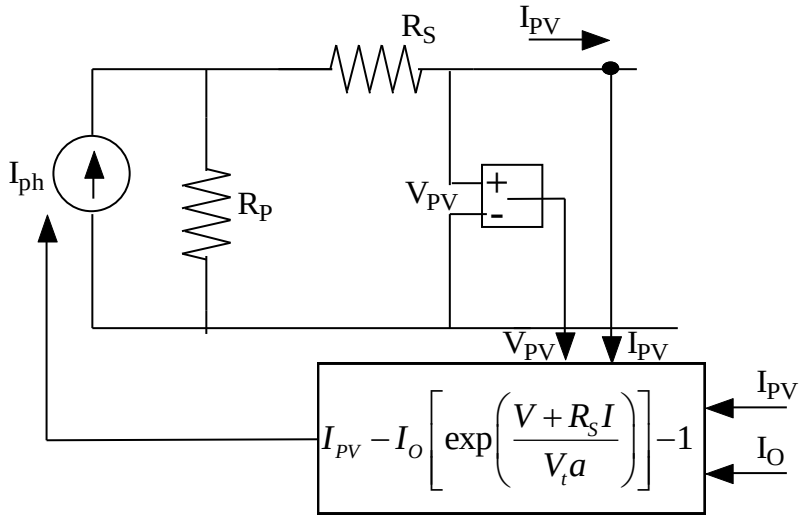

Figure 3.9: Photovoltaic module circuit diagram. (Villalva et al. 2009)

3.3.4 Photovoltaic Array

Multiple photovoltaic modules are linked together to form the PV array. The modelling procedure for the PV module is identical to that for modelling PV cells. Utilise the values specified in the datasheet. The necessary power is generated by connecting PV modules in parallel and series. As shown in Figure 3.10, a solar array consists of numerous modules connected in series and parallel. The sum of the number of modules operating in parallel, denoted by N_{par}, and the number of modules operating in series, denoted by N_{ser}. The parallel and series resistance values vary based on the number of modules. The parallel and series resistance equivalents of the PV array are as follows:

$$R_{s,array} = \frac{R_{s,\mathrm{module}} - N_{ser}}{N_{par}} \tag{3.18}$$

$$R_{p,array} = \frac{R_{s,\mathrm{module}} - N_{ser}}{N_{par}} \tag{3.19}$$

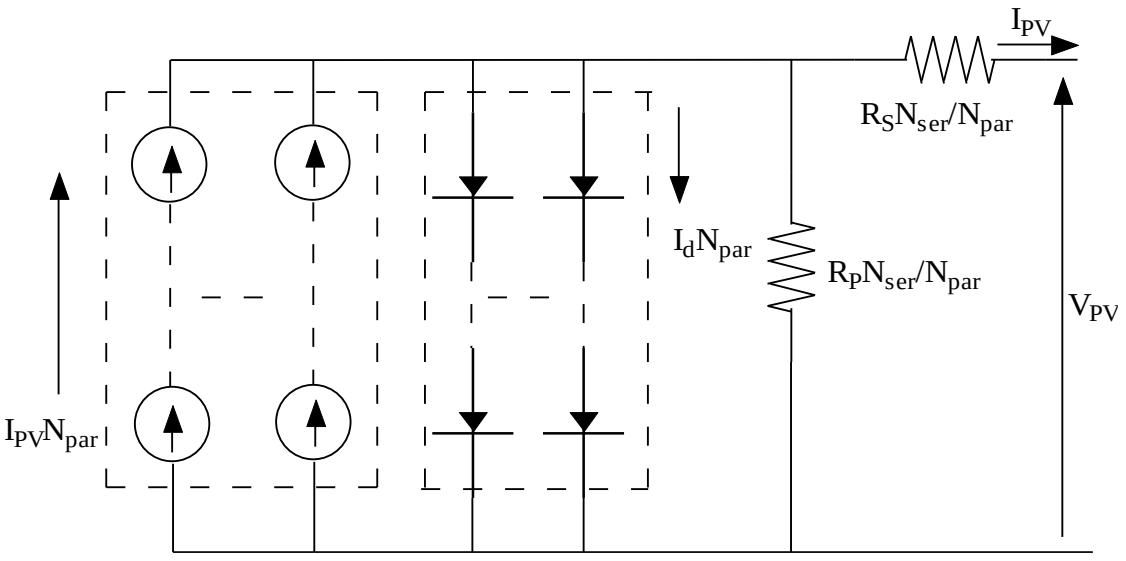

Figure 3.10: Photovoltaic array with modules N_{ser}*N_{par}. (Villalva et al. 2009)

When the current-voltage relationship of PV modules is extended to a PV array, a new relation is found in (Villalva et al. 2009) by

$$I = N_{Par} I_{pv} - N_{Par} I_o \left(\exp\left(\frac{V + IR_S \left(\frac{N_{Ser}}{N_{Par}} \right)}{V_t a N_{Ser}} \right) - 1 \right) - \left(\frac{V + IR_S \left(\frac{N_{Ser}}{N_{Par}} \right)}{R_P \left(\frac{N_{Ser}}{N_{Par}} \right)} \right) \tag{3.20}$$

where the parameters I_o, I_{pv}, V_t is used for a PV module.

This equation applies to each array of similar modules. This equation is used to simulate the photovoltaic array. The simulated circuit needs to incorporate both series/parallel modules. Figure 3.11 depicts the circuit of PV array.

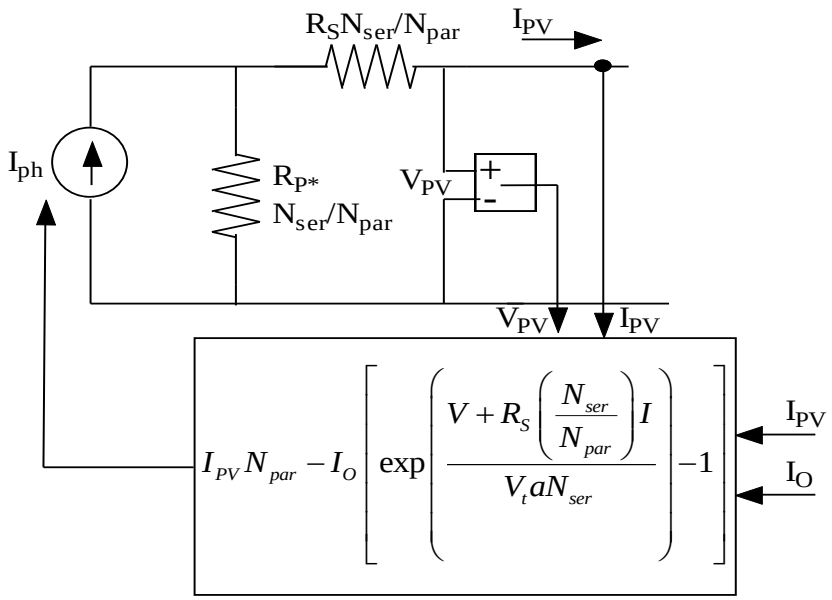

Figure 3.11: Photovoltaic array structural model. (Villalva et al. 2009)

3.4 BOOST CONVERTER

3.4.1 The Boost Converter Working

The primary function of the DC/DC is to enhance the DC input voltage of the PV. For optimum power output, the maximum power point tracker (MPP tracker) utilises the DC/DC converter. A boosting approach is used to improve the limited voltage input of the PV system. For an inverter to function, the photovoltaic (PV) source voltage must be increased by a boost-converter (Hasaneen & Mohammed, 2008). Figure 3.12 depicts the operation of the converter. An inductor L is connected in series with the DC input to provide a source current. Turning on-off a switch T in series with the current source combines the energy derived from the inductance and its source to raise the typical output voltage.

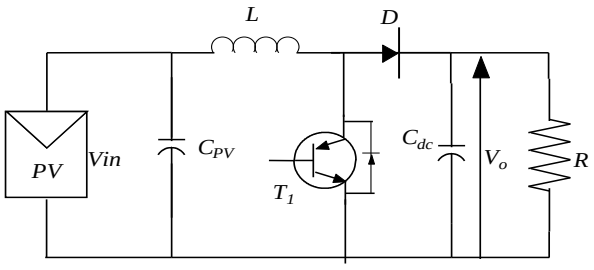

Figure 3.12: Topology of a boost converter

An integral inductor voltage set to zero across the transition time is used to determine the boost converter's voltage ratio. The corresponding voltage ratio is the ratio of the switch's toggling period to its off duration (Mohan, 2003),

$$\frac{V_o}{V_{in}} = \frac{T}{t_{off}} = \frac{1}{1-D} \tag{3.21}$$

The capacitor C_{dc} is sufficiently bulky to maintain a uniform voltage output, and its inductor delivers energy once the switch opens, thereby increasing load voltage. The MPPT controller's duty ratio is used to regulate the converter's switch. It is a PWM pulse that turns on/off to switch as shown in Figure 3.13.

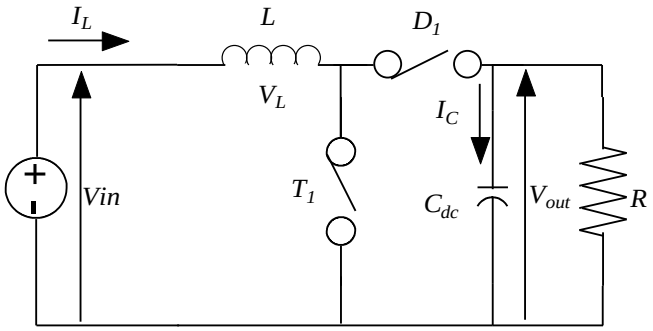

Figure 3.13: Schematic diagram of a boost converter

The T_1 switch is on and switch D_1 is off as shown in Figure 3.14, dividing the circuit into two distinct parts, the inductor is charged by the source, on the left, while the capacitor on the right is responsible for maintaining voltage output using previously stored energy. The current through inductor L is progressively increased.

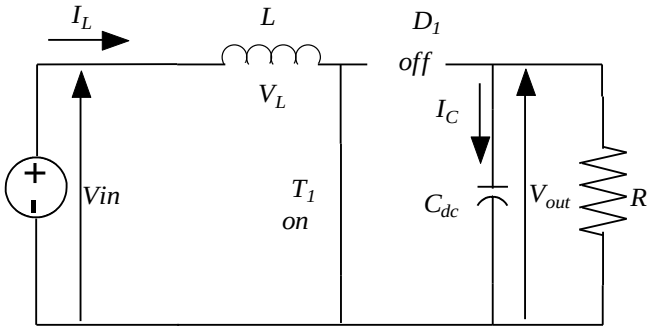

Figure 3.14 Diagram with switch T1 and D1 on-off mode.

During D_1-on and T_1-off as shown in Figure 3.15, the inductor's stored energy and DC source will deliver power from the circuit, increasing the voltage across the load. The current through inductor then progressively decreases. If the toggling sequence is controlled, the voltage across the load can be maintained at a particular desired level.

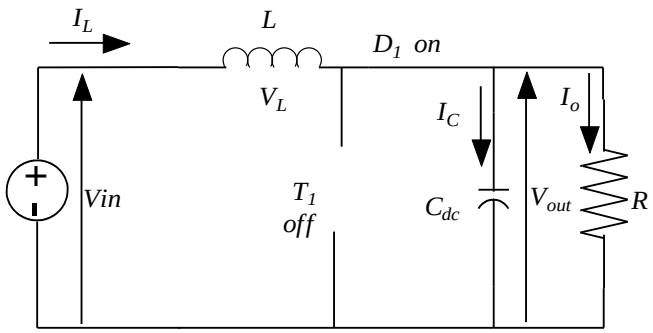

Figure 3.15 The switch T1 off and D1 on converter structure.

While switch T_1 is on and D_1 is turned off, V_L can be as described in (Mohan, 2003):

$$v_L = V_{in} \tag{3.22}$$

$$i_c = \frac{-v_{out}}{R} \tag{3.23}$$

While T_1, and D_1 switch is off and on respectively, resulting:

$$v_L = V_{in} - v_{out} \tag{3.24}$$

$$i_c = i_L - \frac{v_{out}}{R} \tag{3.25}$$

Assuming ripple approximation $v_o \approx V_o$ and $i_L \approx I$

The integral voltage of the integral throughout the length of a certain period must be zero in stabilised circumstances.

$$\int_0^{T_s} V_L(t)dt = (V_{in})DT_s + (V_{in} - V_o)D'T_s \tag{3.26}$$

The voltage output after equal to zero is:

$$V_{out} = \frac{V_{in}}{D'} = \frac{V_{in}}{1-D} \tag{3.27}$$

Assuming a circuit with no losses, $P_{in} = P_{out}$

$$\frac{I_{out}}{I_{in}} = (1-D) \tag{3.28}$$

The output voltage increases as *D* increases, as can be seen. The optimal boost converter can generate any output voltage more than the source voltage.

3.4.1.1 Continuous Conduction Mode

In CCM the switch is held in the ON position for the whole-time span from t to t_{on} as can be seen in Figure 3.16. Positive, linearly increasing current flows via the inductor. V_{in} is the voltage across the inductor. When the switch is turned off (shown in Figure 3.16), the inductor's current gradually decreases until the switch is switched back on. The voltage produced by an inductor is equal to V_{in} - V_{out}. Constant conduction is achieved by making the output voltage a function of both the input voltage V_{in} and the duty cycle *D*.

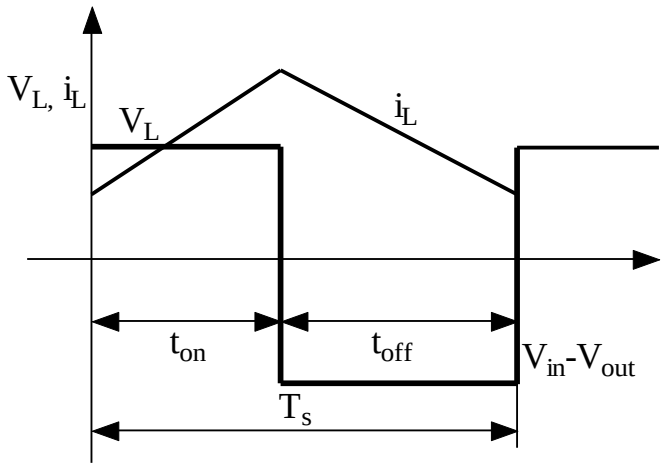

Figure 3.16: Continuous conduction mode (Hasaneen & Mohammed et al. 2008)

3.4.1.2 Discontinuous Conduction Mode

In discontinuous mode (DCM), the boost converter's operation is characterised by a period of sluggishness during which the inductor current drops to zero. Periodically, the inductor current drops to zero. In Figure 3.17, we see this discontinuous conduction mode shown. The connection between the two-voltage levels is established.

$$\frac{V_{out}}{V_{in}} = \frac{D_1 - D}{D_1} \tag{3.29}$$

The average input current is calculated by (Hasaneen & Mohammed et al. 2008)

$$I_{in} = \frac{V_{in}}{2L} DT_s(D + D_1) \tag{3.30}$$

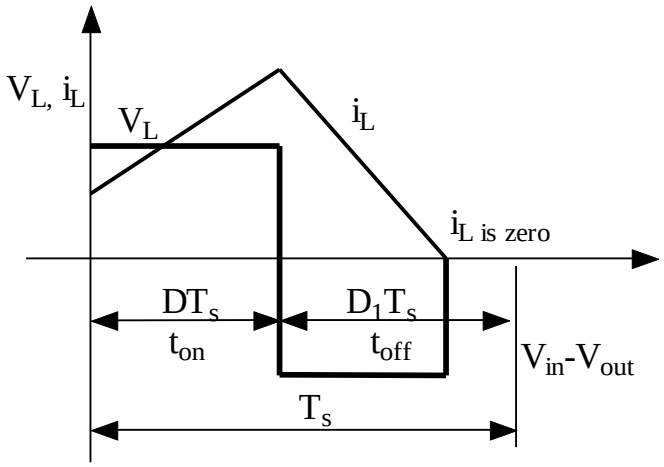

Figure 3.17: conduction mode- Discontinuous (Hasaneen & Mohammed et al. 2008)

A summary of the output currents and voltages of the boost circuit in Figure 3.18 provides. A control switch for the regulation of voltage is shown. The switch toggles between on and off for a given amount of time. When a switch is on, the voltage across it is zero, and when it is off, it is V_{out}. During the on-period of the switch, the voltage across inductor *L* is equivalent to the photovoltaic voltage.

3.4.1.3 Selection of the Inductor

The values of the supply inductor can be calculated using the energy released during the t_{on} and t_{off} periods and the current fluctuations. The boost converter in photovoltaic systems operates in both discontinuous and continuous states of conduction. Based on the conditions in the atmosphere, the conductivity mode of the converter may vary. The inductive component is then determined based on its current and input power. As given by (Mohan, 2003) the inductor is calculated by,

$$L \geq \frac{V_{om} D_m (1 - D_m)}{f_s \left| \Delta I_{Lripple} \right|} \tag{3.31}$$

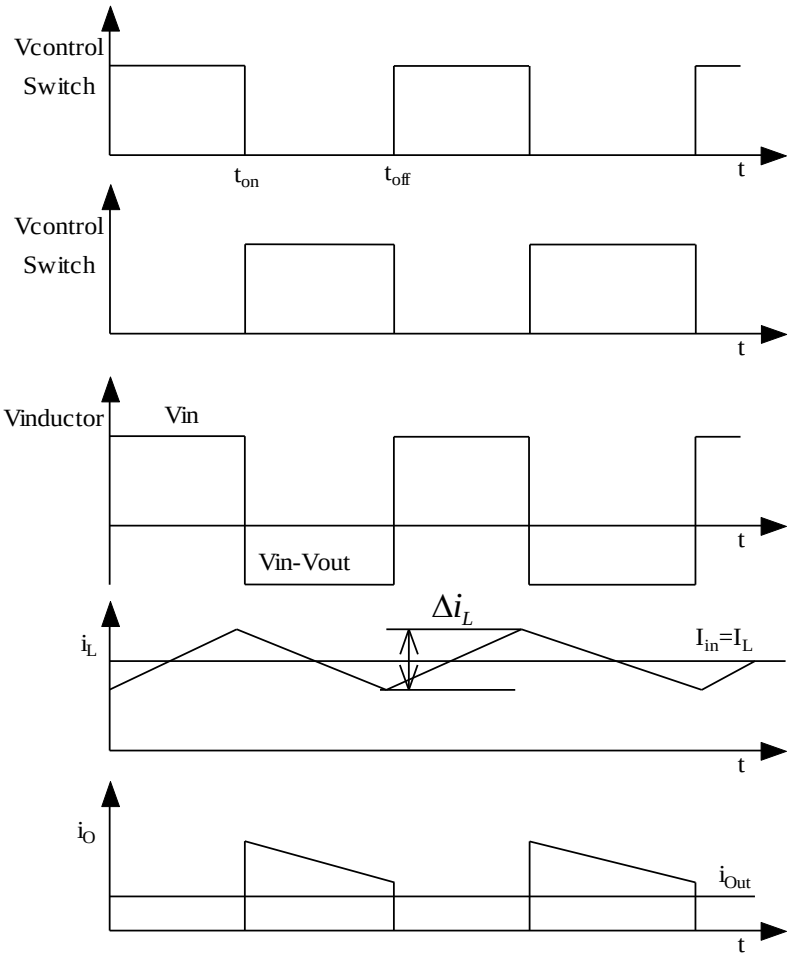

Figure 3.18: DC-DC boost converter output waveform (Mohan, 2003)

3.4.1.4 Power Decoupling Capacitor

The capacitor connected across the photovoltaic array is called the power decoupling capacitor (C_{PV}). This is a capacitor that is at the boost converter's input. The decoupling capacitor can be calculated using (Hasaneen & Mohammed, 2008).

$$C_{PV} \geq \frac{I_{om} D_m^2}{0.02(1-D_m) f_s V_{pv\_mpp}} \tag{3.32}$$

The capacitor's value is dependent on the minimal ripple voltage. According to (Hasaneen & Mohammed, 2008). DC link capacitor across the load is given by,

$$C_{DC} \geq \frac{V_{load}.D}{f_s \Delta V_{load} R_{load}} \tag{3.33}$$

This capacitor is connected across the PV output to mitigate the fluctuating voltage at the output of the PV. It serves to reduce ripples in the voltage while providing storage of energy for a brief period and rapid PV voltage change.

3.5 PV MPPT CONTROL METHODS

3.5.1 P&O MPPT

This strategy has been one of the most widely employed strategies in both the business sector and academia. P&O is divided into measurement and comparison groups in order to monitor and locate the MPP. The PV control system takes measurements of the photovoltaic parameters at the outset of each operating period and then uses those readings to perturb the point at which it operates into a new operating direction. When the voltage derivative of power is zero ($dP/dV = 0$), the maximal power point is reached. Several models have been provided for this method (Killi et al. 2015). Figure 3.19 depicts the controller module.

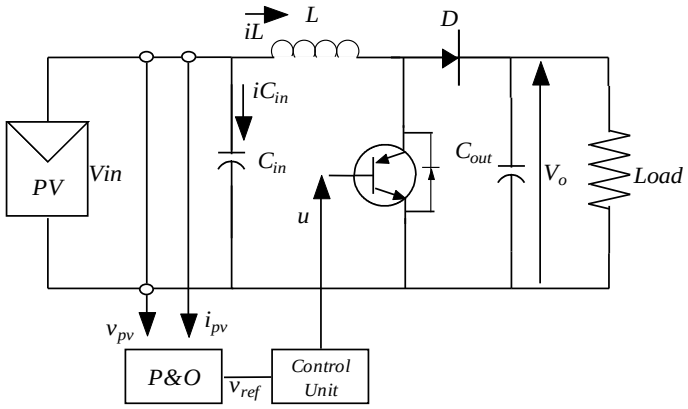

Figure 3.19: Circuit diagram of PV system using PO-MPPT

The maximum power of the photovoltaic system at standard test conditions (1000 W/m^2 and 25^0 C) of 15 panels connected in series with 190 strings totalling 1 MW is considered under study.

The MPP varies as cell temperature and irradiance change. Solar cells have very low efficiency. Appropriately matching the source with the burden is necessary to improve efficiency. Maximum power point tracking (MPPT) is one of these techniques. An MPPT controller controls a converter that is linked to the PV system as the P&O flowchart is shown in Figure 3.20. The MPPT is affected by both radiation and temperature variation. Thus, under any circumstance, the MPPT controller is guided by the P&O MPPT algorithms to adjust the operating point in the direction of the MPP (Islam et al. 2018). Figure 3.21 the adopted PV array characteristics. Thus, the output voltage (DC bus voltage) of the boost converters is maintained at a stable acceptable value. This is given to the inverter to get a 3-ϕ supply to balance the generation and the load using the inverter PQ controller. The DC voltage must constantly remain at an acceptable value for the inverter to control (Ramezani et al. 2017), and this is irrespective of how much ever real power the PV system provides.

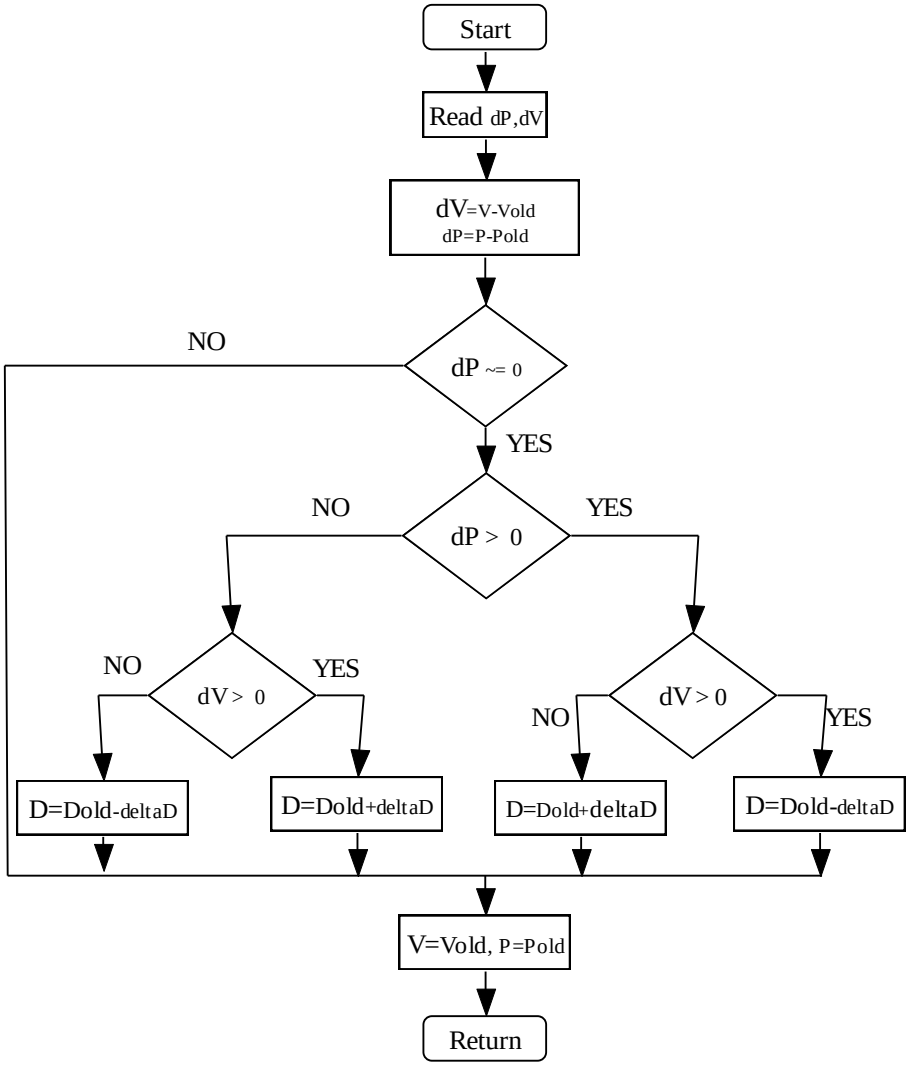

Figure 3.20: The Perturb and Observe algorithm method.

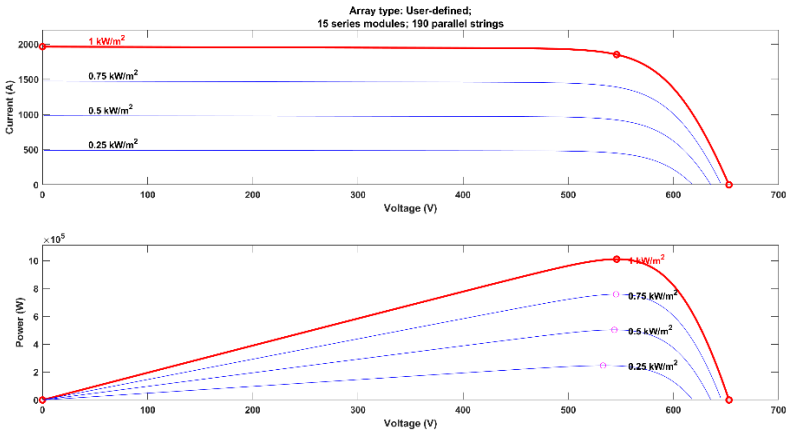

Figure 3.21: The adopted PV array characteristics

3.5.2 PSO-ANFIS MPPT Control

The training and refining of ANFIS requirements have become a difficult challenge for developers. The PSO is simpler to implement and has a more rapid convergence rate than gradient algorithms (Priyadarshi et al. 2020). The PSO also does not require any kind of initial parameter computation or a specific learning rate. In engineering applications, the algorithm known as PSO is regarded as a high-quality search method. This algorithm's fundamental premise is that it attempts to locate an optimized region in which each space contains a degree of potential possible solutions (Sarvi & Azadian, 2022). The PSO optimizer's actions are determined by both its own and its neighbours' past experiences during each particle phase, which is inspired by the flocking behaviour of birds. The PSO algorithm's procedure consists of four stages. In the initial iteration, the PSO optimizer begins to look around for an arbitrary particle value. We've resolved this particle value to maximise the available solution space for a variety of optimisations. The second stage entails comparing the highest fitness values derived for the same space before (P_{bi}) and after (P_{li}). In the final stage, the G_{bi} is computed by comparing the best local positions to the best global positions. The transformed coordinates are then stored for use in the next steps in accordance with Equation (3.34).

$$V_i^{k+1} = w \times V_i^k + r_1 \times C_1 \times (P_{bi} - X_i^k) + r_2 \times C_2 \times (G_{bi} - X_i^k) \tag{3.34}$$

$$X_i^{k+1} = X_i^k + V_i^k \tag{3.35}$$

After a fitness check, the best particle is chosen and stored so that its motion may be fine-tuned with each repetition. These steps are continued indefinitely, or until some stopping condition is satisfied. System accuracy and processing time control requirements inform the suggested stopping condition and total number of iterations. In Figure 3.22, we can see that the ANFIS controller is a five-layered, hierarchical structure whose fundamental components are antecedents and consequent, and therefore a neural network with traditional feedforward topology. These mathematical formulas describe multilayer feedforward networks:

$$L_{1,i} = \mu A_i(e),\ for....i = 1,2...j\ ;\ L_{1,i} = \mu B_i(\Delta e),\ for....i = 1,2...j \qquad (3.36)$$

e and Δe are input A_i and B_i are each node membership function (Gaussian function)

$$L_{2,1} = W_i = \mu A_i(e)\mu B_i(\Delta e),\ for..i = 1,2..j^2 \qquad (3.37)$$

$$L_{3,i} = \overline{W_i} = \frac{W_i}{\sum_{i=1}^{j^2} W_i} \qquad (3.38)$$

$$\left.\begin{aligned} L_{4,i} &= \overline{W_i} f_i = \overline{W_i}(p_i e + q_i \Delta e + r_i) \\ L_{5,i}(x) &= \sum_{i=1}^{j^2} \overline{W}_i f_i = \frac{\sum_{i=1}^{j^2} W_i f_i}{\sum_{i=1}^{j^2} W_i} \end{aligned}\right\} \qquad (3.39)$$

where (p_i, q_i, r_i) constitute the linear elements of the ANFIS network and are frequently referred to as the subsequent parameters of the network, and (W_i) is a normalised firing strength from Layer 3. The least-squares approach is used to fine-tune these parameters during training. The output of this fifth layer is computed using the weighted average method.

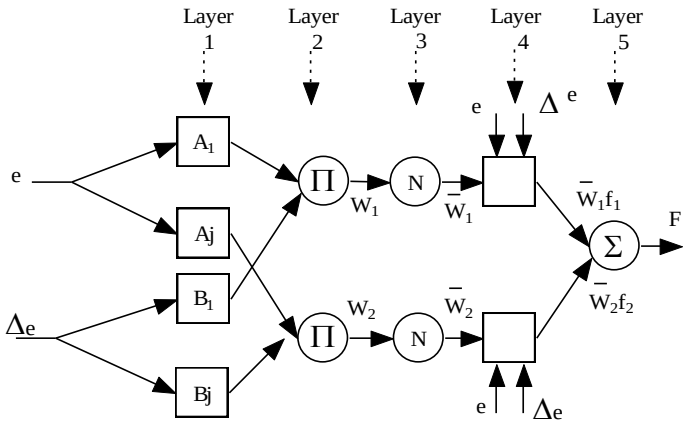

Figure 3.22: Architecture of an ANFIS controller. (Sarvi & Azadian, 2022)

Faster dynamics, a quicker speed of convergence, and a simpler design are just a few benefits this controller provides over conventional MPPT controllers. Crisp results are obtained using the weighted average of the rules consequent using this approach. The weighted values are optimized using PSO. Furthermore, the goal function is the root-mean-square error. The optimum weights of the ANFIS are the target of an algorithm that relies on the PSO technique. These are figured out to improve the model's forecast of output once the weight estimations have been revised. This is accomplished by integrating the PSO algorithm with the ANFIS technique.

Figure 3.23 depicts the comprehensive flowchart arrangement of the PSO-ANFIS-based MPPT control. It is necessary to correctly modify the membership values based on the crisp data gathered utilizing a potent ANFIS algorithm before the error is decreased to an absolute minimum. The trained system can function as a controller as MPPT once the appropriate membership parameters have been adjusted.

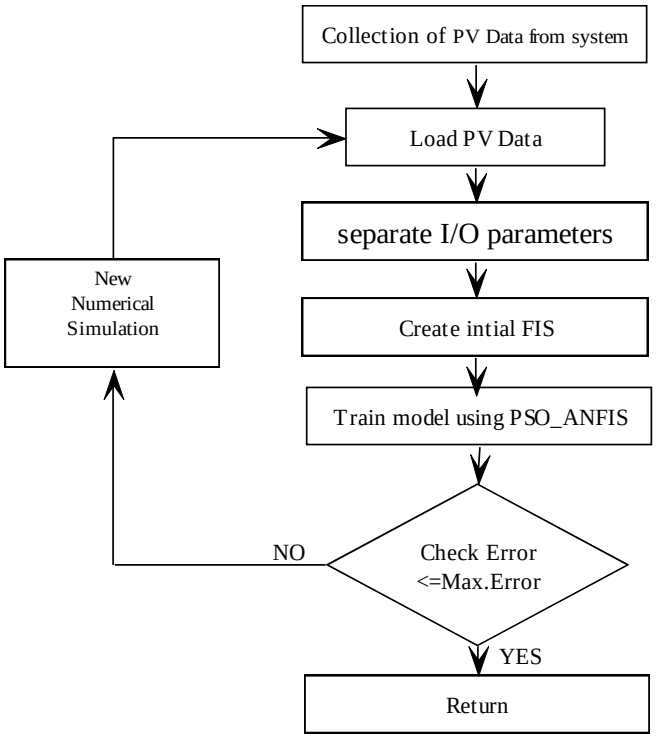

Figure 3.23: Flowchart of PSO_ANFIS-based MPPT.

Table 3.2. PSO-ANFIS Parameters.

Parameters	Nominal Value
No. of operation	25
No. of iteration	100
Weight of inertia	1

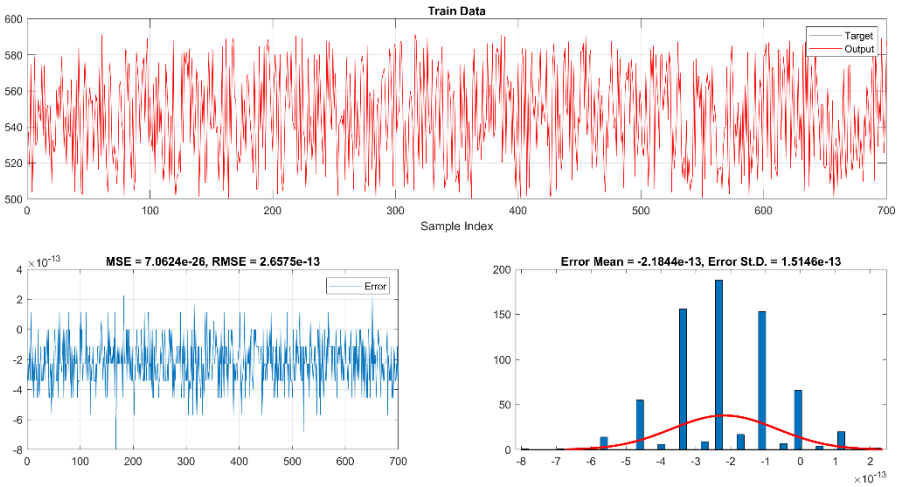

Figure 3.24: Train Data with an error of PSO_ANFIS.

This procedure is used to adapt the boost converter duty ratio determined by the flowchart, and the PSO-ANFIS parameters are listed in Table 3.2.

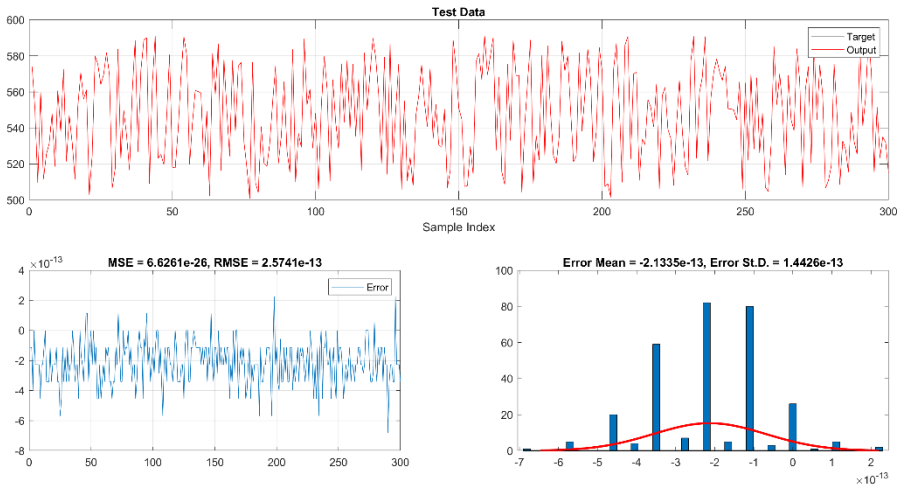

Figure 3.25: Test Data with the error of PSO_ANFIS.

Given an input parameter, the final signal of the pulse-width modulation (PWM) created by the MATLAB/Simulink model of a PSO-ANFIS technique is called the duty ratio. As the proposed ANFIS-PSO based model, the predicted Voltage ($V_{ref.}$) of the PV array at the MPP is calculated using the atmospheric conditions G and T as inputs. Following a PV operating simulink, an actual PV voltage ($V_{act.}$) is measured under identical environmental conditions. Next, the DC-DC converter's D is calculated by comparing the input and output voltages and feeding the resulting error into the PI controller. Equation (3.40) describes the signal control of the PI controller.

$$D = K_P(V_{act.} - V_{ref.}) + \frac{K_I}{S}(V_{act.} - V_{ref.}) \tag{3.40}$$

where K_P and K_I refer to the PI controller's proportional and integral gains. PSO is used to find the optimal parameters for the model's prediction function. The factors of the antecedent/consequent parameters are often examined separately in the conventional method. In this PSO-ANFIS approach, the mean square error is reduced by all parameters being trained and tested simultaneously. The PSO-ANFIS architecture's adaptive learning is calculated through online learning evaluation using the input/output parameters. Figure 3.24 and Figure 3.25 show the trained and tested data with the error of the PSO-ANFIS controller.

3.5.3 ANN Algorithm with PSO

To provide the most precise estimates of output functions, an ANN approach, which is a form of distributed computing (Al-Majidi et al. 2020), needs reliable data. When applied to training data, this algorithm creates a mapping that is nonlinear between the nodes in the input and the nodes in the output. Two varieties of ANN topologies exist feedforward and feedback networks. Because it requires less memory during the implementation stage, the first variant is the most frequently used (Baghban et al. 2015). Additionally, it is extremely efficient when utilising non-linear systems like a PV array. Input, hidden, and output layers make up the typical architecture of a multilayer feedforward ANN, as depicted in Figure 3.26. Furthermore, all layers' neurons are linked through the weights of their predecessors and the bias terms. This distributed computational system is mathematically defined as follows:

$$y = \sum_{i=1}^{n} w_{ij} x_j + bj \tag{3.41}$$

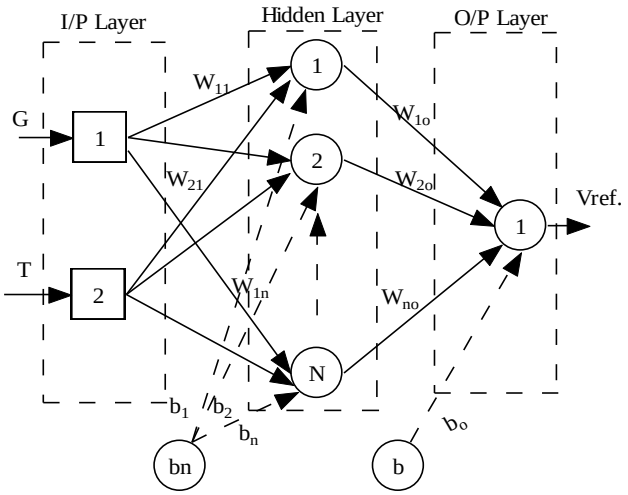

Figure 3.26: An ANN system's block diagram. (Al-Majidi et al. 2020),

In most cases, the backpropagation (BP) technique is used to learn about how a feedforward ANN works. The weights and bias terms of each node are fine-tuned until the desired output is achieved using a complex gradient method. To minimise training errors, the value of the output layer is a forecast that comes as near as possible to the actual outcomes. The standard equation (3.42), representing the MSE as the cost function, is as follows,

$$MSE = \frac{1}{n} \sum_{i=1}^{n} \sum_{j=1}^{m} [Y_j(i) - T_j(i)] \wedge 2 \tag{3.42}$$

A feedforward ANN's framework architecture (the total number of hidden layers and elements inside them) and initial training node weights are two of the most important design considerations.

3.5.3.1 Hidden Layer Size

Because of the trade-off between computing the amount of time and regression of the ANN nodes' population that gives the greatest fit, it is crucial to calculate the appropriate number of hidden layers and units in each for the feedforward ANN design (Basheer & Hajmeer, 2000; Hamdi et al. 2019). An overfitting regression occurs when the calculation time for an ANN model with many units in the hidden layers is too long.

On the other hand, the computing time required to fit a linear regression model using an ANN will be minimal if the model contains too few units within its hidden layers. The thickness of a covert layer is often determined by trial and error. This approach, however, is insufficient since it takes so much time.

3.5.3.2 Initial Training Weights

As mentioned previously, the backpropagation algorithm is utilised to gain knowledge about the error surface-seeking procedure utilised by the feedforward ANN model. As shown in Eq. (3.43), this computation search evolves as a gradient descent proportional to the additional weight increment (ΔW),

$$w_{ji}^{l}(t) = w_{ji}^{l}(t-1) + \Delta w_{ji}^{l}(t) \tag{3.43}$$

An update solution is generated in the first step of the BP algorithm's iteration, and in the second, the *MSE* is calculated and updated with new weights using Eqs. (3.42) and (3.43). This is repeated until the ANN model's training weights are optimal. (Aljarah et al. 2018; Basheer & Hajmeer, 2000) found that it will fail to identify the training weights optimally because it is primarily dependent on the magnitude of ΔW. If large, this can result in accelerated training and a significantly varying study of the error surface, leading to a non-convergent optimizing solution. If ΔW is small, however, training may be protracted and the error surface may be examined seamlessly, leading to the training process being terminated before the global minimum error is discovered. According to this theory, the initial weights have a substantial effect on how near an ANN model approaches the truth.

This process will keep going until the best training weights for the ANN model have been found. It has been shown in several research (Aljarah et al. 2018; Basheer & Hajmeer, 2000), for example, that this approach would fail to determine the optimised training weights since it largely relies on the size of ΔW. A non-converged optimising solution may be the consequence of rapid training and substantial fluctuations in the study of the error surface if ΔW is big. However, if ΔW is low, training will be sluggish, and the researcher may encounter fluctuations in the error surface without ever reaching

a global minimum. In this regard, an appropriate ANN model construction relies heavily on the anticipated starting weights.

In this study, we propose the data-driven feedforward ANN (artificial neural network) method for estimating the MPPT of a PV array. Significant challenges are posed to an ANN model training method by variations in training and operating parameters of a solar system. Particle Swarm Optimisation (PSO) is used to identify the optimal design and generate the optimal initial weights of the ANN model, enhancing the ANN model's accuracy. Not only is the mean squared error reduced, but also the trade-off between processing time and the ANN model's best-fitting regression is resolved.

3.5.3.3 PSO Algorithm with PV system

For this study, a PSO ANN based MPPT controller has been developed to generate *D*. As the output of the proposed model, the predicted Voltage ($V_{ref.}$) of the PV array at the MPP is calculated using the atmospheric conditions G and T as inputs. Following a PV operating Simulink, an actual PV voltage ($V_{act.}$) is measured under identical environmental conditions. Then, the two voltages undergo comparison, thus the error is passed to tune the controller to determine the converter's *D*. The control signal is given by Equation (3.44):

$$D = K_P(V_{act.} - V_{ref.}) + \frac{K_I}{S}(V_{act.} - V_{ref.}) \tag{3.44}$$

A MATLAB-Simulink model is used to propose an intelligent ANN-MPPT approach based on a large set of actual PV system data. As stated previously, the training approach of the ANN network has a significant impact on the accuracy of PV voltage forecasts made using the ANN technique. First, the configuration of the ANN model is selected, and then its initial weight values are optimized using PSO. Additionally, the *MSE* is the objective function. Figure 3.27 depicts a flowchart of the development approach of the PSO–ANN algorithm.

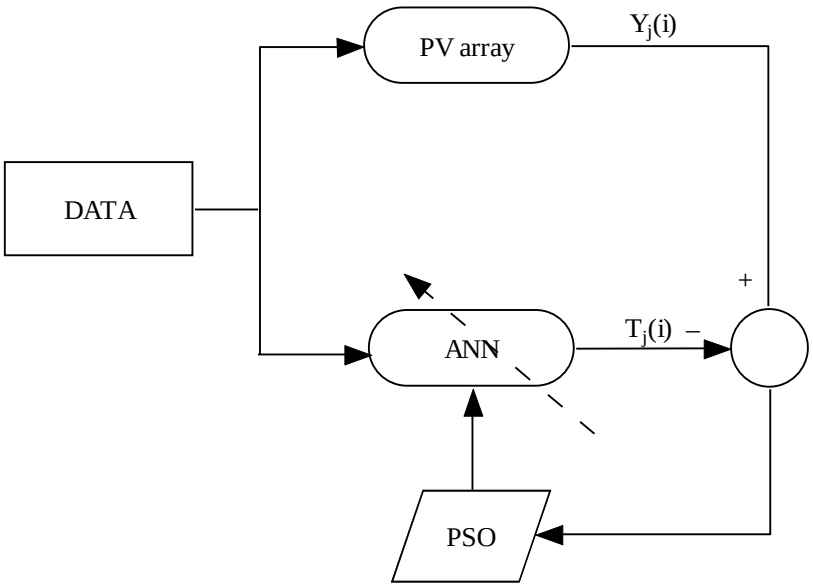

Figure 3.27: Illustration of the training approach.

Once the topology of the ANN network has been determined, the objective of a PSO-ANN algorithm is to determine the optimal initial weights for the ANN model. Once the incorrectly estimated weights have been corrected, they are calculated to enhance the output prediction of the model. To achieve this, the PSO algorithm and ANN technique are coupled. The text Algorithm describes the fundamental stages of the hybrid algorithm. After running this hybrid algorithm, the optimal weights are determined. Following the selection of optimal initial weights, the neural network model is trained. After the optimal starting weights have been determined, they are substituted with the standard training weights. Consequently, the ANN-PSO model based on the optimal training method utilising real-world data generates more accurate predictions than conventional ANN models. Thus, a lower MSE and epochs, approximately 0.01909 and 100, as shown in Figure 3.28.

Algorithm: The suggested algorithm focuses mostly on determining the base values for the ANN's weights.

Steps

1. Loading the data;
2. Input samples for testing and training,
3. Select neurons to represent the hidden layer on the initial modification,

4. Set ANN starting weights,
5. Set PSO algorithm main parameters,
6. Generate (for loop) to obtain ANN random weights using netff,
7. After training the ANN, construct (for loop) to obtain the optimised initial weights,
8. Using Eq. (3.42) determines each particle's MSE,
9. The MSE measured for each particle should be updated
10. For each particle, compare its P_{li} against its P_{bi} by the PSO method,
11. Evaluate each particle's G_{pi} using the PSO method and compare it to its P_{bi},
12. Modify the PSO algorithm's current velocity and position values
13. Display the outcome (the ANN's optimal initial weights) if the halting condition is met or the maximum number of iterations has been reached; otherwise, continue with step 7.

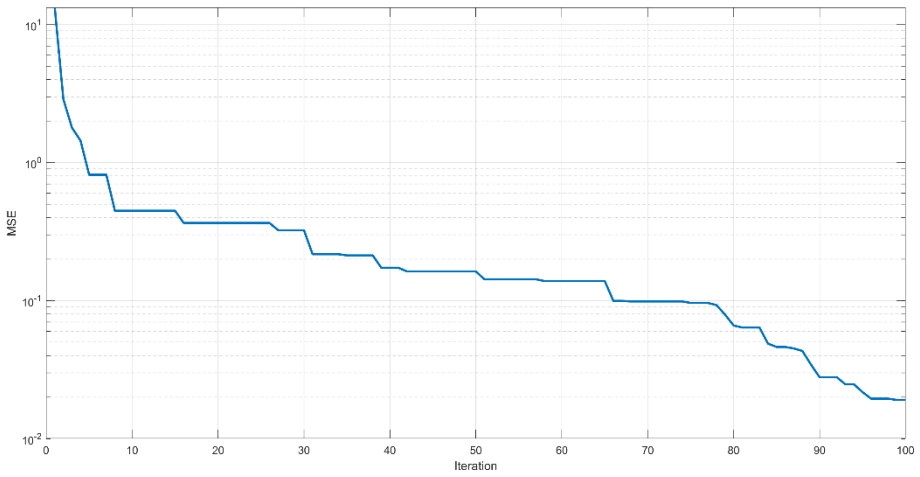

Figure 3.28: MSE vs Iteration using PSO-NN.

3.5.4 SMC with PSO

Nonlinear control systems, such as sliding mode control(SMC), are used to build efficient controllers for higher-order nonlinear dynamical plants that must function in an uncertain environment (Bartoszewicz & Zuk, 2010; Z. Meng et al. 2018).

The fundamental principle of SMC is shown in Figure 3.29 (a).

- First, create a state space sliding surface.
- Selection of a control principle that forces the system's state trajectory to approach a predetermined surface within a finite amount of time.
- Keeping it about this surface with the proper switching logic.

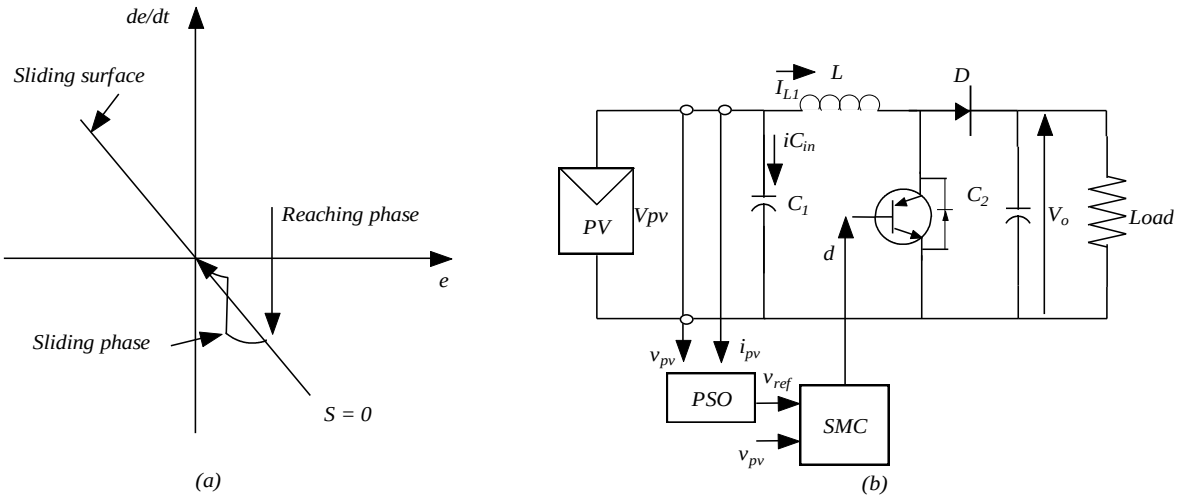

Figure 3.29: (a) Basic SMC principle. (b) Topology of PVs boost using PSO-SMC

The use of the PSO-SMC approach with a photovoltaic (PV) system is depicted in Figure 3.29 The dynamic model of the DC/DC boost converter is as follows:

$$\left.\begin{aligned} \dot{V}_{pv} &= \frac{1}{C_1} I_{pv} - \frac{1}{C_1} I_{L1} \\ \dot{I}_{L1} &= \frac{1}{L_1} V_{pv} - \frac{1}{L_1}(1-d)V_o \\ \dot{V}_o &= \frac{1}{C_2} I_{L1}(1-d) - \frac{1}{C_3 R} V_o \end{aligned}\right\} \qquad (3.45)$$

A nonlinear controller designed specifically for nonlinear systems is the sliding mode controller (SMC). The purpose of this controller, which is implemented by varying the Boost converter's duty cycle, is to follow a reference of the desired voltage as determined by this study. During the SMC design process, the PV voltage V_{pv} and the optimum voltage reference V_{ref}, denoted by the output reference y_{ref}, must be defined.

The following steps (Komurcugil et al. 2021)

$$s = (\lambda + \frac{d}{dt})^{r-1} e \tag{3.46}$$

where,
e: The tracking error, it is equal V_{pv} - V_{ref}.
r: The relative degree.
The output of derivative *y* is:

$$\dot{y} = \frac{1}{C_1} I_{pv} - \frac{1}{C_1} I_{L1} \tag{3.47}$$

Thus, by using Equ. (3.45) and Equ. (3.46), *y* the double derivative is as follows:

$$\ddot{y} = \frac{1}{C_1} I'_{pv} - \frac{1}{C_1 L_1} V_{pv} - \frac{1}{L_1}(1-d)V_o \tag{3.48}$$

The subsequent derivation of y reveals the principle of control, i.e, the converter's duty cycle. Therefore, r = 2 is the relative degree. As a result, we can write down the equation (3.46) and its equivalent for a sliding surface and its derivative is,

$$s = \lambda e + \dot{e}, \quad \dot{s} = \lambda \dot{e} + \ddot{e} \tag{3.49}$$

Where the tracking error derivative *e* and the double-derivative of *e* are as follows:

$$\dot{e} = \dot{y} - \dot{y}_{ref} = \dot{V}_{pv} - \dot{V}_{ref}, \quad \ddot{e} = \ddot{y} - \ddot{y}_{ref} = \ddot{V}_{pv} - \ddot{V}_{ref} \tag{3.50}$$

Replacing Equ. (3.48) In Equ. $\ddot{e}$ the expression is:

$$\ddot{e} = \frac{1}{C_1} I'_{pv} - \frac{1}{C_1 L_1}\left[V_{pv} - \frac{1}{L_1}(1-d)V_o \right] - \ddot{V}_{ref} \tag{3.51}$$

Therefore, considering $\dot{Vref}$ and $\ddot{Vref}$ equal to zero and the derivative of the sliding surface is:

$$\dot{s} = \lambda \dot{V}_{pv} + \frac{1}{C_1} I'_{pv} - \frac{1}{C_1 L_1}\left[V_{pv} - \frac{1}{L_1}(1-d)V_o \right] \tag{3.52}$$

To ensure stability, $\dot{s} = -ksign(s)$ and So, Equation (3.52) can be:

$$\dot{s} = -ksign(s) = \lambda \dot{V}_{pv} + \frac{1}{C_1} I'_{pv} - \frac{1}{C_1 L_1}\left[V_{pv} - \frac{1}{L_1}(1-d)V_o \right] \tag{3.53}$$

Duty cycle of converter is,

$$d = \frac{C_1 L_1}{V_o}\left[\lambda \dot{V}_{pv} + \frac{1}{C_1} I'_{pv} - \frac{1}{C_1 L_1}\left[V_{pv} - V_o \right] + ksign(s) \right] \tag{3.54}$$

So, equation (3.54) The constant gains and settings of the DC/DC boost converter, along with the PSO-SMC dynamic model, ensure that the suggested technique is carefully implemented. The subsequent flowchart provides a brief description of the procedure:

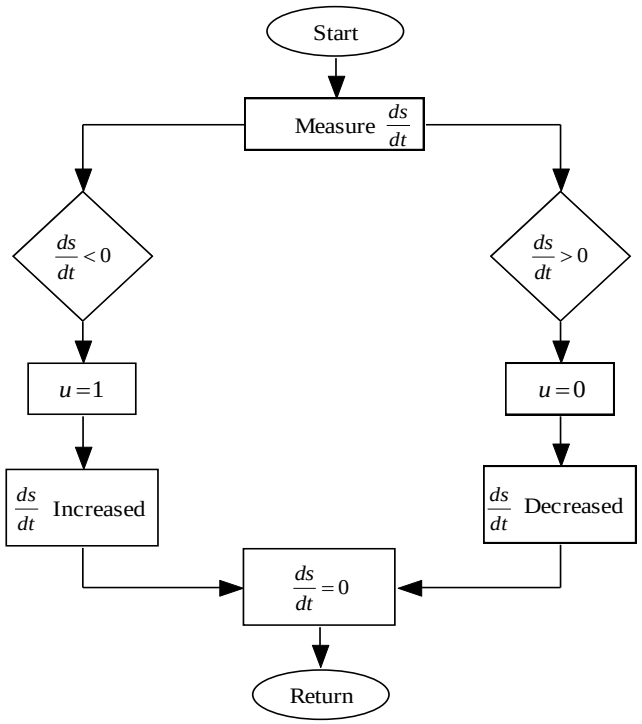

Figure 3.30: Flowchart of PSO-SMC for PV MPPT.

3.6 VSI CONTROLLER DESIGN

The VSI converts DC/AC power (Ramezani et al. 2017) shown in Figure 3.31. PWM techniques are used to control the output of the VSI. The SPWM compares

balanced sinusoidal control 3-ϕ voltages to the triangular wave. The switching frequency of the triangular waveform, also known as carrier frequency, is typically significantly greater than the frequency of the regulating voltages. The same frequency sinusoidal control signals modify the duty ratios of pulses of switching for switches. Inductance with resistance devices is used to represent an AC load.

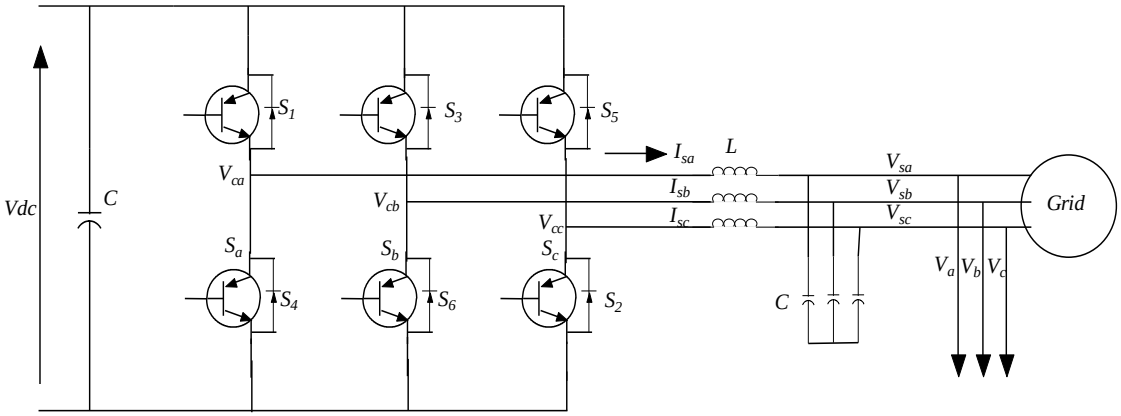

Figure 3.31: Schematic diagram of the control system. (Ramezani et al. 2017)

The simplified circuit is subjected to a power flow study, with the impedance substituting for the transformer and filter combined inductance. The active as well as reactive power exchanges from the VSC are governed by the phase and amplitude of the converter's voltage output about the utility parameters (Mohamed et al. 2020). The active power flow is controlled by modulating the phase difference, whereas the reactive power injection is controlled by modifying the output magnitude of the inverter. To a fixed grid voltage, both the phase shift and amplitude can be adjusted. The amplitude can be modified by adjusting the modulation index, while the phase variation can be fine-tuned by adjusting the synchronization and phase angle of the modulating sine wave. Real and reactive power supplied to the utility is described by the following relations.

$$P = \frac{EV_s}{Z}\cos(\theta_z - \delta) - \frac{E^2}{Z}\cos(\theta_z) \qquad (3.55)$$

$$Q = \frac{EV_s}{Z}\sin(\theta_z - \delta) - \frac{E^2}{Z}\cos(\theta_z) \tag{3.56}$$

where,

$Z = \sqrt{R^2 + X^2}$

$Q_z = \tan^{-1}\frac{1}{XR}$

The active and reactive power control scheme (PQ control) is used when the inverter is operating to meet a given real and reactive power set point, and the active power and voltage control scheme (PV control) is used when the inverter is operating to supply the load with a fixed voltage and frequency values.

3.6.1 Active Power and Reactive Power Control

The PQ, or active and reactive, control mechanism is frequently employed by grid-connected systems. The grid supplies the requisite standards for voltage and frequency. An LC filter is connected to the inverter's output terminals to reduce harmonics. Figure 3.31 depicts the schematic of an inverter. Real and reactive powers are completely dependent on the amplitude and phase of the voltage source at the transmission end in this system. The ac output voltage of the inverter and the voltage reduction across the filter act as the main influences of the dc bus voltage. The dc bus voltage is constrained by the relationship (3.57) at the unity power factor (Mohan, 2003).

$$\frac{\sqrt{3}}{2\sqrt{2}} m_a V_{dc} \geq \sqrt{V_{LL}^2 + 3(\omega L_f I_{ac})^2} \tag{3.57}$$

where,

V_{LL} = Line- line RMS voltage on the inverter side, L_f = Filter inductance, I_{ac} = Maximum possible RMS value of the ac load current, m_a = Modulation index of the inverter.

The 3-ϕ voltages can be written as

$$V_{ca} = \frac{V_{dc}}{3}(2S_a - S_b - S_c) \tag{3.58}$$

$$V_{cb} = \frac{V_{dc}}{3}(-S_a + 2S_b - S_c) \tag{3.59}$$

$$V_{cc} = \frac{V_{dc}}{3}(-S_a - S_b + 2S_c) \tag{3.60}$$

The 3-ϕ current can be given as

$$\frac{di_{ca}}{dt} = i_{ca} = -(R_c / L_c)i_{ca} + (V_{sa} - V_{ca}) / L_c \tag{3.61}$$

$$\frac{di_{cb}}{dt} = i_{cb} = -(R_c / L_c)i_{cb} + (V_{sb} - V_{cb}) / L_c \tag{3.62}$$

$$\frac{di_{cc}}{dt} = i_{cc} = -(R_c / L_c)i_{cc} + (V_{sc} - V_{cc}) / L_c \tag{3.63}$$

The total instantaneous power in the 3-ϕ system can be written as

$$p(t) = v_a i_a + v_b i_b + v_c i_c \tag{3.64}$$

The active power can be represented in the synchronous frame as

$$P = \frac{3}{2}(V_{gd} i_d + V_{gq} i_q) \tag{3.65}$$

$$Q = \frac{3}{2}(V_{gq} i_d - V_{gd} i_q) \tag{3.66}$$

When the reference frame is synchronized with voltage, the active and reactive power can be written as

$$P = \frac{3}{2}(V_{gd} i_d) \tag{3.67}$$

$$Q = \frac{3}{2}(-V_{gd} i_q) \tag{3.68}$$

The d and q-axis components in synchronous frame with decoupling terms are given as

$$u_d = R_c i_d + L_c \frac{di_d}{dt} + V_{gd} - \omega L_c i_q \tag{3.69}$$

$$u_q = R_c i_q + L_c \frac{di_q}{dt} + V_{gq} - \omega L_c i_d \tag{3.70}$$

The PQ control relies on the inverter to regulate the actual and reactive power that is transferred to and from the grid to maintain the reference power. On an isolated grid, PQ control cannot function without a voltage reference.

3.6.1.1 VSC Voltage and Current Controller

The d-q rotating frame current feed-forward control method is used to regulate the VSC as shown in Figure 3.32. (Pogaku et al. 2007) The Park transformation has been employed to transform the 3-ϕ voltage and current values into the DC values in the *d-q* frame. The *d-q* axis current components (I_{od}. I_{oq}) were individually controlled with their respective reference commands (I_{dref}, I_{qref}) with ωL_{ff} as a feed-forward factor in the controller loops, where L_{ff} is the VSC-side filter inductance. For determining the phase angle, the PLL block employs the static reference frame of the voltage signals. Then I_{dref} and I_{qref}=0 as the reference current is derived by feeding both the measured dc-link (V_{dc}) voltage and the reference voltage ($V_{dc\text{-}ref}$) into the voltage loop. This reference current and the measured current are given to the current control loop to get the reference voltage, V_{dref} and V_{qref} which is given to the pulse generator to get the pulses for inverter switches. The voltage control PI regulator is given by,

$$\left.\begin{aligned} I_{dref} &= (k_{pvpv} + \frac{k_{iviv}}{s})(V_{dc-ref} - v_{dc}) \\ I_{qref} &= 0 \end{aligned}\right\} \tag{3.71}$$

The processed currents which are obtained from the voltage regulator are fed to the Current Regulator(Ramezani et al. 2017).

$$\left.\begin{aligned} V_{dref} &= (k_{pib} + \frac{k_{iib}}{s})(I_{dref} - I_{od}) \\ &+V_d - \omega L_{ff} I_{qref} \\ V_{qref} &= (k_{pib} + \frac{k_{iib}}{s})(I_{qref} - I_{oq}) \\ &+V_q + \omega L_{ff} I_{dref} \end{aligned}\right\} \tag{3.72}$$

Where, k_{pvpv} and k_{ivpv} are the gains of the PV voltage loop PI controller, and the current controller PI gains are k_{pipv} and k_{iipv}.

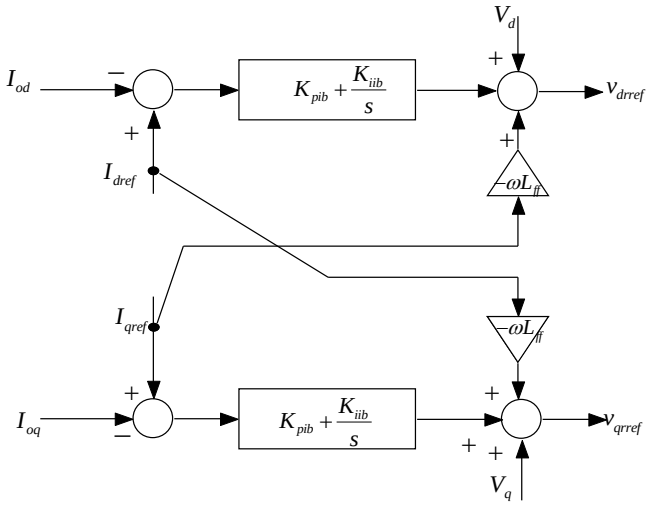

Figure 3.32: VSC current controller.

Non-dispatchable resources, such as solar photovoltaics, are often given grid-following control methods. To the AC grid generated by a grid-following source, these inverters work as current-controlled sources, exporting active and reactive power in predetermined proportions (Rocabert et al. 2012). The adjustment of the DC-link voltage under fluctuating power output by the PV array is a crucial function for the dependable functioning of the PV-VSC (Yazdani & Dash, 2009). The DC link voltage (VDC) from the d-q axis current references (I_{dref}, I_{qref}). The DC-link voltage reference (V_{dc_ref}) is set to 800V and is regulated by balancing the power flow-in and flow-out of the DC-link. The PWM generation will receive the V_{dref} and V_{qref} after they have been transformed into a-b-c format. The abc-dq and dq-abc conversions, as well as grid synchronisation, all rely on the angle reference provided by the PLL.

Parameters for both voltage and current loops are derived using the equations given by (Pogaku et al. 2007). High-frequency noise may be reduced using an LC filter. (K. H. Ahmed et al. 2007; Dursun & Dosoglu, 2018) provide expressions for the cutoff frequencies of LC circuits.

$$f = \frac{1}{2\pi\sqrt{LC}} \tag{3.73}$$

For inductor and capacitance calculations, the ripple current and voltage may be set between 10% and 15% of the rated current and power.

$$\Delta i_{L\max} = \Delta i_L \times V_{dc} \times L \times f_s \tag{3.74}$$

$$C = \frac{\%Q \times \mathrm{P}_{rated}}{2\pi \times f \times V_{rated}^2} \tag{3.75}$$

3.7 RESULTS AND DISCUSSION

The results for the test microgrid with the proposed grid following mode (P-Q) and MPPT control's simulation are carried out in this section using MATLAB/Simulink software package. The method presented in this section is to operate in MPP point using four MPPT control's those are P&O, PSO-ANFIS, PSO-ANN, and PSO-SMC MPPT controller. In this chapter, the grid-connected mode with the coordinated P-Q control method is considered. The PV system coupled with the PCC scenario is discussed in detail.

Table 3.3: Photovoltaic System Data

Symbol	Description	Nominal Value
K_{ppv}	Power regulator Proportional gain	0.05
K_{ipv}	Power regulator Integral gain	2
K_{pvpv}	Current regulator Proportional gain	6
K_{ivpv}	Current regulator Integral gain	30
K_{pipv}	Voltage regulator Proportional gain	0.2
K_{iipv}	Voltage regulator Integral gain	15
F_{sw}	PWM switching freq. Hz	2700
K_{psvn}	Sync. Proportional gain (Kpsyn)	0.075
Kisvn	Sync. Integral gain	0.03

3.7.1 Grid Connected Mode

The study on grid-connected (P-Q) controllers with integrated MPPT control is summarized here. Table 3.3 shows the controller gain parameters. The proposed methods for the PV array are working in MPPT mode, tracking the voltage reference (V_{MPPT}) estimated by the MPPT algorithm. The loads are connected to the bus. Depending on the quantity of power generated by the PV system, the grid's capacity

and demand, the power grid (P_{grid}) absorbs or releases power to maintain a balance. Figure 3.33 Figure 3.34 illustrates PV-grid power sharing and voltages of the system under PQ control with MPPT with coordinated control.

Power is balanced by either absorbing or releasing power, depending on the quantity of generation by the PV system and the demand, the grid (P_{grid}) balances. Power injecting and voltages in the PV-grid system under grid following mode management with integrated MPPT and PQ control are shown in Figure 3.33 and Figure 3.34.

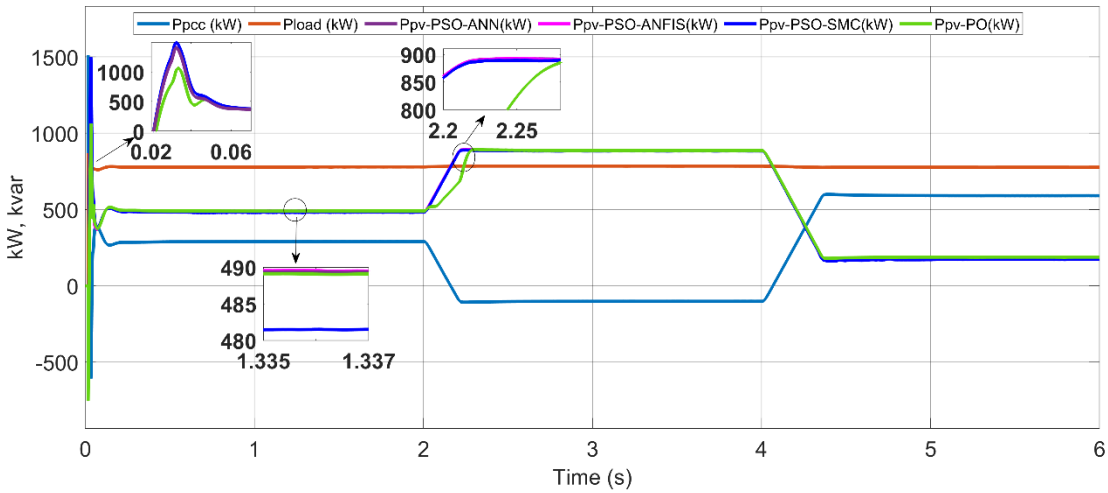

Figure 3.33: Power sharing of the system with MPPTs comparison.

As, 2s before, the PV power P_{PV} is about 500kW, and the utility grid power P_{grid} is 280 kW which is shared to meet the load demand P_{grid} = 780 kW. The power delivery to the grid in this period is around 280 kW since to meet additional power is demanded by the load, where PV power available was only 500 kW. At around 2 s, as the utility demand decreases instead the power flows towards the grid i.e., around (-100 kW), meaning that the PV the power available was more than the load demand the 100kW extra power is sent to the grid. At 4 s, the grid demand increases again, as to meet demand, the PV power at this moment is only around 100 kW due to its weather condition. Hence the load generation balance is taken care of by a grid-coordinated controller. The grid can balance the energy as a buffer. The waveforms which are shown below are the same in all methods, to analyze easily one of the methods waveforms are shown.

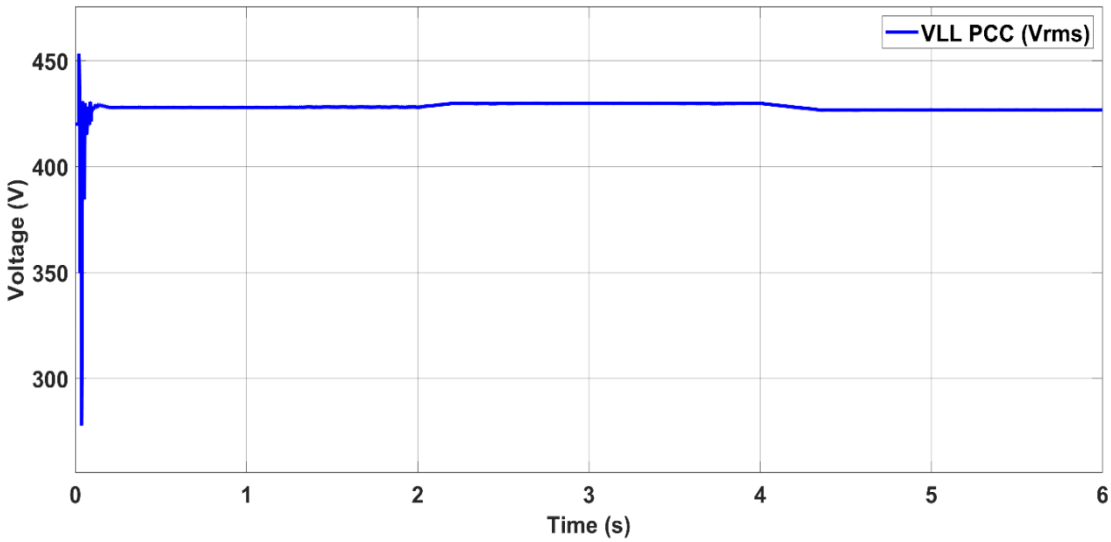

Figure 3.34: RMS PCC Voltage.

During these variations, the PCC voltages are controlled across the load terminal voltage V_{rms} as shown in Figure 3.34, as the voltage stays almost constant at around 420 V irrespective of load variation. In Figure 3.35 the time-varying voltages between PCC and bus are shown.

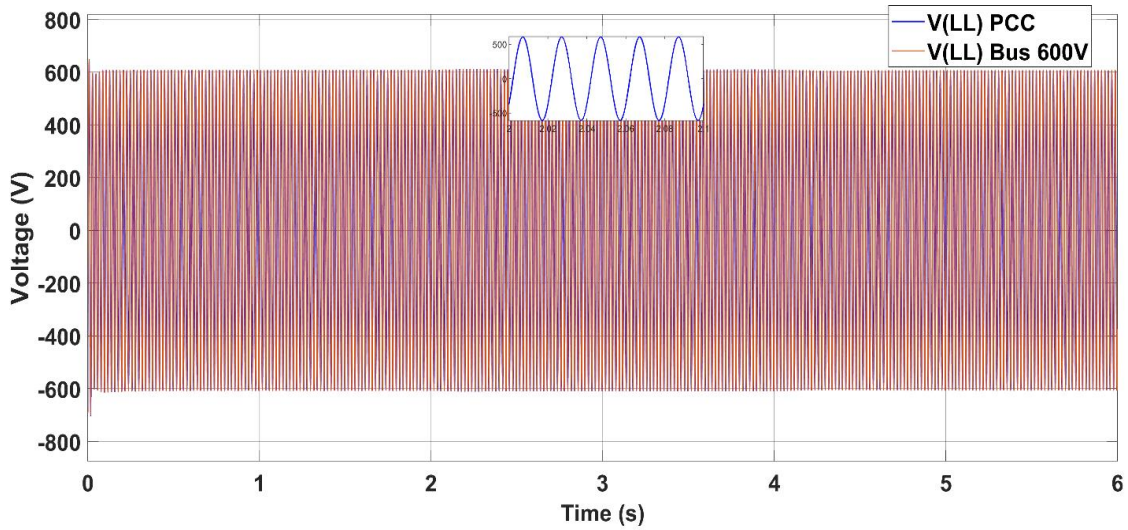

Figure 3.35: Instantaneous PCC Voltage.

In Figure 3.36 and Figure 3.37 frequency between PCC and bus along with phase angle as shown, are stably maintained, which is operating in current control mode by the utility.

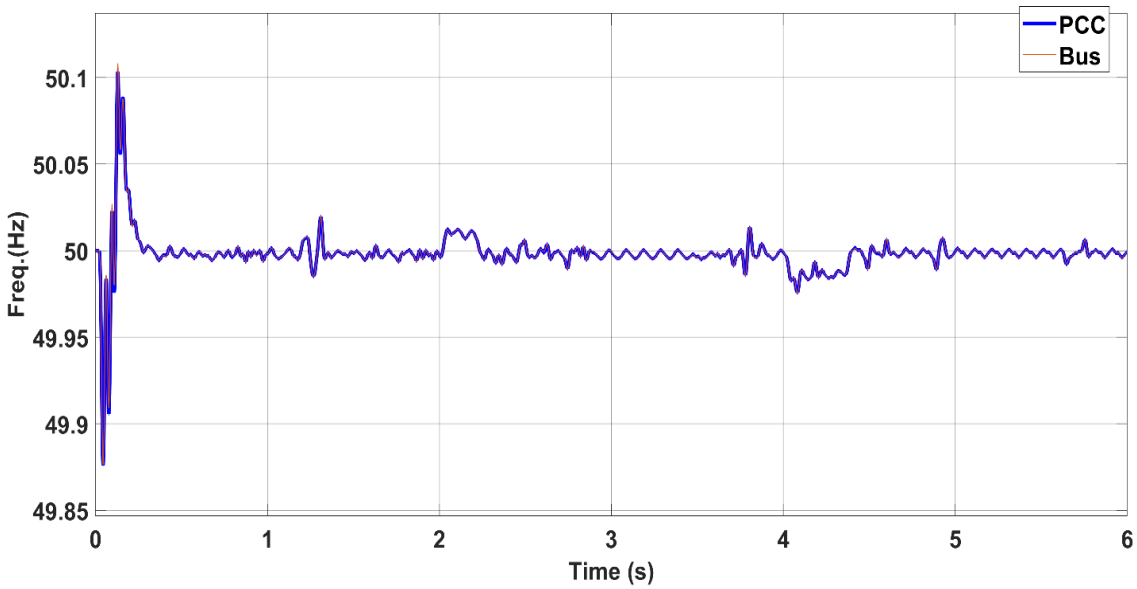

Figure 3.36: Frequency of PCC and Bus.

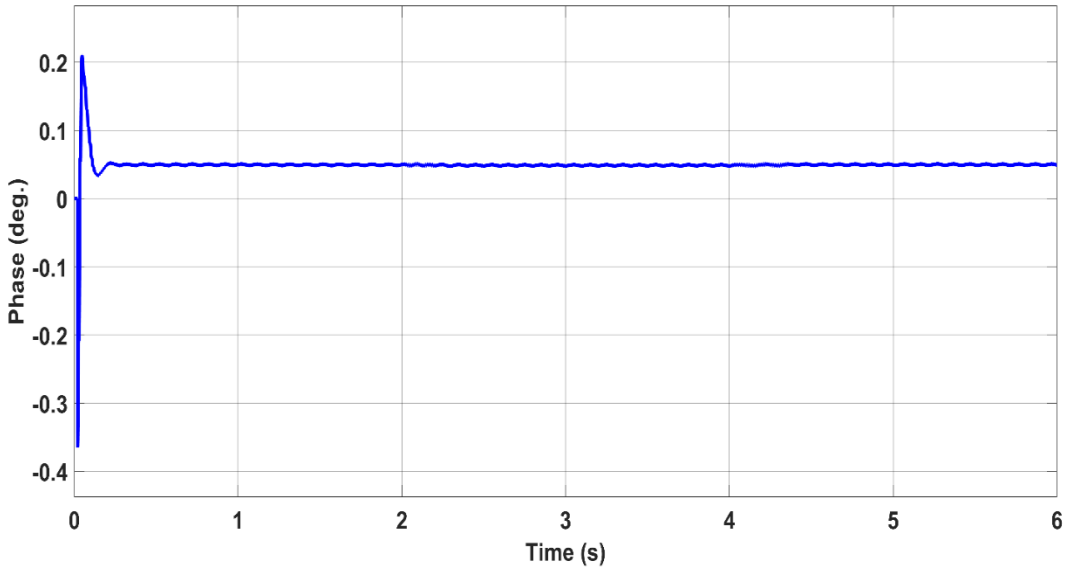

Figure 3.37: Phase angle between voltages.

As the load demand, which is constant around 800 kW, the instantaneous load current is also constant as shown in Figure 3.38. The power production of the PV system is concerned with irradiance; hence its load current is drawn by the load as shown in Figure 3.39, the deficit power is drawn from the grid to meet the load generation balance.

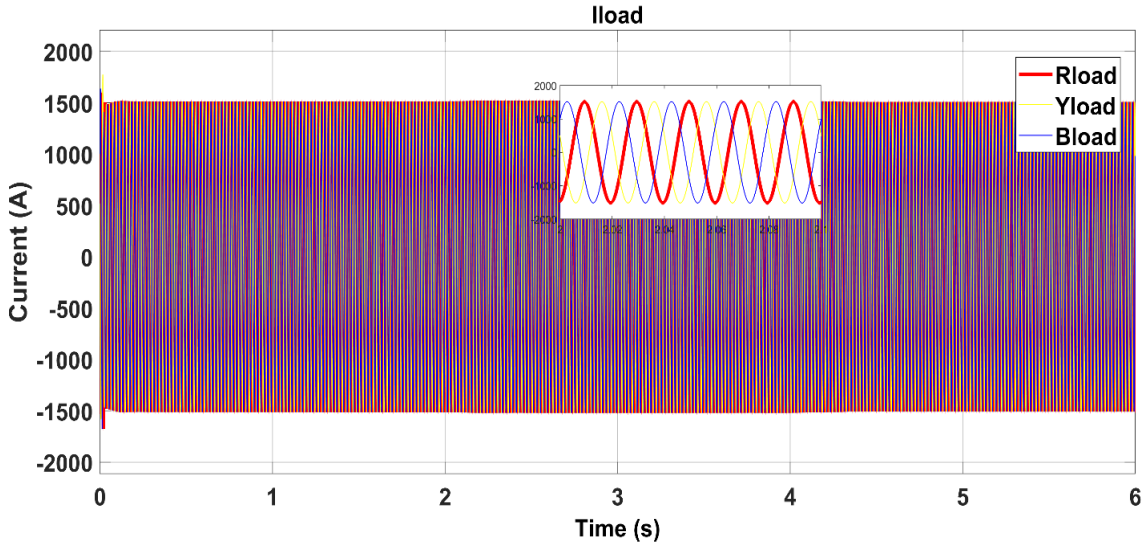

Figure 3.38: PV system load current.

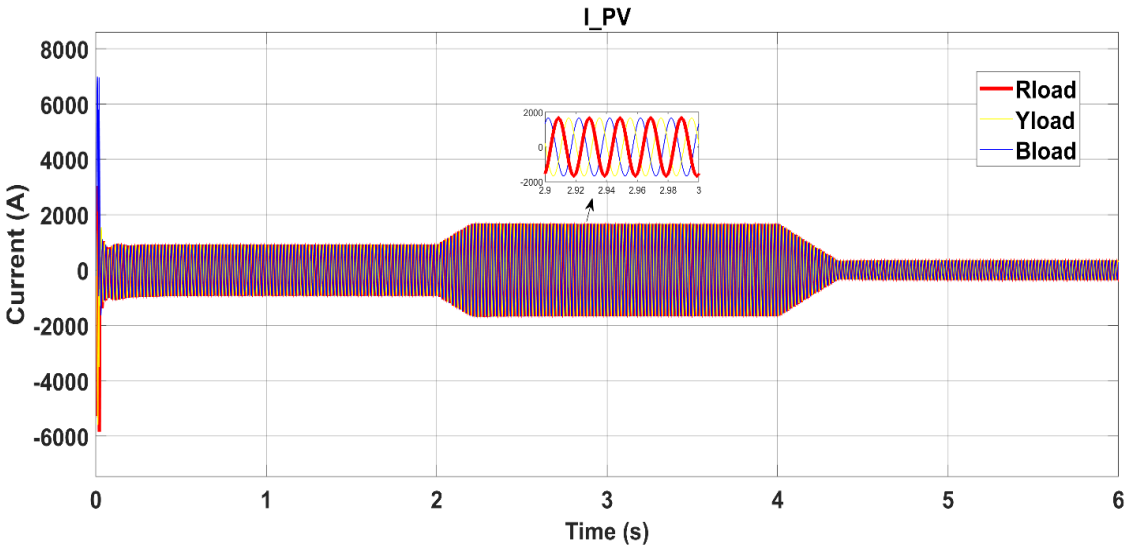

Figure 3.39: PV system output current.

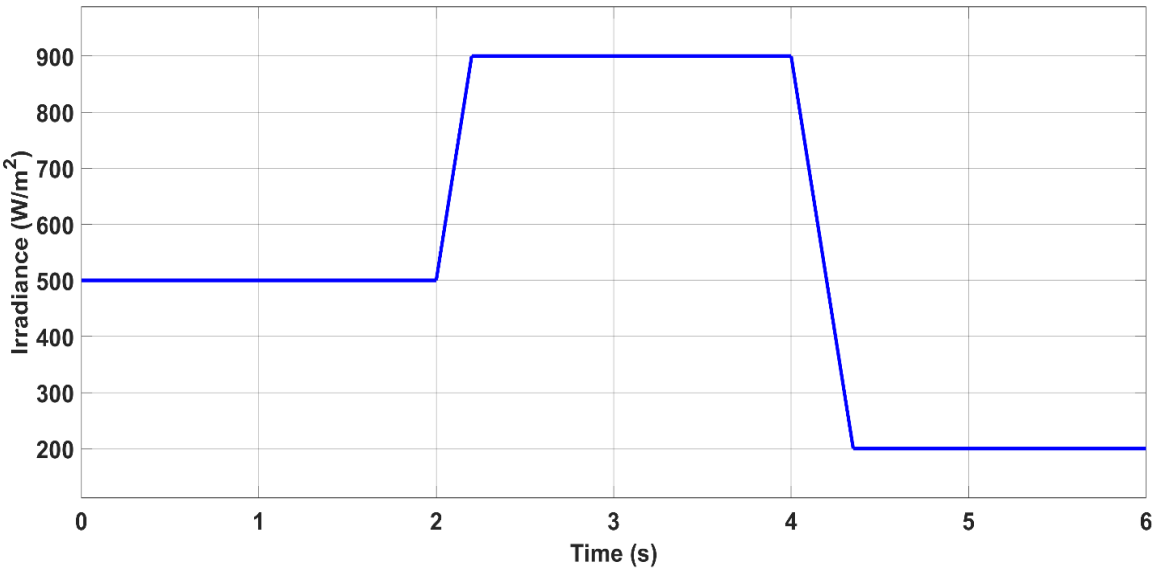

Figure 3.40: Solar irradiation.

The solar PV system with proposed MPPT controllers tracks MPP as it is shown in Figure 3.33 following irradiance as depicted in Figure 3.40, the PV system produces maximum power accordingly during the simulation's time frame. From 0s to 2s around 500 kW, from 2s to 4s around 900 kW and 4s to 6s around 200 kW.

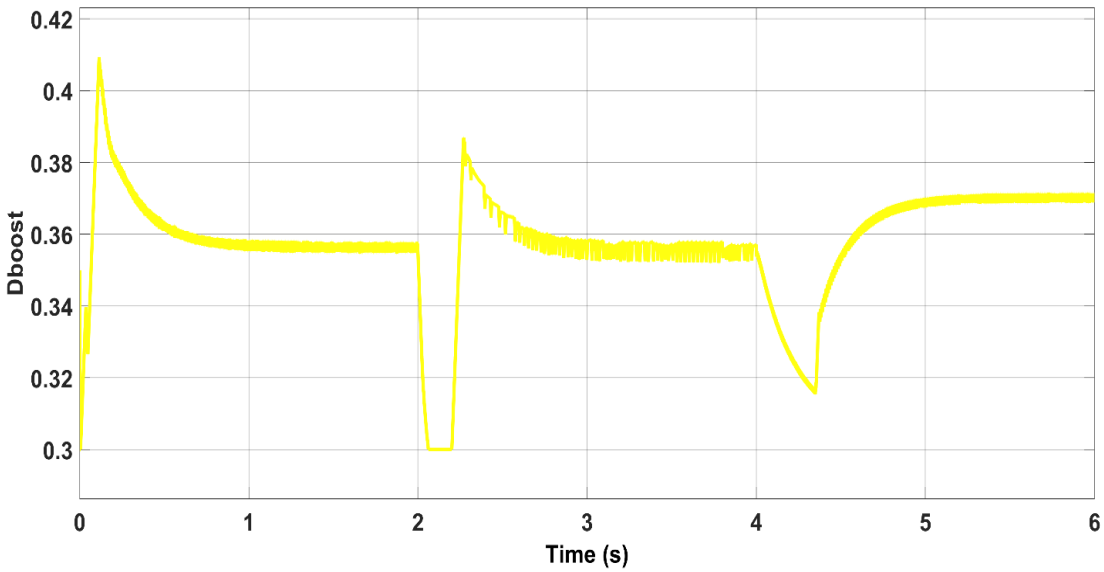

Figure 3.41: PV converter duty ratio.

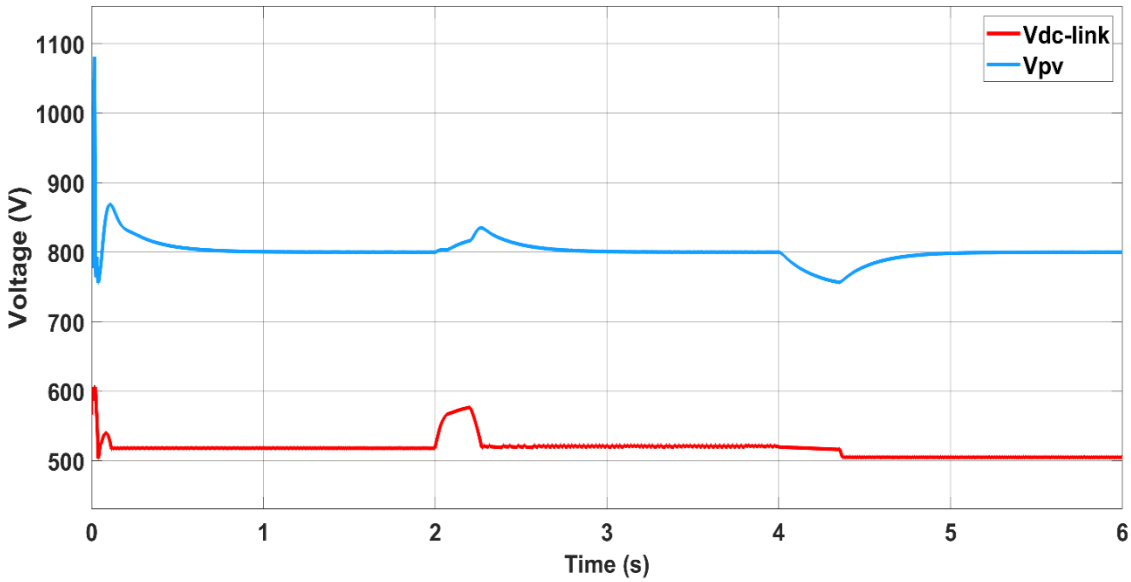

Figure 3.42: Output voltage of PV and DC link.

Irrespective of variations in irradiance the duty ratio is maintained constant as shown in Figure 3.40. As depicted in this figure, during any change of irradiation, the proposed MPPT methods successively iterate until reach the optimum voltage that matches the global maximal power points. AT 2 s and 4 s the variations are due to the irradiation change. Following that the output voltage of the PV and DC link along with the PV output current as shown in Figure 3.42 and Figure 3.43.

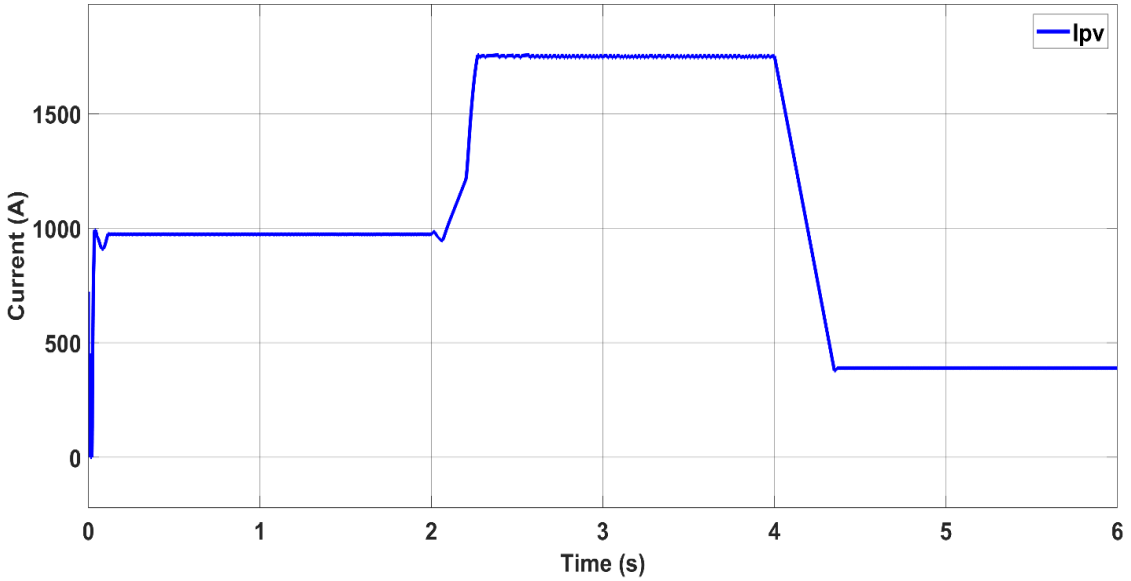

Figure 3.43: PV output current.

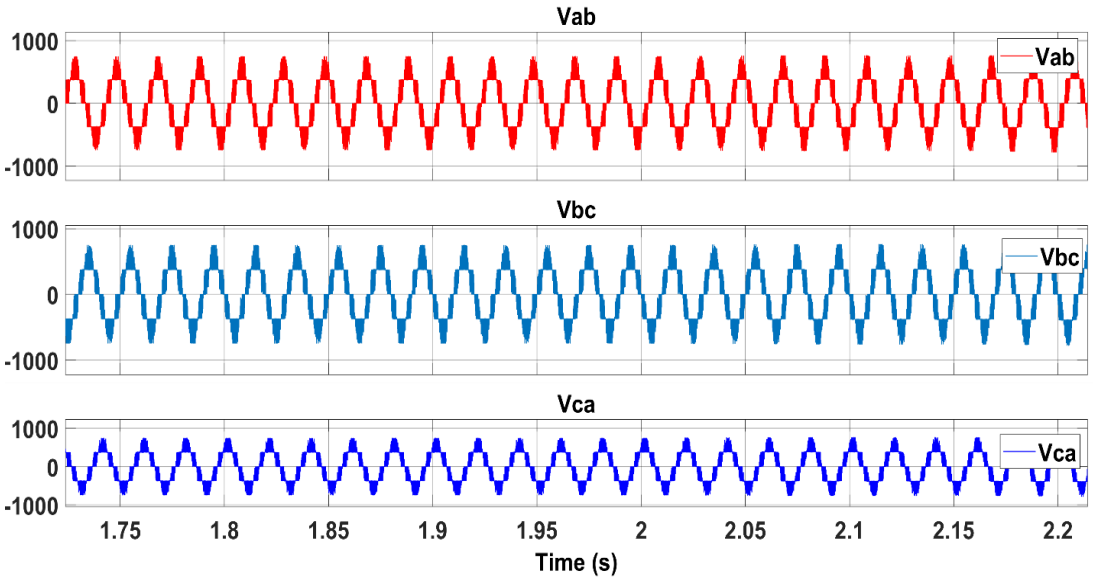

Figure 3.44: PV inverter output voltages.

Figure 3.44 shows PV inverter output voltages and Figure 3.45 is the modulation index of PV inverter which is about around 0.8. and the THD of load current and PV system current are shown in Figure 3.46 and Figure 3.47 which meets as in IEEE 519 std.

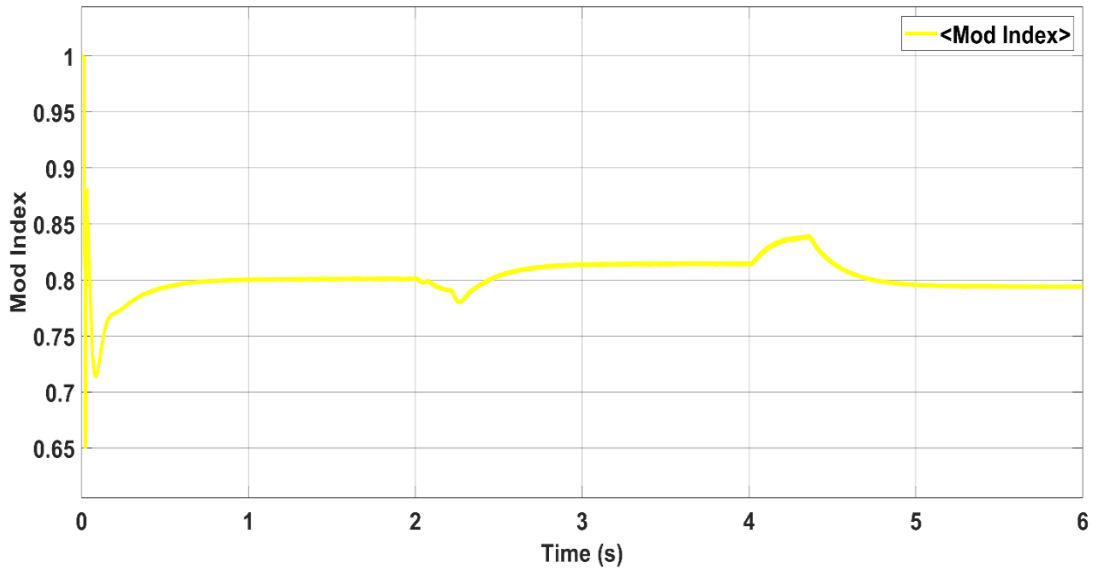

Figure 3.45: Modulation index of PV inverter

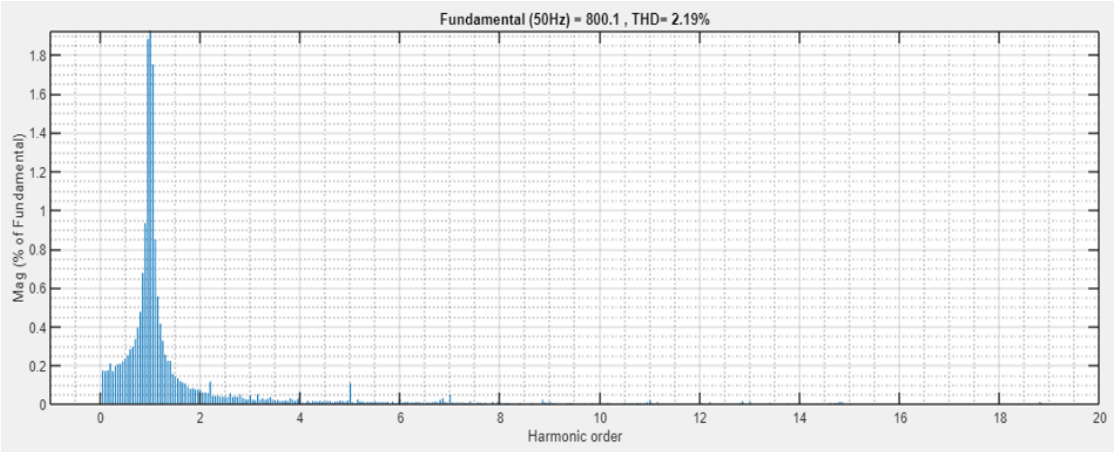

Figure 3.46: THD of ac load current.

Table 3.4: Hybrid MPPT algorithms

Hybrid methods (first/ second)	Description	Advantages	Disadvantages
P&O	Identify the VMPP from P&O algorithm to reach the MPP accurately	Easy implementation, accurate, convenient convergence speed	Slow tracking of rapid changes in irradiance.
ANN-PSO	PSO is used for prediction and reduces the root mean square error, main optimization and GMPP	High efficiency and appropriate performance.	Requires prior knowledge training of ANN, Complex implementation
ANFIS-PSO	PSO is tuned to the ANFIS membership function to get crisp output using the weighted average method	High PV tracking efficiency and convergence speed is fast,	Complex implementation, prior training of ANFIS is required.
PSO-SMC	PSO is tuned to get global optimum value for the SMC function	Tracking speed is fast and moderately efficient	Moderately difficult in Implementation.

The power-sharing among all the sources to meet the demand as shown in Figure 3.31. The compared simulation results of different proposed MPPT methods

such as PSO-ANFIS, ANN-PSO and PSO-SMC are compared with perturb and absorb methods.

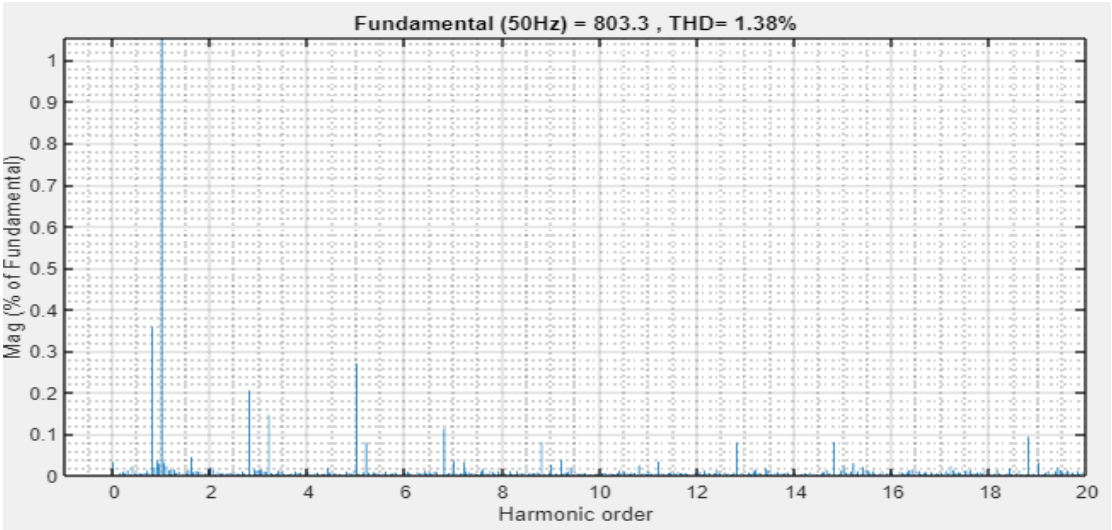

Figure 3.47: THD of PV system ac load current.

From the results, it can be interpreted that the first transient peak is more in the case of PSO-SMC than followed by PSO-ANFIS, ANN-PSO and the least is in the P&O method. The steady-state value operating at the MPP, the efficiency is highest in PSO-ANFIS followed by ANN-PSO and P&O methods whereas PSO-SMC is lesser than those three methods with different irradiation. During the rise in irradiation, the steady-state time of P&O takes 10% more compared with other methods. Overall, the proposed methods are operating in MPP mode. The other merits and demerits are listed in Table 3.4.

3.8 SUMMARY

The implementation of a 3-ϕ grid-interactive PV-based microgrid with coordinated control of MPPT and VSI control approach has been made with a P-Q controller in grid-connected mode. In this work, the photovoltaic system is run with four different algorithms to obtain maximum power point (MPP). A PSO-based ANFIS, ANN and sliding mode technique is compared with the P&O method for the extraction of maximum power from the PV system in grid-connected mode. The PSO-ANFIS algorithm is quick, accurate and better than the other three algorithms in exact PV tracking under variable irradiance. The work carried out demonstrates the proposed

MPPT algorithm along with coordinated (P-Q) techniques for the grid using a photovoltaic system. The utility balances the load based on the PV array generation, as the PV system depends on the weather conditions. Overall, the response of a 3-ϕ grid interactive PV-based microgrid has been found efficient as shown in results under different PV irradiation and loads.

Chapter 4

PV-BESS MICROGRID OF BOTH GRID AND ISLANDED MODES

4.1 INTRODUCTION

Photovoltaic (PV) systems typically employ battery storage to balance out the power changeability caused by the unique character of PV i.e., variations in irradiance. Methods for managing PV-battery systems must be capable of regulating power transfers flexibly while keeping stable bus voltages. In this research, we present a completely Integrated power and control management system for grid-connected and island PV-battery hybrid microgrids utilising ac buses. Despite complications from switching operating modes, variations in sunlight, and changes in loads, the proposed method is effective at governing the PCC voltages as well as frequency, regulating the individual unit, and managing the transfer of power in the network with ease under varying operating conditions. Simulations are used to examine the effectiveness of the proposed strategy.

4.2 PV-BESS CONTROL SYSTEM

PV at times produces insufficient energy and may not meet the voltage and frequency requirements set by the grid operator. Therefore, the ability to operate the battery energy storage device as a grid-supporting (Brenna et al. 2018; X. Li & Wang, 2021b) can be essential for maintaining stable and dependable operation in such isolated regions. The PV-BESS are allotted to form the power utility in a multi-master arrangement under this approach. By employing a droop strategy, the functioning of the BES system and Photovoltaic system as grid-forming resources coupled in parallel can be realised. Though, this would enforce the benefit of extracting the openly available maximum power of the PV array with the MPPT controller, as explained in

section (3.5), along with the PV-VSC controller. Figure 4.1 shows the block diagram BESS controller, which generates a reference voltage to the PWM block. The controller consists of a battery model, voltage source inverter with droop control, power and voltage regulator and current controller, and filter. To ensure the system frequency and voltage while ensuring the generation load balance. The control methodology is explained below.

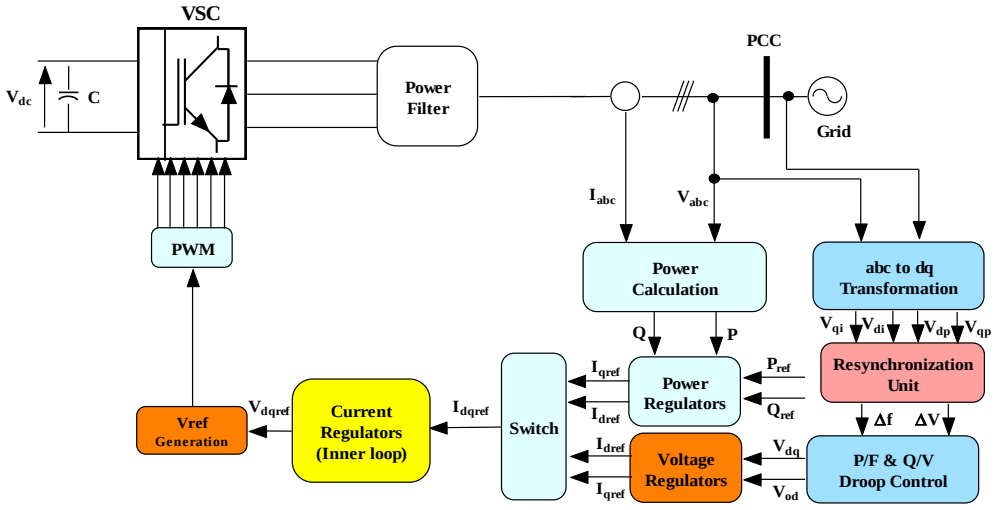

Figure 4.1: The storage system inverter controller.

4.2.1 Battery Energy Storage System

The BESS consists of a storage element, which is taken from the MATLAB SimPowerSystem library. As given in the thesis about the battery model the deep cycle battery is necessary due to the uncertain weather. The parameters are appropriately used as needed for the controller. The equation of discharge and charge Lithium-ion Iron Phosphate (LFP) battery model is given,(Tremblay & Dessaint, 2009)

$$V_{BAT} = V_0 - R.i - K\frac{Q}{(Q-\text{it})}(\text{it}+\text{t}^*) + A.\exp(-B.it) \tag{4.1}$$

$$V_{BAT} = V_0 - R.i - K\frac{Q}{(\text{it}-0.1Q)}i^* - K\frac{Q}{(Q-\text{it})}.\text{it} + A\exp(-B.it) \tag{4.2}$$

Where V_{BAT} is the battery voltage (V), V_o is the battery constant voltage (V), K is polarization constant (V/Ah) Q is battery capacity (Ah), i_t is the actual battery charge

(Ah), R is the internal resistance (Ω), i is battery current (A), i^* is filtered current (A), A is exponential zone amplitude (V), B is exponential zone time constant inverse (Ah),

The solar power output varies and also load variability is the reason to use a storage system for the microgrid application. The battery system has 1 MWh of backup energy to balance PV power for the critical load and frequency control.

4.2.2 Voltage and Frequency Control

A stable output voltage and frequency are essential for off-grid applications (Rocabert et al. 2012). Modulating the inverter's control signal's amplitude and frequency can change the system's operating frequency. The inverter maintains a constant frequency and voltage supply to the load. The park transformation is used to determine the direct reference voltage (V_{dref}) and the quadrature reference voltage (V_{qref}). The necessary frequency of the reference signal can be generated internally as a voltage signal. (Ramezani et al. 2017) gives an expression for the voltage at the inverter terminal.

$$\begin{bmatrix} V_a \\ V_b \\ V_c \end{bmatrix} = \begin{bmatrix} V_{a1} \\ V_{b1} \\ V_{c1} \end{bmatrix} + R_c \begin{bmatrix} I_a \\ I_b \\ I_c \end{bmatrix} + L_c \frac{d}{dt} \begin{bmatrix} I_a \\ I_b \\ I_c \end{bmatrix} \tag{4.3}$$

Where R_c is resistance, L_c is the inductance of the filter and I_a, I_b and I_c are load currents. The d-q-axis load voltage can *be* written as

$$V_{dref} = R_c i_d + L_c \frac{di_d}{dt} + V_d - \omega L_c i_q \tag{4.4}$$

$$V_{qref} = R_c i_q + L_c \frac{di_q}{dt} + V_q - \omega L_c i_d \tag{4.5}$$

The PWM pulses are controlled by the reference voltages V_{dref} and V_{qref}. The parameters of the voltage and current loops are determined by (Pogaku et al. 2007).

4.2.3 Grid-Island-Grid Transition Mode

The microgrid out-of-phase recloses with the supply system, leading to incredibly high inrush currents. Instead, the microgrid voltage is in phase with the

distribution voltage, the resynchronization system will prevent a blackout. Doing this will ensure a soft reconnection to the supply system. Three seconds will pass during the synchronization process. The voltage and frequency will gradually catch up to that of the central grid using PI regulators. The voltage and frequency deviations computed using PLL are computed using the resynchronization block (Golestan et al. 2018; Tran et al. 2014). The primary droop will be modified to include these deviations to account for the altered voltage or frequency (Pogaku et al. 2007). The instantaneous complex powers of the inverter in *dq* reference frame and the power on the DC side P_{dc} of the inverter are represented as.

$$P_{dc} = V_{dc} I_{dc} \tag{4.6}$$

$$\left.\begin{aligned} P &= \frac{3}{2}(V_{od} I_{od} + V_{oq} I_{oq}) \\ Q &= \frac{3}{2}(V_{od} I_{od} - V_{oq} I_{oq}) \end{aligned}\right\} \tag{4.7}$$

Whether the system is operating in grid-connected, or island mode is decided by the control method of the inverter. As depicted in Figure 4.2, a phase-locked loop (PLL) (Golestan et al. 2018) is used to derive the phase-A bus angle θ while operating in grid-connected mode. A ramp signal locally generated from 0 to 2π of frequency is caused θ in islanded mode. By applying Park transformation to the time-dependent 3-phase PCC voltages and inverter output currents, the d-q frame quantities V_{od} and V_{oq}, and I_{od} and I_{oq} are obtained, respectively. Based on the operating mode, the controller determines which decides of quantities to regulate. By setting the "Islanded" signal to 1, the converter enters islanded mode and begins controlling the V_{od} and V_{oq} voltages on the AC bus. The frequency (*f*) of the AC bus voltages in a system has been fixed at 50 Hz. The AC bus voltage must be synced with the grid before the breaker may be closed and the PV-battery system reconnected. In autonomous mode, the controller has full control of the PCC voltage through modification of the references, and the "Sync" signal is set to 0. The PCC voltage and bus voltages should be synchronised when changing to the utility mode by setting "Sync" to 1 just before the breaker is closed.

Therefore, the AC voltages following the breaker in the d-q frame, V_{od}^{*} and, V_{oq}^{*} will be used as the references in island mode and V_{d}^{ref} and V_{q}^{ref} are when synchronization initiated as shown in Figure 4.2, respectively; they will be synchronised to the θ of PLL output angle. In utility mode (Islanded = 0), the converter regulates the reactive power. Additionally, the inner loop of the controller's current references (I_{dref} and I_{qref}) can be imposed to suitable constraints in both modes to avoid the inverter overloading.

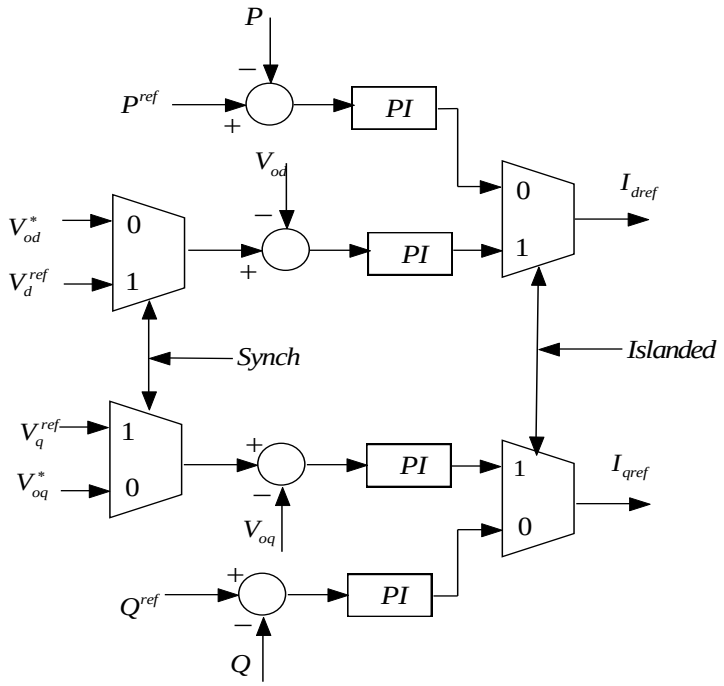

Figure.4.2: Control scheme of the inverter.

4.2.4 Droop Controller

In the microgrid under the grid-forming mode, the BESS must control the microgrid's voltage and frequency. The BESS has a droop P/F put to 0.5%, (the inverter produces its nominal active power). The microgrid voltage at the PCC bus can be adjusted by the adjustment of the droop Q/V put to 3%. Hence, droop control serves two purposes: it regulates real/reactive power using frequency/voltage control (Meng et al. 2019; Tayab et al. 2017). The following is how a droop control equation is created: A transmission line's actual and reactive power are as follows:

$$\left.\begin{aligned} P &= \frac{V_1 V_2}{X}\sin\delta \\ Q &= -\frac{V_1 V_2}{X}\cos\delta + \frac{V_1^2}{X} \end{aligned}\right\} \tag{4.8}$$

The power angle (δ) is much lower, so $Sin\delta = \delta$ and $Cos\delta = 1$. Hence equations become,

$$\delta = \frac{PX}{V_1 V_2} \tag{4.9}$$

$$V_2 - V_1 \cong -\frac{XQ}{V_1} \tag{4.10}$$

The preceding equations demonstrate that power angle control can be done using real power. The voltage can be managed using reactive power. Frequency control results in power angle regulation, which controls the actual power flow. So, the frequency and voltage droop control can be calculated as follows (Guerrero et al. 2011)

$$\left.\begin{aligned} f &= f_s + k_{pf}(P - P^s) \\ V &= V_s + k_{QV}(Q - Q^s) \end{aligned}\right\} \tag{4.11}$$

The measured and set values of frequency, voltage, active and reactive power are denoted as *f*, *V*, *P*, *Q*, and f_s, V_s, P_s, Q_s respectively. Droop proportional constants are k_{pf} and k_{QV}.

4.2.5 Voltage and Power Regulators

In microgrid mode, the voltage regulator is set. Computes I_{dref} and I_{qref} from the measured *dq* voltages and the voltage reference V_{od}^* which is generated by the droop controller as shown in Figure 4.3. Under the grid mode, the active and reactive power regulators are set. The power regulators are to produce I_{dref} and I_{qref} reference currents using the measured and reference active/reactive power. The processed currents which are obtained from the voltage regulator or power regulator are fed to the

Current Regulator. The voltage regulator and power regulator governing equation with PI controller is given in (4.11 & 4.12) as (Hamad et al. 2023; Pogaku et al. 2007).

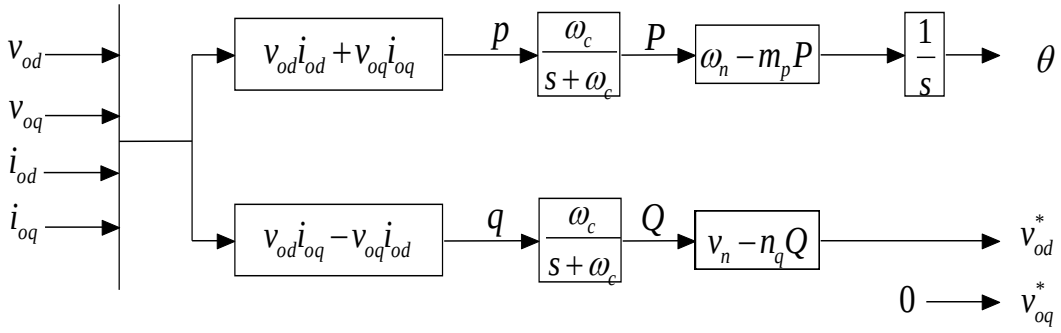

Figure 4.3: Power controller source.

$$\left.\begin{aligned} I_{dref} &= (k_{pvb} + \frac{k_{ivb}}{s})(V_{od}^* - V_{od}) \\ I_{qref} &= (k_{pvb} + \frac{k_{ivb}}{s})(0 - V_{oq}) \end{aligned}\right\} \tag{4.11}$$

$$\left.\begin{aligned} I_{dref} &= (k_{ppb} + \frac{k_{ipb}}{s})(P - P_{ref}) \\ I_{qref} &= (k_{pqb} + \frac{k_{iqb}}{s})(Q - Q_{ref}) \end{aligned}\right\} \tag{4.12}$$

Where k_{pvb} k_{ivb} and k_{ppqb}, k_{ipqb} are the PI gains of the BESS voltage controller and the power controller respectively.

4.2.6 Current Regulators

The processed currents which are obtained from the voltage regulator (isolated) mode or power regulator (grid mode) through the switch are fed to the Current Regulator as shown in Figure 4.4. To produce the required dq voltages to generate pulses for the inverter. It is important to note that the regulators use feedforward computation to achieve a high dynamical response. Current control functions as an inner loop section on the control of inverters. The PI controllers control keeps track of current reference values, respectively. The PI controller output, the *dq* voltage, and the

cross voltage drop in the inductor L_{ff} are combined to generate the reference voltages V_{dref} and V_{qref}. This reference voltage is used to generate the PWM, which creates the necessary commands for the switches on the connected inverter. The equation is given as (Ramezani et al. 2017)

$$\left.\begin{aligned} V_{dref} &= (k_{pib} + \frac{k_{iib}}{s})(I_{dref} - I_d) \\ &+V_d - \omega L_{ff} I_q \\ V_{qref} &= (k_{pib} + \frac{k_{iib}}{s})(I_{qref} - I_q) \\ &+V_q - \omega L_{ff} I_q \end{aligned}\right\} \quad (4.13)$$

Where k_{pib} and k_{iib} are the PI values for the BESS current loop controller. The translated and scaled V_{dref} and V_{qref} are used to generate a 3-phase reference signal V_{ref}, then fed to the PWM block to produce pulses for the inverter switches.

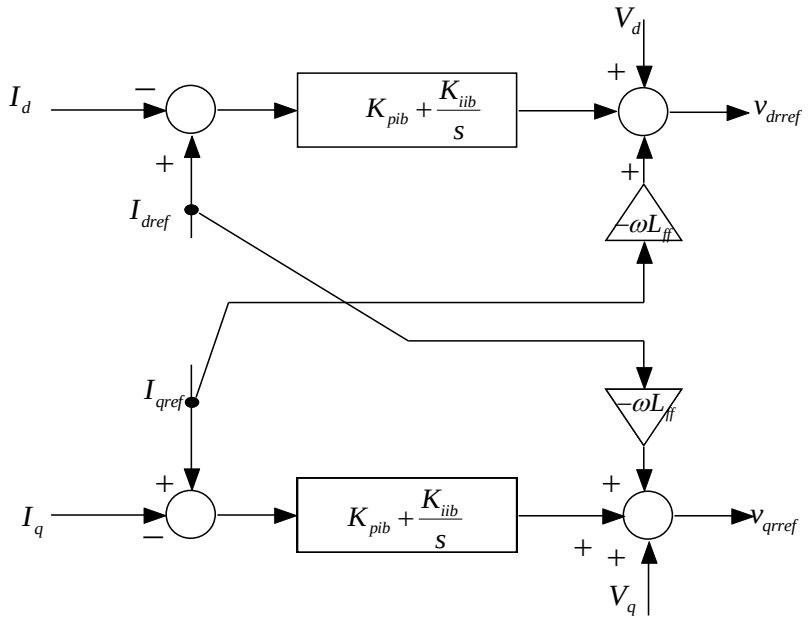

Figure 4.4: Current Controller source: (Pogaku et al. 2007)

4.2.7 Battery Controller

A PV system can't balance its power output without a battery bank serving as a storage buffer. The BES is managed by a bidirectional converter (Figure 4.1) which is

connected to the PCC and has control to manage both charging and discharging. The detailed control procedure is shown in Figure 4.5. In utility mode, with 0 as the command, the converter controls the power flow in or out of the battery, wherein discharging mode $P_{battery} > 0$, and charging mode $P_{battery} < 0$. The final output of the battery controller is a switching signal. In Islanded mode, the control command is set to "1", which switches the converter to work in voltage reference mode (Gadalla et al. 2018; Hasabelrasul et al. 2022).

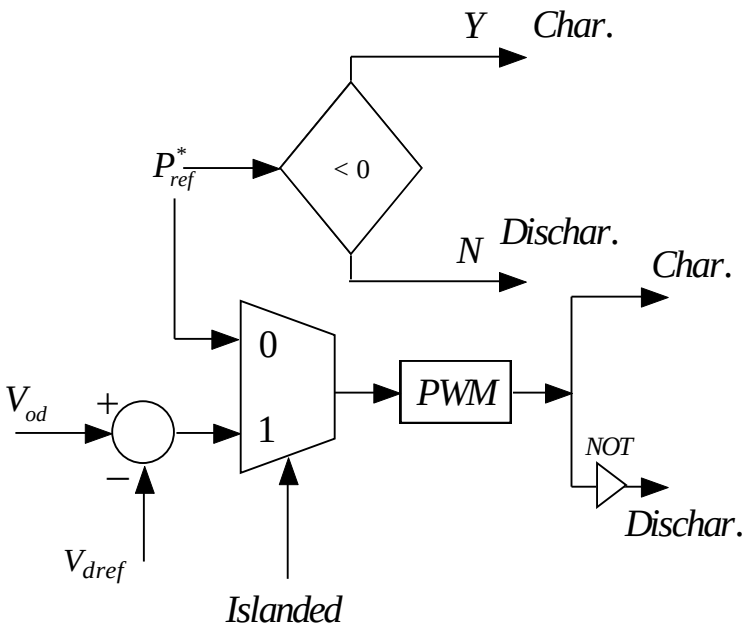

Figure 4.5: Battery charging/discharging controller.

Table 4.1: The battery parameters.

Quantity	**Value**
Nominal Voltage	780
Rated capacity (Ah)	1360
Initial SOC (%)	50

4.3 RESULTS AND DISCUSSION

An additional case study demonstrates the dynamic features of the suggested control algorithms during grid-to-microgrid and back-to-grid transitions. In this study, the system first acts as a standard grid, and then the tie switch is opened after two seconds to make an intentional island. As a result, the microgrid is solely reliant on the PCC's solar farm and BESS. The combined real and reactive power infusion from the BESS inverter and solar plant with proposed MPPT controllers during microgrid mode is shown in Figure 4.6. The proposed controllers instruct the solar plant to produce an assuring of active power at MPP during grid-connected and microgrid mode based on the irradiance considered.

Table 4.2: Battery Energy Storage System Data

Symbol	Description	Nominal Value
K_{pf}	Frequency droop	0.5
K_{QV}	Voltage droop	3
K_{ppb}	Power regulator Proportional gain	1.5
K_{ipb}	Power regulator Integral gain	15
K_{pib}	Current regulator Proportional gain	0.2
K_{iib}	Current regulator Integral gain	15
K_{pvb}	Voltage regulator Proportional gain	2
K_{ivb}	Voltage regulator Integral gain	25
F_{sw}	PWM switching freq. Hz	2700

In a microgrid-connected mode i.e., when it transits to the islanded condition, the PV system is managed to provide real power and the deficit power required for the load is covered by the BESS inverter system with reactive power. As the microgrid transits to the islanded situation, both active as well reactive power injections from PV and Battery.

In the first scenario, the PV battery system operates normally in connection to the grid. The PV array is operating in MPPT mode and is tracking the voltage reference (VMPPT) as estimated by the MPPT module. AC loads are connected to the bus. Depending on the quantity of generation, usage, and demand requested by the grid (P_{grid}), the battery is either absorbing (-ve) or releasing (+ve) power to maintain a balance. The sharing of power and rms voltages of the PV-BES system under the suggested coordinated control are depicted in Figure 4.6 and Figure 4.8. Before 2s, the

power generated by PV around 650 kW in MPPT mode, and the AC load required is P_{load} AC = 780 kW, and the difference is provided by the utility grid (P_{grid} = 130 kW).

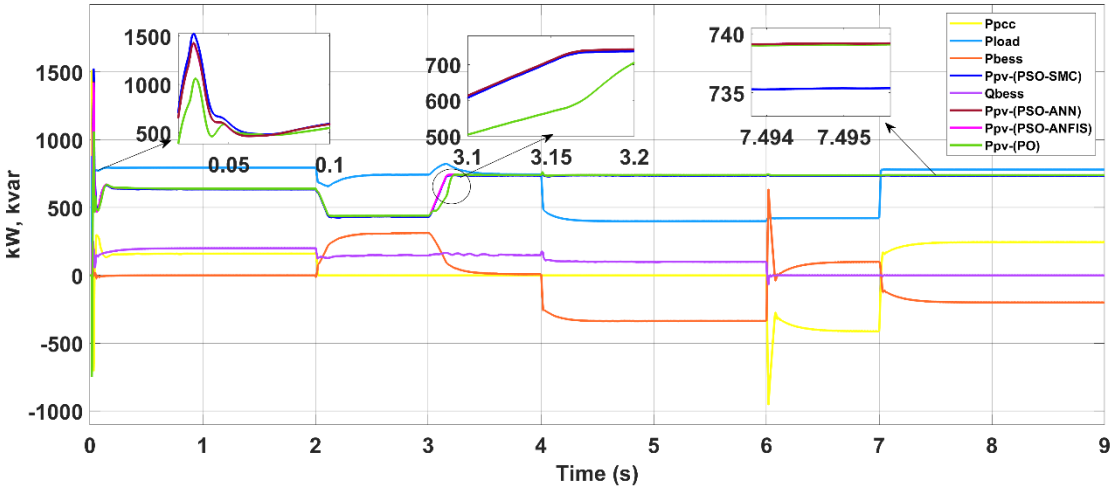

Figure 4.6: Power sharing of the system.

During this time, the battery's reactive power is discharged. Since the VSC has complete control over both the DC link voltage and the reactive power in grid-connected mode, it can supply reactive power to the utility if required. Figure 4.6 depicts the waveforms that are corresponding to this case, where all and pink graph represent the active as well as reactive power, respectively. P_{load} and Q_{load}, delivered from the PV-BES hybrid system to the demand. The VSC regulates reactive power in an adaptable manner.

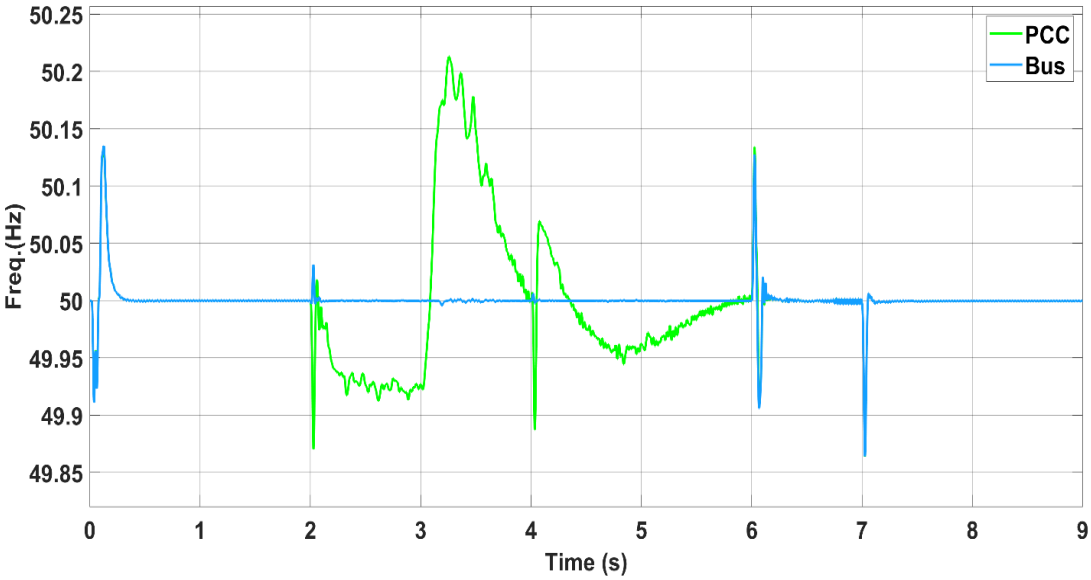

Figure 4.7: Frequencies of microgrid and PCC.

The PV battery system has been demonstrated to operate in both grid-connected and island configurations. In the event of utility grid instability or severe failures at the AC bus, for example, the circuit breaker at PCC will be opened, converting the system to islanded mode so that it does not draw current from the power grid. After the circuit breaker is tripped, the battery inverter is switched to control frequency and AC bus voltage (Figures 4.7 and 4.8), where these parameters resolve more rapidly.

The power balancing criterion is $P_{PV}+P_{bat} = P_{load}$ when the PV-battery system is operating in islanded mode, which means that all available power is supplied by the PV and battery alone. As discussed in Chapter 3, MPPT controllers provide V_{MPPT}, which is followed by the PV array to power loads. Depending on the required capacity and PV output, the battery converter's direction of power transfer may change. As depicted in Figure 4.6, power can be shared between the PV system and the battery bank. To meet the system's demand, the battery's delivering power (P_{bat}) increases from zero to approximately 330 kW when the AC bus load is 780 kW at 2s. Since photovoltaic energy can provide approximately 450 kW. At two-second change in solar irradiance may result in a change in PV power, which in turn impacts the burden on AC buses. By modifying the power supply from the battery converter, the battery bank's controllers can effectively compensate for the decrease in PV power. Figure 4.6 depicts how battery power (orange curve) responds to a decrease in PV power when solar

irradiance decreases. Consequently, it can regulate the battery and achieve precise power balance.

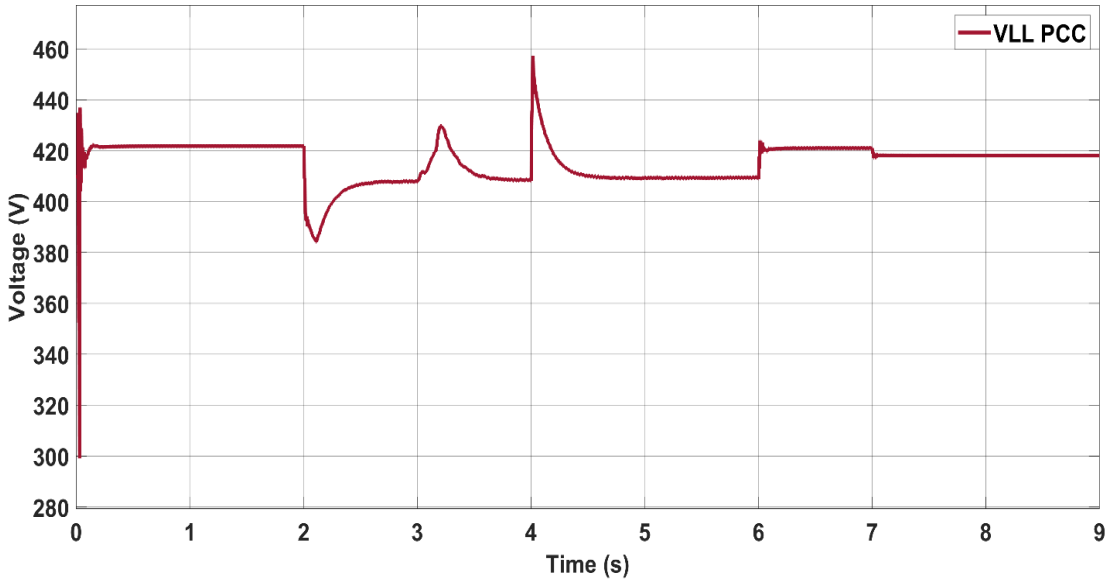

Figure 4.8: PCC RMS Voltage.

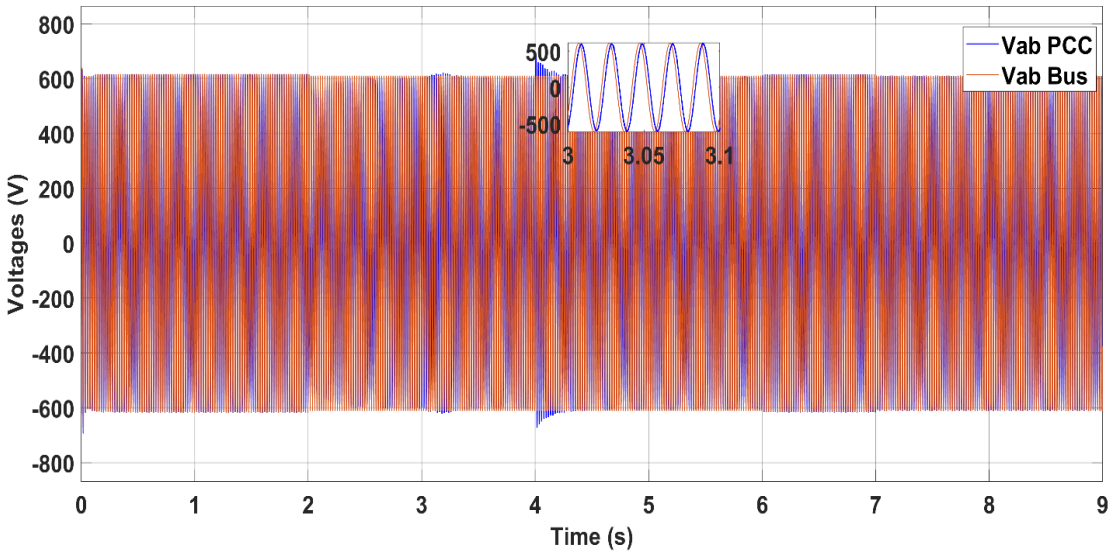

Figure 4.9: The sinusoidal PCC and Bus voltages.

In grid forming mode, the battery inverter independently regulates the voltages (v_{ab}, v_{bc} and v_{ca}). To provide consistent power to applications, bus voltages must frequently be maintained at specific levels. Nonetheless, the controller has full control over these voltages as well.

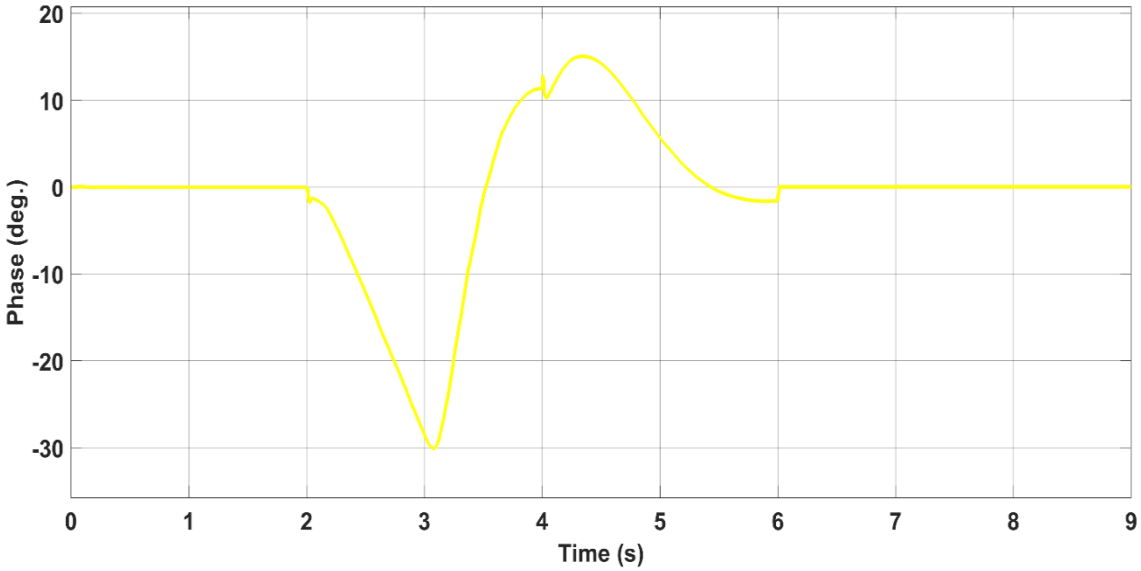

Figure 4.10: The phase angle between PCC and Bus voltages

The bus voltages can be maintained constant (Figure 4.8) at 2, 3 4 and 6s irrespective of changes in the environment such as planned islanding, synchronization signal to the microgrid, one load disconnected, and grid connected respectively. In all of these cases, V_{rms} maintained around 420 V and its sinusoidal waveforms of PCC and bus are also shown in Figure 4.9. The phase angle between those voltages is shown in Figure 4.10.

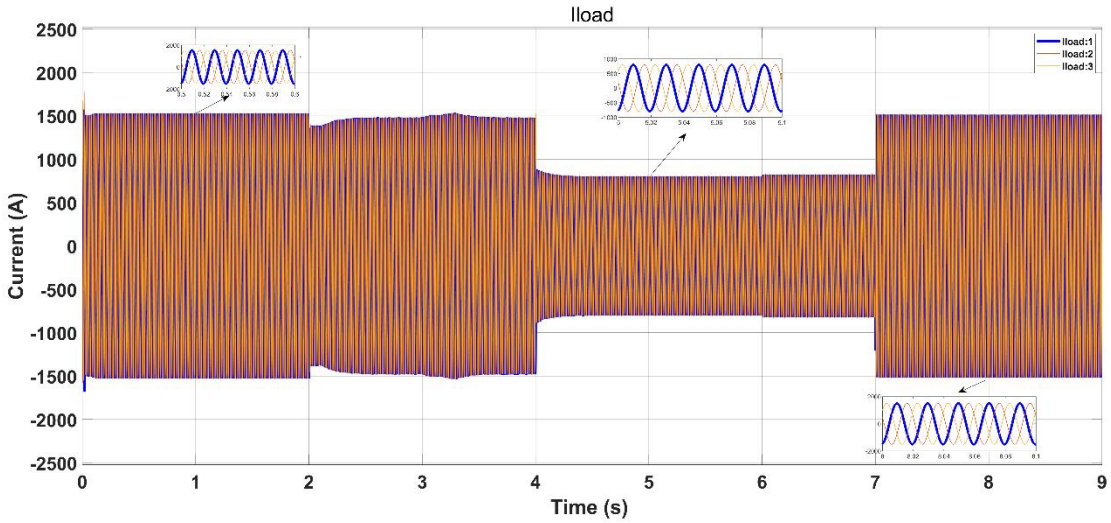

Figure 4.11: The sinusoidal load current

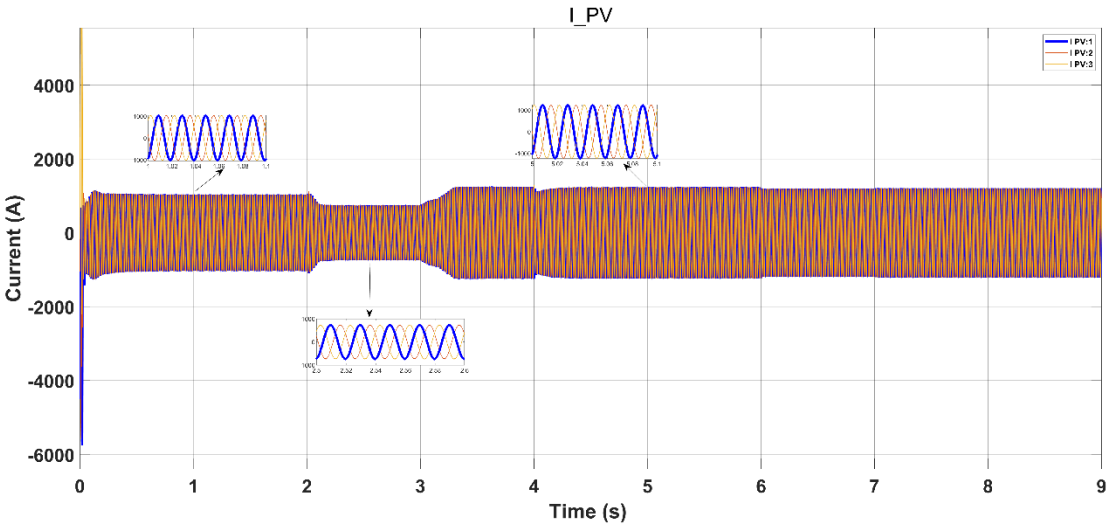

Figure 4.12: The sinusoidal PV load current

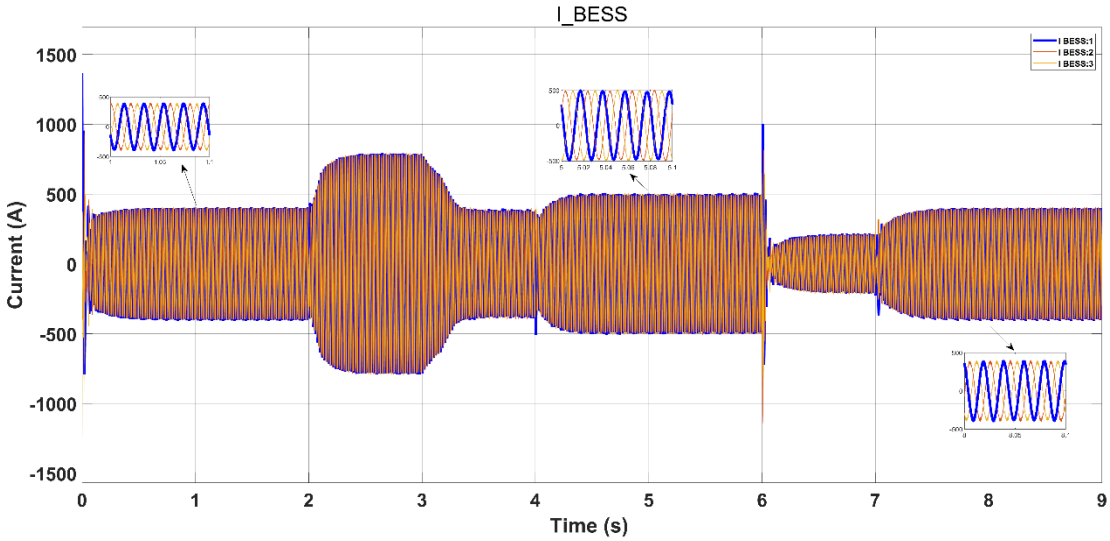

Figure 4.13: The sinusoidal battery load current

As the load demand and power generation change with these sources based on the condition, the instantaneous load current also changes in all sources (Figure 4.11, Figure 4.12 and Figure 4.13).

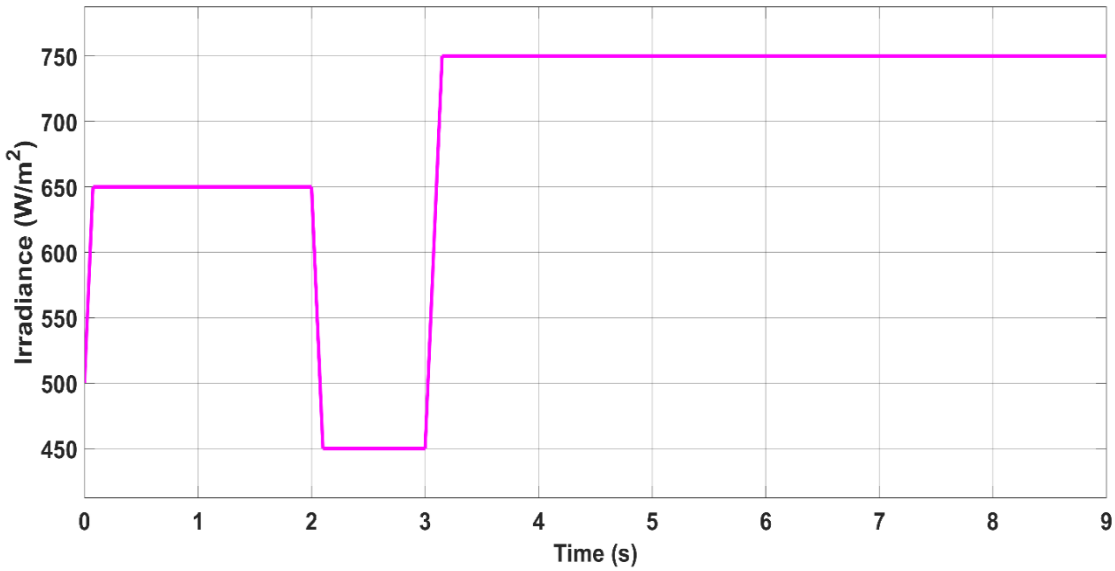

Figure 4.14: The irradiance W/m^2

The solar PV system with proposed MPPT controllers tracks MPP as it is shown in Figure 4.6 with irradiance change as depicted in Figure 4.14, PV system produces maximum power accordingly during the simulation's time frame. From 0 to 2s around 650 kW, from 2 to 3 around 450 kW and 4 to 9 around 900 kW.

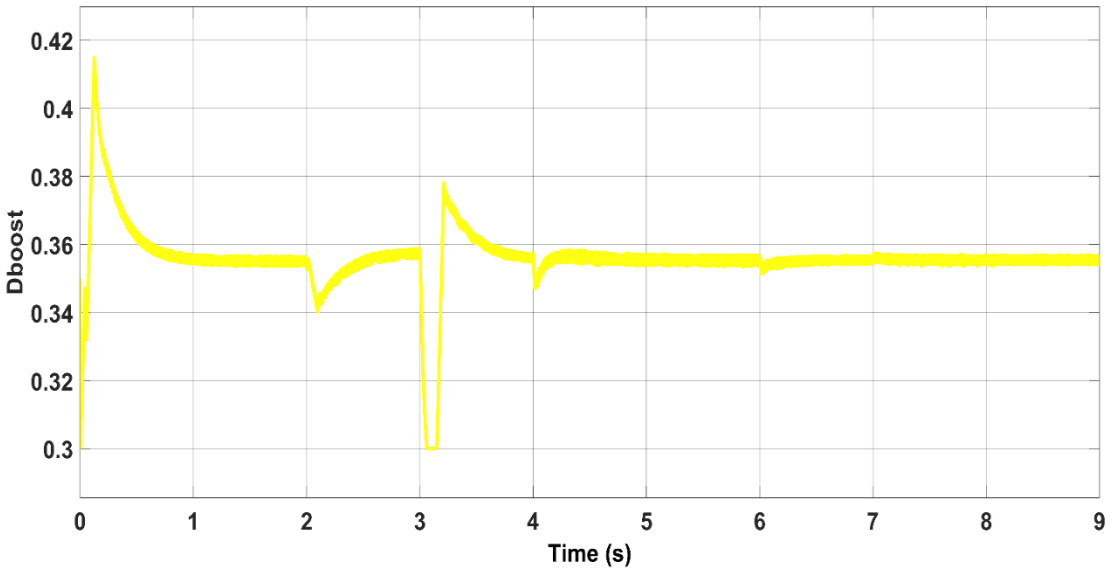

Figure 4.15: The PV boost converter duty ratio.

Irrespective of variations in irradiance the duty ratio is maintained constant as shown in Figure 4.15. Following that the output voltage of PV and output current as

shown in Figure 4.16 and Figure 4.17. As depicted in this figure, during any change of irradiation, the proposed MPPT methods successively iterate until reach the optimal voltage that corresponds to the global maximal power points.

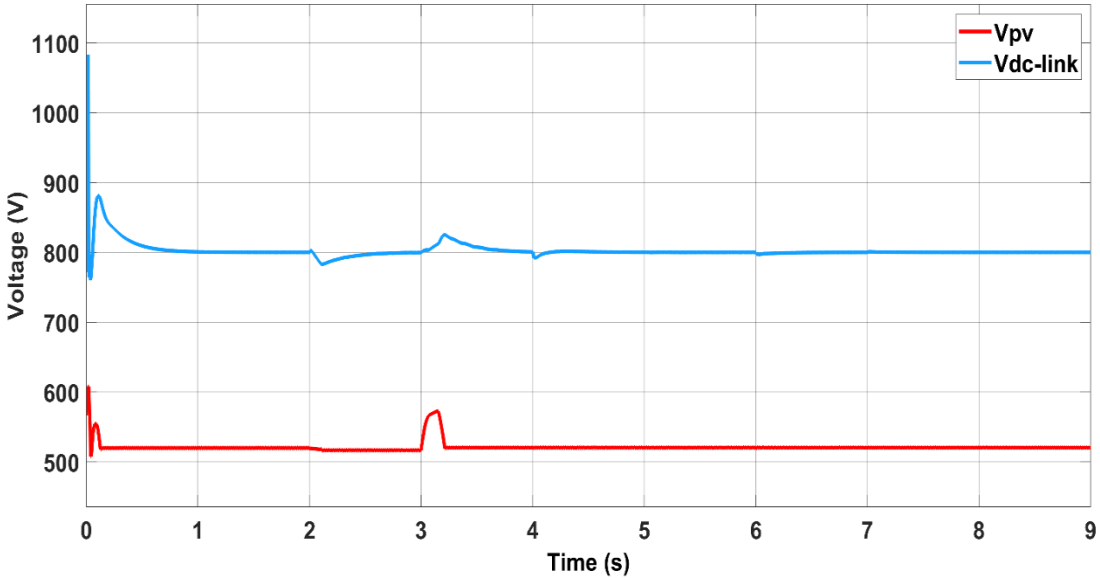

Figure 4.16: Output voltage of PV boost converter.

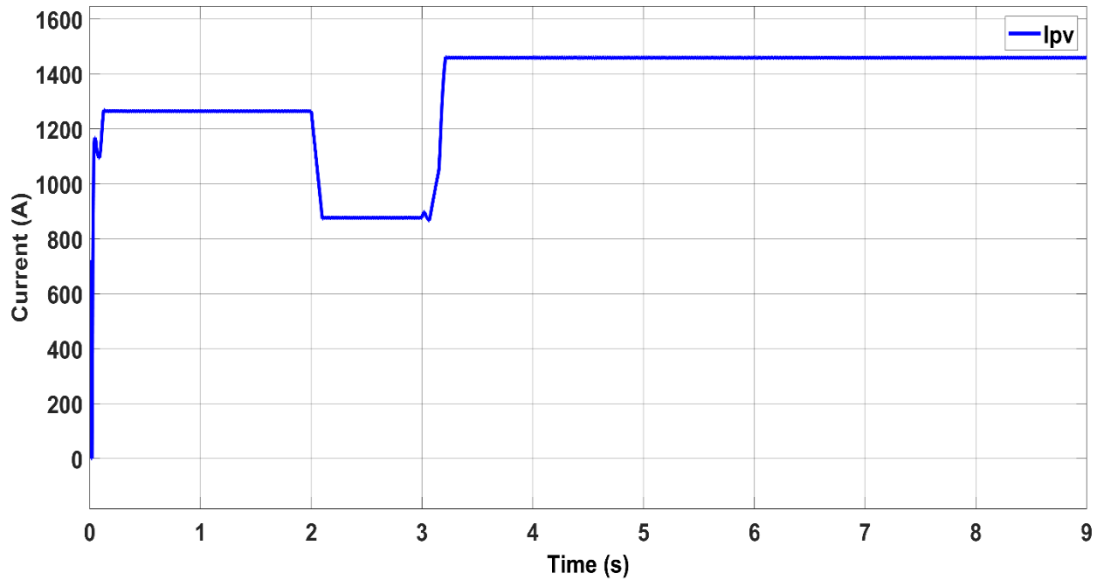

Figure 4.17: Output current of PV boost converter.

As the load changes the inverter controller maintained the battery voltage constant as shown in Figure 4.18. and its output current is also shown in Figure 4.19.

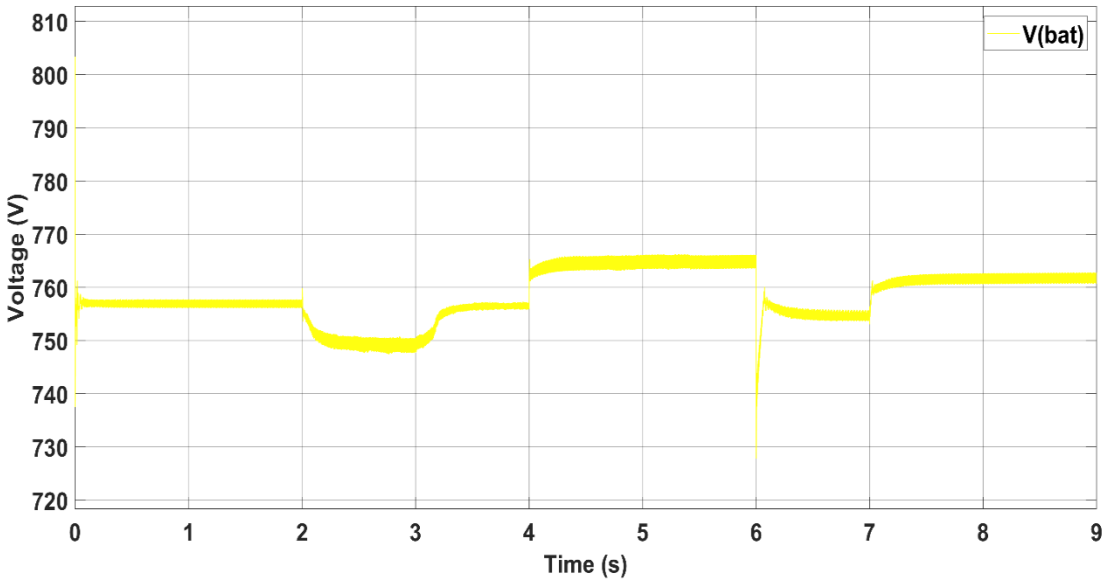

Figure 4.18: Energy storage Voltage.

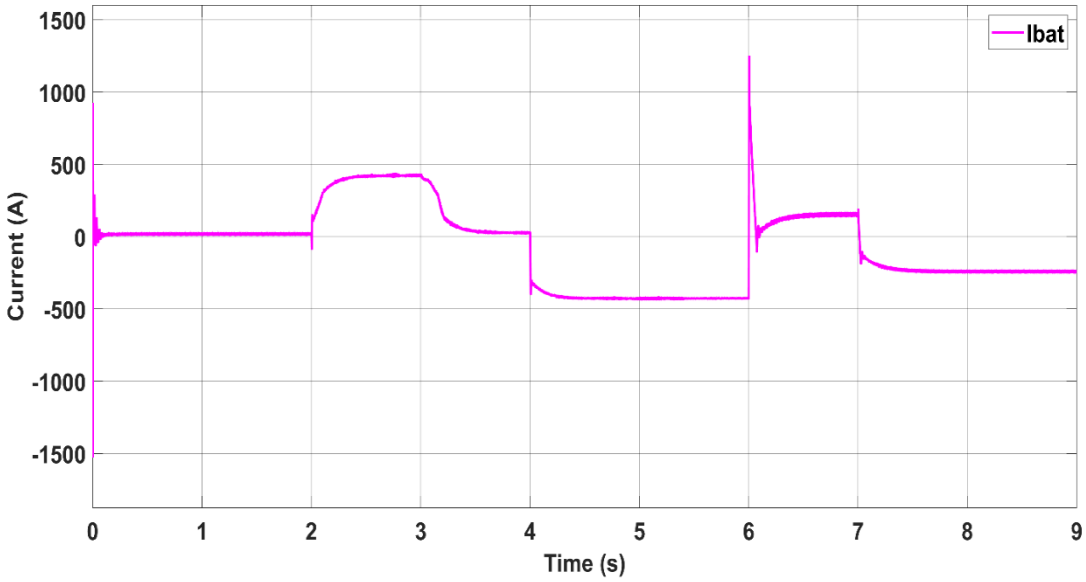

Figure 4.19: Energy storage current.

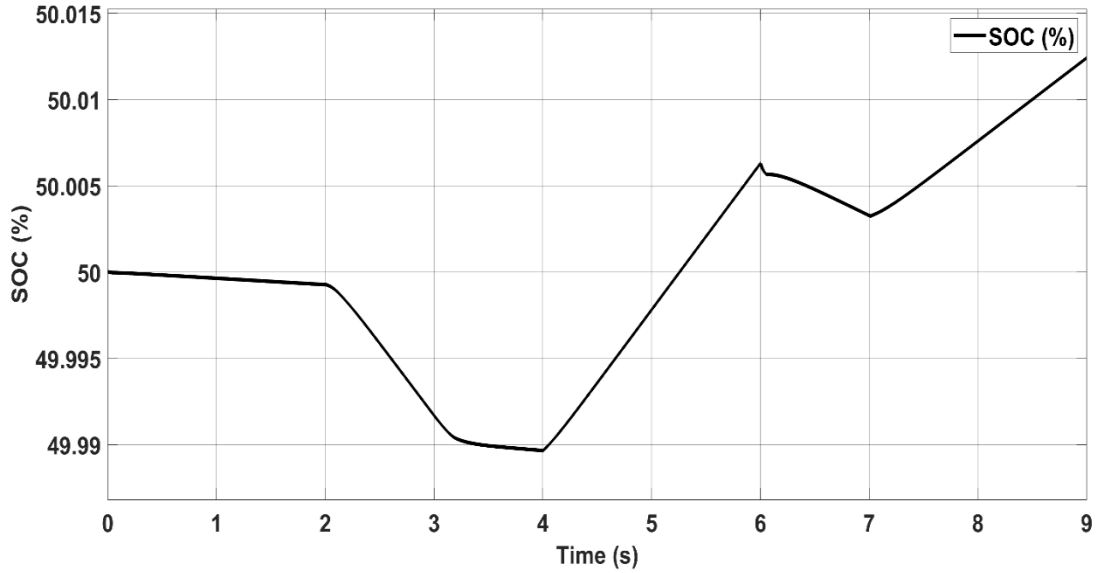

Figure 4.20: Battery energy storage SOC.

In Figure 4.20 from 0 to 2 s, the battery's active power is not delivering any power, hence it will be at its initial SOC of 50%. At 2 s, utility is disconnected, the battery starts delivering power to load up to 4s, slope changes based on load current. Again at 4 s, some load turned off, but PV power was generating more than the demand and started charging the battery, till 6 s. This continues based on the demand. Hence the proposed battery controller efficiently works under these conditions in both modes.

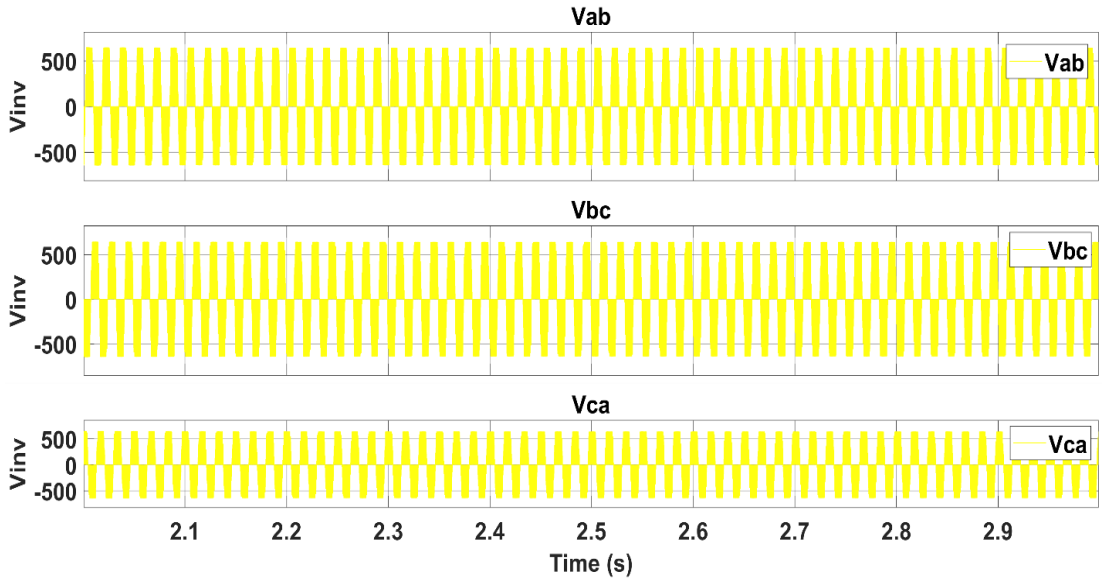

Figure 4.21: BES microgrid inverter output voltages

PV-BES inverter output voltages as shown in Figure 4.21, and Figure 4.22 and Figure 4.23 is the modulation index of the PV-BES inverter which is about around 0.8. and the THD of load current and PV system current are shown in Figure 4.24 to Figure 4.26 which is well within IEEE 519 std.

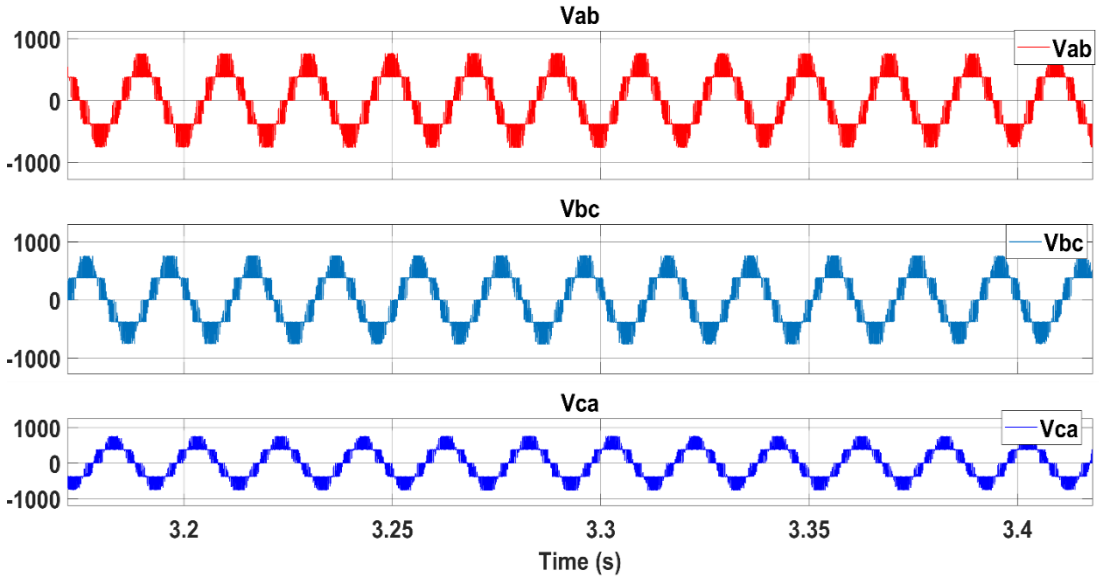

Figure 4.22: microgrid inverter PV output voltages

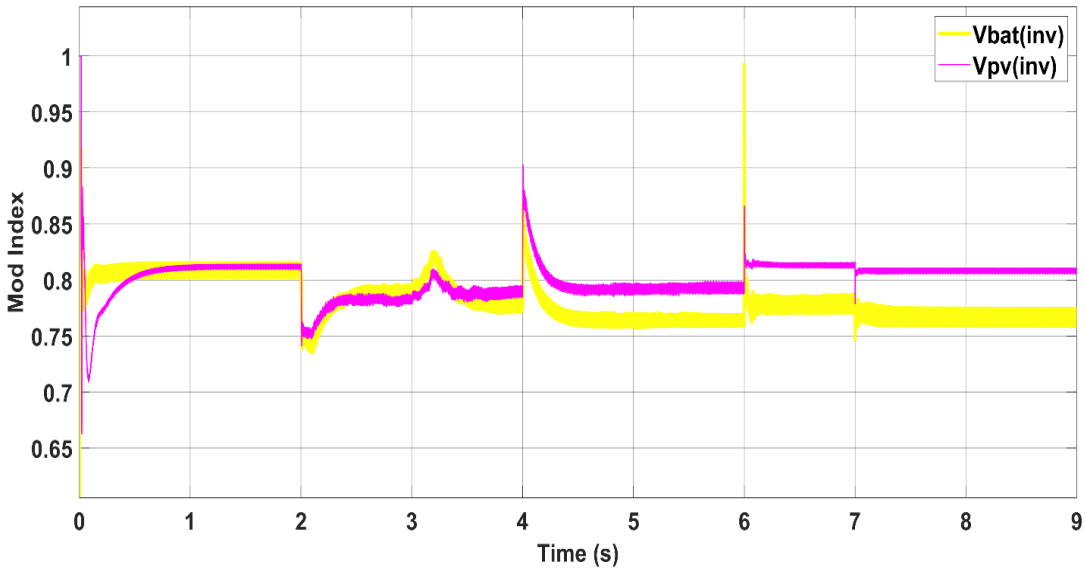

Figure 4.23: Modulation index of PV-BES inverter

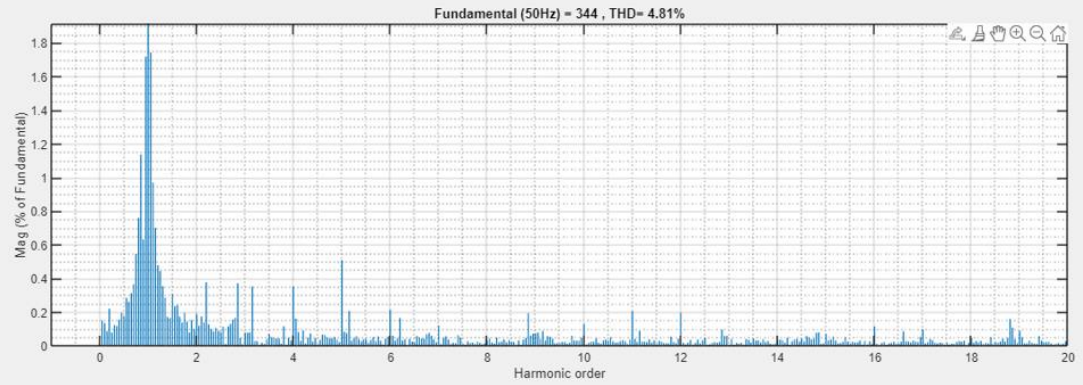

Figure 4.24: THD of BES system AC load current.

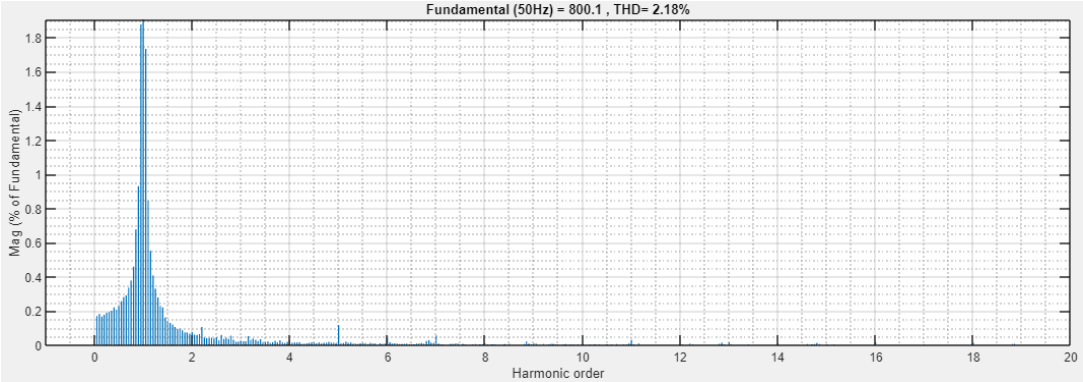

Figure 4.25: THD of microgrid ac load current.

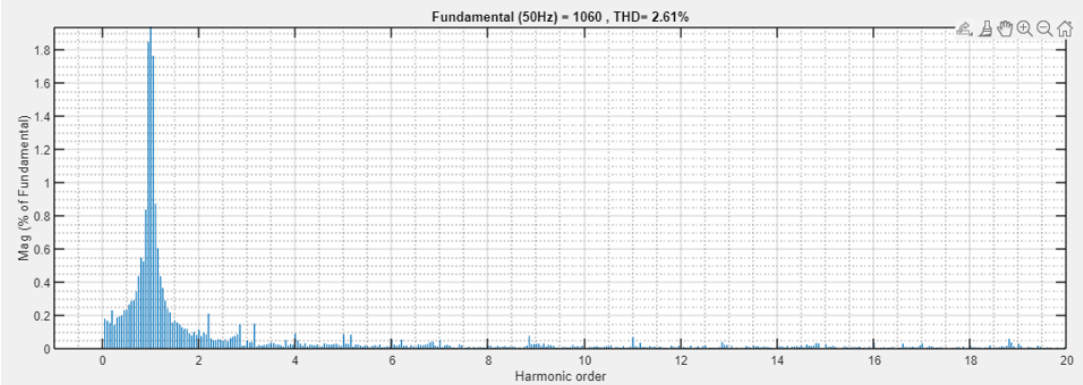

Figure 4.26: THD of PV system ac load current.

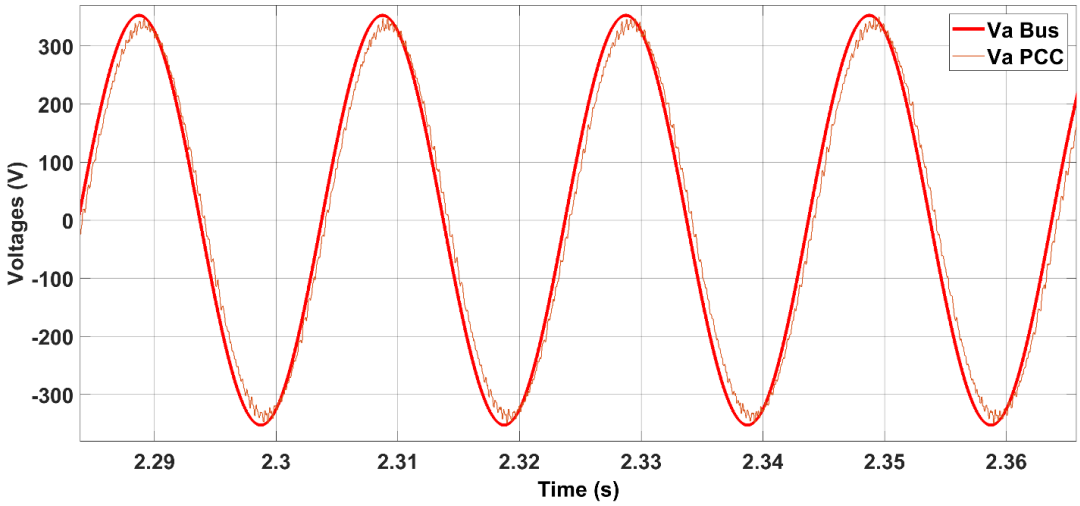

Figure 4.27: Islanding AC voltage.

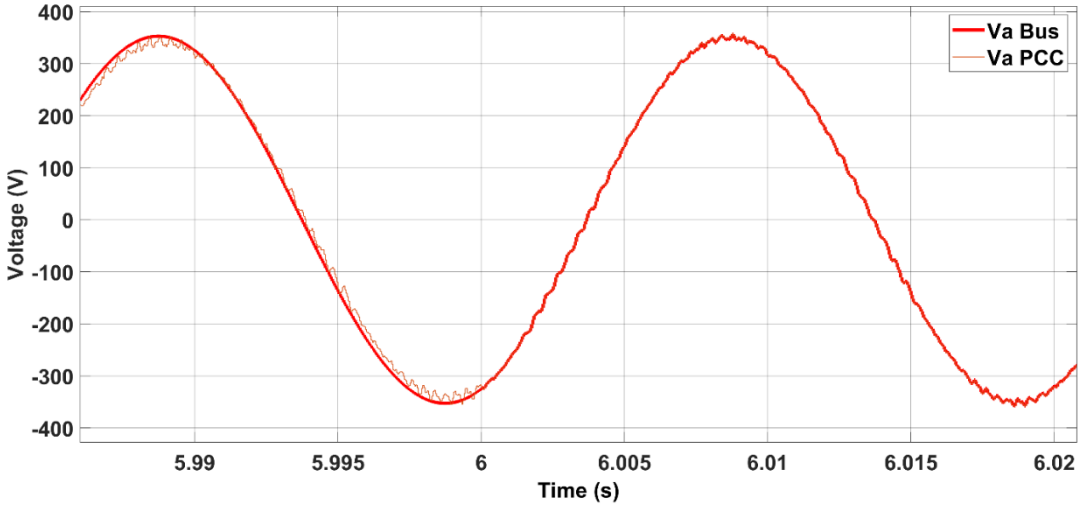

Figure 4.28: Synch. AC voltage.

Accidental acts of the PCC circuit breaker could result in the disconnection of the PV-battery system. However, reconnection to the utility is usually arranged in advance, so the provider will have plenty of time to position the independent PV battery system for smooth reconnection before closing the breaker. In order to avoid disruptions brought on by the breaker's operation, the 3-ϕ voltage of PCC must be synchronised with the grid side voltage. The following scenario compares the situations in which the voltages are synchronised by the proposed controller and those in which it is not before the breaker is closed. In Figure 4.27, the distortion of waveform can be witnessed at the

beginning of islanding (after 2 s) without voltage synchronization. In contrast, Figure 4.28 presents the synchronizing process, which takes successfully at 6 s and avoids distortion. When the PV battery system is connected to the grid, disturbances are significantly reduced, ensuring that the bus loads receive a reliable power supply.

4.4 SUMMARY

The work carried out demonstrates the proposed MPPT algorithm along with coordinated (V-f)/(P-Q) techniques for the grid and islanded mode using a photovoltaic system, battery storage and utility. In this thesis, the PV system is run with dissimilar algorithms to attain maximum power point (MPP). Among all the PSO-ANFIS algorithm is quick, accurate and is better than the other three algorithms in better PV tracking under different operating conditions. In addition, with the proposed control method, the transition from grid-connected side P-Q control to autonomous V-f supervision and back to grid synchronization, respectively, was seamless and effective. In the suggested microgrid the V-f control mechanism brings back the microgrid frequency and PCC voltage with the use of battery installations. The battery storage acts as a buffer to inject and receive power as needed via the charge/discharge cycle to make up for any shortfalls or surpluses. Also, the coordinated P-Q control method under the grid following mode, the active power requirement by the load met by the grid, the solar PV system, and the storage device. The excess generation by PV will be stored in the battery storage device.

Chapter 5

CONCLUSIONS AND SUGGESTIONS FOR FUTURE STUDY

5.1 GENERAL

This thesis has primarily focused on the implementation and analysis of control algorithms for PV arrays and BES, as well as the operation of 3-ϕ microgrids. The three phases of the proposed microgrid system are the battery storage's connection to the converter and the microgrid's connection to the power distribution network. In microgrids, a bidirectional converter is used to link the BES bank to the AC connection. The following are the primary focuses of this study.

1. Control, implementation and analysis of 3-ϕ grid interactive microgrids with PV system along with different MPPT algorithms for boost converter to extract maximum power. The proposed 3-ϕ microgrid is tested, which is subjected to variable atmospheric conditions with grid connection under different load conditions.
2. The control of seamless transitions of 3-ϕ PV-BES microgrids has been carried out in detail. The battery is connected directly to the AC bus through the bidirectional converter. In 3-ϕ PV-BES microgrids, processes such as synchronisation, islanding, and resynchronization ensure secure operation and a smooth transition between the three phases.

5.2 MAIN CONCLUSIONS

In this thesis, the 3-ϕ grid interactive microgrids based on PV array and battery storage, have been explored in detail. The functionalities have been achieved by modifying the control algorithms. The control of the voltage source converter (VSC)

has been made more robust so that it can inject the extracted PV power to the utility and provides additional functionalities such as load balancing and transition between modes. Maximum power point tracking (MPPT) is typically carried out by power converters and is associated with the PV panels and DC link capacitor of the voltage source converter (VSC). To enhance the efficacy of the PV module, MPPT must provide improved performance in a wide range of environmental conditions. In this thesis, precise models of PV systems with MPPT methods such as P&O, PSO-Sliding, PSO-ANN and PSO-ANFIS are proposed. When PV generation is available, it works as a power quality conditioner and injects extracted PV power into the utility. In deficit PV generation, it works with the availability of the grid to meet the demand and under outage of the grid, with the battery feeding the power to the load using this converter by operating it into voltage control mode. This way the microgrid is used rather than shut down when the PV source and the grid are not available. The proposed control method a seamless change from grid-connected side PQ control to island V-f management back to grid resynchronization, respectively, was seamless and successful. In the suggested microgrid the V-f control mechanism brings back the microgrid frequency and PCC voltage with the use of battery installations. The battery storage acts as a buffer to inject and receive power as needed via the charge/discharge cycle to make up for any shortfalls or surpluses. Also, the coordinated PQ control method under the grid forming, the power demand from the load supplied by the utility, the solar PV system, and the storage device. The excess generation by PV will be stored in the battery storage device.

Some of the most salient outcomes of this work are as follows:

- The frequency and phase of the utility network have been evaluated using numerous mode transition algorithms. By coupling these techniques with the suggested controls, the conventional phase-locked loop (PLL) system's deficiencies are mitigated. Large frequency fluctuations and phase leaps affected PLL-based grid phase and frequency estimations during unanticipated power disruptions and restorations. This is because frequency and phase angle are evaluated simultaneously.

- These microgrids provide seamless transitions between the dual mode. In the event of a power outage from grid, the voltage source converter (VSC) is switched from current control to voltage control while remaining continuously present. Consequently, the effectiveness of the PV with efficient MPPT algorithms and BES microgrid is increased, to receive uninterrupted power. The simulation performances of the microgrids have been demonstrated under sudden outages and recovery of the utility grid.
- Utility-connected microgrids that are powered by solar PV with MPPT techniques and battery storage systems are intended to be in precise phase and frequency coordination with the distribution grid's voltage waveform. For safety reasons, conventional PV inverters are mandated to close autonomously in the event of a grid failure. The intended multitasking PV-BES microgrid will ensure that the demand does not experience any interruptions in power. Therefore, these microgrid systems are more reliable and efficient as compared to grid-tied microgrids.

5.3 SUGGESTIONS FOR FURTHER WORK

In this thesis work, a wide variety of the 3-ϕ standalone and grid interactive PV-BES microgrids have been investigated in detail. This research work can be extended for further work, and it can be explained in the following ways.

1. The PV-BES microgrids with additional DGs and load compensation can be synchronised and de-synchronized unintentionally using an efficient smooth transition control technique. Also, the effect of grid fault also may be analysed to see performance and the effect of unbalance load performance can be studied on operation of the microgrid.
2. Here, to control the battery energy storage, a bidirectional inverter is used. However, an analysis of various converters such as flyback converters, push-pull converters, and high gain DC-DC converters with coupled inductors can be used for control of charging/discharging of the battery storage.

3. In this work, the partial shading situation is not addressed. The suggested microgrid can be studied with the use of partial shading situations and nonlinearities in PV arrays.
4. Developing efficient SOC estimation techniques for battery energy storage is still a challenging task. For safe operation and the longer life span of the battery, some investigations can be made to develop some SOC estimation techniques.
5. The hydrogen energy storage can be considered to replace the battery for the PV-BES microgrids with additional DGs for greener sustainability.

LIST OF PUBLICATIONS

REFEREED JOURNALS

1. Siddaraj, S., Yaragatti, U. R., Nagendrappa, H., & Jhunjhunwala, V. K. (2020). Autonomous microgrid based parallel inverters using droop controller for improved power sharing. Bulletin of Electrical Engineering and Informatics, 9(6), 2302-2310.
2. SIddaraj, S., Yaragatti, U. R., & Harischandrappa, N. (2023). Coordinated PSO-ANFIS-Based 2 MPPT Control of Microgrid with Solar Photovoltaic and Battery Energy Storage System. Journal of Sensor and Actuator Networks, 12(3), 45.

CONFERENCE PROCEEDINGS

1. Siddaraj, S., Yaragatti, U. R. & Nagendrappa, H. (2022). Autonomous microgrid using New Perspective on Droop Control in AC Microgrid. International conference on advances in Renawable Energy & Electric Vehicles, Nitte, Karnataka. (Lecture Notes in Electrical Engineering-Springer)

BIBLIOGRAPHY

Abbes, D., Martinez, A., & Champenois, G. (2012). Eco-design optimisation of an autonomous hybrid wind-photovoltaic system with battery storage. *IET Renewable Power Generation*, *6*(5). https://doi.org/10.1049/iet-rpg.2011.0204

Abo-Sennah, M. A., El-Dabah, M. A., & Mansour, A. E. B. (2021). Maximum power point tracking techniques for photovoltaic systems: A comparative study. *International Journal of Electrical and Computer Engineering*, *11*(1), 57–73. https://doi.org/10.11591/ijece.v11i1.pp57-73

Abu-Rub, H., Iqbal, A., Ahmed, S. M., Peng, F. Z., Li, Y., & Baoming, G. (2013). Quasi-Z-source inverter-based photovoltaic generation system with maximum power tracking control using ANFIS. *IEEE Transactions on Sustainable Energy*, *4*(1). https://doi.org/10.1109/TSTE.2012.2196059

Adhikari, S., & Li, F. (2014). Coordinated V-f and P-Q control of solar photovoltaic generators with MPPT and battery storage in microgrids. *IEEE Transactions on Smart Grid*, *5*(3), 1270–1281. https://doi.org/10.1109/TSG.2014.2301157

Ahmad, F. F., Ghenai, C., Hamid, A. K., & Bettayeb, M. (2020). Application of sliding mode control for maximum power point tracking of solar photovoltaic systems: A comprehensive review. In *Annual Reviews in Control* (Vol. 49). https://doi.org/10.1016/j.arcontrol.2020.04.011

Ahmed, K. H., Finney, S. J., & Williams, B. W. (2007). Passive filter design for three-phase inverter interfacing in distributed generation. *5th International Conference-Workshop Compatibility in Power Electronics, CPE 2007*. https://doi.org/10.1109/CPE.2007.4296511

Ahmed, M., Abdelrahem, M., Farhan, A., Harbi, I., & Kennel, R. (2021). DC-link sensorless control strategy for grid-connected PV systems. *Electrical Engineering*, *103*(5). https://doi.org/10.1007/s00202-021-01228-2

Alam, M. S., Azeem, M. F., & Alouani, A. T. (2014). Modified queen-bee algorithm-based fuzzy logic control for real-Time robust load matching for a solar PV System. *IEEE Transactions on Sustainable Energy*, *5*(2). https://doi.org/10.1109/TSTE.2013.2271449

Alaraj, M., Kumar, A., Alsaidan, I., Rizwan, M., & Jamil, M. (2022). An Advanced and Robust Approach to Maximize Solar Photovoltaic Power Production. *Sustainability (Switzerland)*, *14*(12). https://doi.org/10.3390/su14127398

Al-Gizi, A. G., Craciunescu, A., & Al-Chlaihawi, S. J. (2017a). The use of ANN to supervise the PV MPPT based on FLC. *2017 10th International Symposium on Advanced Topics in Electrical Engineering, ATEE 2017*. https://doi.org/10.1109/ATEE.2017.7905128

Al-Gizi, A. G., Craciunescu, A., & Al-Chlaihawi, S. J. (2017b). The use of ANN to supervise the PV MPPT based on FLC. *2017 10th International Symposium on Advanced Topics in Electrical Engineering, ATEE 2017*. https://doi.org/10.1109/ATEE.2017.7905128

Ali, M. N., Mahmoud, K., Lehtonen, M., & Darwish, M. M. F. (2021). An Efficient Fuzzy-Logic Based Variable-Step Incremental Conductance MPPT Method for Grid-Connected PV Systems. *IEEE Access*, *9*. https://doi.org/10.1109/ACCESS.2021.3058052

Aljarah, I., Faris, H., & Mirjalili, S. (2018). Optimizing connection weights in neural networks using the whale optimization algorithm. *Soft Computing*, *22*(1), 1–15. https://doi.org/10.1007/S00500-016-2442-1/METRICS

Al-Majidi, S. D., Abbod, M. F., & Al-Raweshidy, H. S. (2020). A particle swarm optimisation-trained feedforward neural network for predicting the maximum power point of a photovoltaic array. *Engineering Applications of Artificial Intelligence*, *92*, 103688. https://doi.org/10.1016/J.ENGAPPAI.2020.103688

Asakura, J., & Akagi, H. (2009). State-of-Charge (SOC)-Balancing Control of a Battery Energy Storage System Based on a Cascade PWM Converter. *IEEE Transactions on Power Electronics*, *24*(6). https://doi.org/10.1109/TPEL.2009.2014868

Ashwin, D., Ilango, K., & Gopal, V. K. (2018). Design and simulation of stand-alone three phase power supply system using solar photo voltaics for industrial load application. *Proceedings of 2017 IEEE International Conference on Technological Advancements in Power and Energy: Exploring Energy Solutions for an Intelligent Power Grid, TAP Energy 2017*, 1–6. https://doi.org/10.1109/TAPENERGY.2017.8397266

Baghban, A., Ahmadi, M. A., & Shahraki, B. H. (2015). Prediction carbon dioxide solubility in presence of various ionic liquids using computational intelligence approaches. *The Journal of Supercritical Fluids*, *98*, 50–64. https://doi.org/10.1016/J.SUPFLU.2015.01.002

Balcells, J., Lamich, M., Griful, E., & Corbalan, M. (2016). Influence of data resolution in nonlinear loads model for harmonics prediction. *IECON Proceedings (Industrial Electronics Conference)*. https://doi.org/10.1109/IECON.2016.7793266

Bartoszewicz, A., & Zuk, J. (2010). Sliding mode control - Basic concepts and current trends. *IEEE International Symposium on Industrial Electronics*. https://doi.org/10.1109/ISIE.2010.5637990

Basheer, I. A., & Hajmeer, M. (2000). Artificial neural networks: fundamentals, computing, design, and application. *Journal of Microbiological Methods*, *43*(1), 3–31. https://doi.org/10.1016/S0167-7012(00)00201-3

Bei, T. Z., & Wang, P. (2016). Robust frequency-locked loop algorithm for grid synchronisation of single-phase applications under distorted grid conditions. *IET Generation, Transmission and Distribution*, *10*(11). https://doi.org/10.1049/iet-gtd.2015.0914

Bendrat, F., Chhor, J., & Sourkounis, C. (2017). Novel computation-efficient three-phase EPLL-based grid synchronization techniques considering power quality issues. *2017 25th Mediterranean Conference on Control and Automation, MED 2017*. https://doi.org/10.1109/MED.2017.7984214

Bhoyar, R. R., Bharatkar, S. S., & Khadtare, S. A. (2014). Measurement of harmonics at HT end users in power distribution system. *1st International Conference on Automation, Control, Energy and Systems - 2014, ACES 2014*. https://doi.org/10.1109/ACES.2014.6807992

Bisht, R., Subramaniam, S., Bhattarai, R., & Kamalasadan, S. (2018). Active and reactive power control of single phase inverter with seamless transfer between grid-connected and islanded mode. *2018 IEEE Power and Energy Conference at Illinois, PECI 2018*, *2018-January*. https://doi.org/10.1109/PECI.2018.8334989

Biswas, S., Mohan, N., & Robbins, W. P. (2017). A Systematic Design Method and Verification of a Zero Current Ripple Interface for PV-to-Battery Applications. *IEEE Transactions on Industry Applications*, *53*(2). https://doi.org/10.1109/TIA.2016.2624748

Borowy, B. S., & Salameh, Z. M. (1996). Methodology for optimally sizing the combination of a battery bank and PV array in a Wind/PV hybrid system. *IEEE Transactions on Energy Conversion*, *11*(2). https://doi.org/10.1109/60.507648

Brenna, M., Foiadelli, F., Longo, M., & Zaninelli, D. (2018). Energy Storage Control for Dispatching Photovoltaic Power. *IEEE Transactions on Smart Grid*, *9*(4). https://doi.org/10.1109/TSG.2016.2611999

Campanhol, L. B. G., Da Silva, S. A. O., De Oliveira, A. A., & Bacon, V. D. (2017). Single-stage three-phase grid-tied pv system with universal filtering capability applied to DG systems and AC microgrids. *IEEE Transactions on Power Electronics*, *32*(12). https://doi.org/10.1109/TPEL.2017.2659381

Chakraborty, S., Arvind, P., Bera, S., & Kumar, D. (2020). Coordinated Frequency Based Demand Side Management Scheme with Active Power Curtailment of Solar PV in a Battery Hybrid Stand-Alone Microgrid. *Proceedings - 2020 IEEE India Council International Subsections Conference, INDISCON 2020*. https://doi.org/10.1109/INDISCON50162.2020.00028

Chan, D. S. H., & Phang, J. C. H. (1987). Analytical Methods for the Extraction of Solar-Cell Single- and Double-Diode Model Parameters from I-V Characteristics. *IEEE Transactions on Electron Devices*, *34*(2). https://doi.org/10.1109/T-ED.1987.22920

Chen, Y. M., Huang, A. Q., & Yu, X. (2013). A high step-up three-port DC-DC converter for stand-alone PV/battery power systems. *IEEE Transactions on Power Electronics*, *28*(11). https://doi.org/10.1109/TPEL.2013.2242491

Choi, J., Illindala, M. S., Mondal, A., Renjit, A. A., & Pulcherio, M. C. (2018). Cascading Collapse of a Large-Scale Mixed Source Microgrid Caused by Fast-Acting Inverter-Based Distributed Energy Resources. *IEEE Transactions on Industry Applications*, *54*(6). https://doi.org/10.1109/TIA.2018.2854748

Craciunescu, D., & Fara, L. (2023). Investigation of the Partial Shading Effect of Photovoltaic Panels and Optimization of Their Performance Based on High-Efficiency FLC Algorithm. *Energies*, *16*(3). https://doi.org/10.3390/en16031169

Dai, W., Xie, Y., & Yang, H. (2009). A PLL control based on algorithm of BP neural network. *2009 IEEE International Conference on Computational Intelligence for Measurement Systems and Applications, CIMSA 2009*. https://doi.org/10.1109/CIMSA.2009.5069926

Dayal, R., Modepalli, K., & Parsa, L. (2013a). A new optimum power control scheme for low-power energy harvesting systems. *IEEE Transactions on Industry Applications*, *49*(6). https://doi.org/10.1109/TIA.2013.2264043

Dayal, R., Modepalli, K., & Parsa, L. (2013b). A new optimum power control scheme for low-power energy harvesting systems. *IEEE Transactions on Industry Applications*, *49*(6), 2651–2661. https://doi.org/10.1109/TIA.2013.2264043

Delghavi, M. B., & Yazdani, A. (2009). A control strategy for islanded operation of a distributed resource (DR) unit. *2009 IEEE Power and Energy Society General Meeting, PES '09*. https://doi.org/10.1109/PES.2009.5275592

Dong, H., Yuan, S., Han, Z., DIng, X., Ma, S., & Han, X. (2018a). A Comprehensive Strategy for Power Quality Improvement of Multi-Inverter-Based Microgrid with Mixed Loads. *IEEE Access*, *6*. https://doi.org/10.1109/ACCESS.2018.2826923

Dong, H., Yuan, S., Han, Z., DIng, X., Ma, S., & Han, X. (2018b). A Comprehensive Strategy for Power Quality Improvement of Multi-Inverter-Based Microgrid with Mixed Loads. *IEEE Access*, *6*, 30906–30916. https://doi.org/10.1109/ACCESS.2018.2826923

Dursun, M., & Dosoglu, M. K. (2018). LCL Filter Design for Grid Connected Three-Phase Inverter. *ISMSIT 2018 - 2nd International Symposium on Multidisciplinary Studies and Innovative Technologies, Proceedings*. https://doi.org/10.1109/ISMSIT.2018.8567054

Elgendy, M. A., Zahawi, B., & Atkinson, D. J. (2013). Assessment of the incremental conductance maximum power point tracking algorithm. *IEEE Transactions on Sustainable Energy*, *4*(1). https://doi.org/10.1109/TSTE.2012.2202698

Elgendy, M. A., Zahawi, B., & Atkinson, D. J. (2015). Operating characteristics of the P&O algorithm at high perturbation frequencies for standalone PV systems. *IEEE Transactions on Energy Conversion*, *30*(1), 189–198. https://doi.org/10.1109/TEC.2014.2331391

Errouissi, R., Muyeen, S. M., Al-Durra, A., & Leng, S. (2016). Experimental Validation of a Robust Continuous Nonlinear Model Predictive Control Based Grid-Interlinked Photovoltaic Inverter. *IEEE Transactions on Industrial Electronics*, *63*(7). https://doi.org/10.1109/TIE.2015.2508920

Esram, T., & Chapman, P. L. (2007). Comparison of photovoltaic array maximum power point tracking techniques. *IEEE Transactions on Energy Conversion*, *22*(2). https://doi.org/10.1109/TEC.2006.874230

Fernández-Guillamón, A., Gómez-Lázaro, E., Muljadi, E., & Molina-García, Á. (2019). Power systems with high renewable energy sources: A review of inertia and frequency control strategies over time. In *Renewable and Sustainable Energy Reviews* (Vol. 115). https://doi.org/10.1016/j.rser.2019.109369

Gadalla, A. S., Yan, X., & Hasabelrasul, H. (2018). State-of-charge balancing control strategy for battery energy storage systems based on a modern cascaded multilevel PWM converter. *Proceedings - 2018 IEEE 12th International Conference on Compatibility, Power Electronics and Power Engineering, CPE-POWERENG 2018*. https://doi.org/10.1109/CPE.2018.8372534

Golestan, S., Guerrero, J. M., & Vasquez, J. C. (2018). A PLL-Based Controller for Three-Phase Grid-Connected Power Converters. *IEEE Transactions on Power Electronics*, *33*(2). https://doi.org/10.1109/TPEL.2017.2719285

Golestan, S., Vidal, A., Yepes, A. G., Guerrero, J. M., Vasquez, J. C., & Doval-Gandoy, J. (2016). A True Open-Loop Synchronization Technique. *IEEE Transactions on Industrial Informatics*, *12*(3). https://doi.org/10.1109/TII.2016.2550017

Golsorkhi, M. S., Shafiee, Q., Lu, D. D. C., & Guerrero, J. M. (2017). A distributed control framework for integrated photovoltaic-battery-based islanded microgrids. *IEEE Transactions on Smart Grid*, *8*(6). https://doi.org/10.1109/TSG.2016.2593030

Gonzalez Montoya, D., Ramos Paja, C. A., & Giral, R. (2016). Maximum power point tracking of photovoltaic systems based on the sliding mode control of the module admittance. *Electric Power Systems Research*, *136*. https://doi.org/10.1016/j.epsr.2016.02.001

Gow, J. A., & Manning, C. D. (1999). Development of a photovoltaic array model for use in power-electronics simulation studies. *IEE Proceedings: Electric Power Applications*, *146*(2). https://doi.org/10.1049/ip-epa:19990116

Gowtham, N., & Shankar, S. (2018). UPQC: A Custom Power Device for Power Quality Improvement. *Materials Today: Proceedings*, *5*(1). https://doi.org/10.1016/j.matpr.2017.11.172

Gradella Villalva, M., Rafael Gazoli, J., & Ruppert Filho, E. (2009). Modeling And Circuit-based Simulation Of Photovoltaic Arrays. *Eletrônica de Potência*, *14*(1). https://doi.org/10.18618/rep.2009.1.035045

Gray, M. K., & Morsi, W. G. (2015b). Power quality assessment in distribution systems embedded with plug-in hybrid and battery electric vehicles. *IEEE Transactions on Power Systems*, *30*(2), 663–671. https://doi.org/10.1109/TPWRS.2014.2332058

Guan, Y., Vasquez, J. C., Guerrero, J. M., Wang, Y., & Feng, W. (2015). Frequency Stability of Hierarchically Controlled Hybrid Photovoltaic-Battery-Hydropower Microgrids. *IEEE Transactions on Industry Applications*, *51*(6). https://doi.org/10.1109/TIA.2015.2458954

Guerrero, J. M., Vasquez, J. C., Matas, J., De Vicuña, L. G., & Castilla, M. (2011). Hierarchical control of droop-controlled AC and DC microgrids - A general approach toward standardization. *IEEE Transactions on Industrial Electronics*, *58*(1). https://doi.org/10.1109/TIE.2010.2066534

Gupta, A., Doolla, S., & Chatterjee, K. (2018). Hybrid AC-DC Microgrid: Systematic Evaluation of Control Strategies. *IEEE Transactions on Smart Grid*, *9*(4). https://doi.org/10.1109/TSG.2017.2727344

Hamad, B., Al-Durra, A., El-Fouly, T. H. M., & Zeineldin, H. H. (2023). Economically Optimal and Stability Preserving Hybrid Droop Control for Autonomous Microgrids. *IEEE Transactions on Power Systems*, *38*(1). https://doi.org/10.1109/TPWRS.2022.3169801

Hamdi, H., Ben Regaya, C., & Zaafouri, A. (2019). Real-time study of a photovoltaic system with boost converter using the PSO-RBF neural network algorithms in a MyRio controller. *Solar Energy*, *183*. https://doi.org/10.1016/j.solener.2019.02.064

Harirchi, F., Simões, M. G., Babakmehr, M., Al-Durra, A., & Muyeen, S. M. (2015a). Designing smart inverter with unified controller and smooth transition between grid-connected and islanding modes for microgrid application. *IEEE Industry Application Society - 51st Annual Meeting, IAS 2015, Conference Record*. https://doi.org/10.1109/IAS.2015.7356800

Harirchi, F., Simões, M. G., Babakmehr, M., Al-Durra, A., & Muyeen, S. M. (2015b, December 14). Designing smart inverter with unified controller and smooth transition between grid-connected and islanding modes for microgrid application. *IEEE Industry Application Society - 51st Annual Meeting, IAS 2015, Conference Record*. https://doi.org/10.1109/IAS.2015.7356800

Hasabelrasul, H., Cai, Z., Sun, L., Suo, X., & Matraji, I. (2022). Two-Stage Converter Standalone PV-Battery System Based on VSG Control. *IEEE Access*, *10*. https://doi.org/10.1109/ACCESS.2022.3165664

Hasaneen, B. M., & Mohammed, A. A. E. (2008). Design and simulation of DC/DC boost converter. *2008 12th International Middle East Power System Conference, MEPCON 2008*. https://doi.org/10.1109/MEPCON.2008.4562340

Huynh, D. C., & Dunnigan, M. W. (2016). Development and comparison of an improved incremental conductance algorithm for tracking the MPP of a solar PV panel. *IEEE Transactions on Sustainable Energy*, *7*(4). https://doi.org/10.1109/TSTE.2016.2556678

Islam, H., Mekhilef, S., Shah, N. B. M., Soon, T. K., Seyedmahmousian, M., Horan, B., & Stojcevski, A. (2018). Performance evaluation of maximum power point tracking approaches and photovoltaic systems. *Energies*, *11*(2). https://doi.org/10.3390/en11020365

Jedari Zare Zadeh, M., & Fathi, S. H. (2017). A New Approach for Photovoltaic Arrays Modeling and Maximum Power Point Estimation in Real Operating Conditions. *IEEE Transactions on Industrial Electronics*, *64*(12). https://doi.org/10.1109/TIE.2017.2711571

Kampen, D., Parspour, N., Probst, U., & Thiel, U. (2008). Comparative evaluation of passive harmonic mitigating techniques for six pulse rectifiers. *11th International Conference on Optimization of Electrical and Electronic Equipment, OPTIM 2008*. https://doi.org/10.1109/OPTIM.2008.4602412

Karimi Ghartemani, M., Khajehoddin, S. A., Jain, P. K., & Bakhshai, A. (2012). Problems of startup and phase jumps in PLL systems. *IEEE Transactions on Power Electronics*, *27*(4). https://doi.org/10.1109/TPEL.2011.2169089

Karimi, Y., Oraee, H., Golsorkhi, M. S., & Guerrero, J. M. (2017). Decentralized Method for Load Sharing and Power Management in a PV/Battery Hybrid Source Islanded Microgrid. *IEEE Transactions on Power Electronics*, *32*(5), 3525–3535. https://doi.org/10.1109/TPEL.2016.2582837

Karimi, Y., Oraee, H., & Guerrero, J. M. (2017). Decentralized Method for Load Sharing and Power Management in a Hybrid Single/Three-Phase-Islanded Microgrid Consisting of Hybrid Source PV/Battery Units. *IEEE Transactions on Power Electronics*, *32*(8). https://doi.org/10.1109/TPEL.2016.2620258

Karimi-Ghartemani, M. (2014). Linear and pseudolinear enhanced phased-locked loop (EPLL) structures. *IEEE Transactions on Industrial Electronics*, *61*(3). https://doi.org/10.1109/TIE.2013.2261035

Killi, M., & Samanta, S. (2015). Modified perturb and observe MPPT algorithm for drift avoidance in photovoltaic systems. *IEEE Transactions on Industrial Electronics*, *62*(9). https://doi.org/10.1109/TIE.2015.2407854

Kjaer, S. B., Pedersen, J. K., & Blaabjerg, F. (2005). A review of single-phase grid-connected inverters for photovoltaic modules. In *IEEE Transactions on Industry Applications* (Vol. 41, Issue 5). https://doi.org/10.1109/TIA.2005.853371

Koad, R. B. A., Zobaa, A. F., & El-Shahat, A. (2017a). A Novel MPPT Algorithm Based on Particle Swarm Optimization for Photovoltaic Systems. *IEEE Transactions on Sustainable Energy*, *8*(2). https://doi.org/10.1109/TSTE.2016.2606421

Koad, R. B. A., Zobaa, A. F., & El-Shahat, A. (2017b). A Novel MPPT Algorithm Based on Particle Swarm Optimization for Photovoltaic Systems. *IEEE Transactions on Sustainable Energy*, *8*(2), 468–476. https://doi.org/10.1109/TSTE.2016.2606421

Komurcugil, H., Biricik, S., Bayhan, S., & Zhang, Z. (2021). Sliding Mode Control: Overview of Its Applications in Power Converters. *IEEE Industrial Electronics Magazine*, *15*(1), 40–49. https://doi.org/10.1109/MIE.2020.2986165

Krithiga, S., & Gounden, N. G. A. (2014). Power electronic configuration for the operation of PV system in combined grid-connected and stand-alone modes. *IET Power Electronics*, *7*(3). https://doi.org/10.1049/iet-pel.2013.0107

Kumar, S., Suryawanshi, H. M., Singh, B., Verma, V., & Chakraborty, C. (2020). Synchronization and de-synchronization of single stage PV-battery based microgrid for enhancing power grid resilience. *2020 IEEE International Conference on Computing, Power and Communication Technologies, GUCON 2020*. https://doi.org/10.1109/GUCON48875.2020.9231262

Kuo, Y. C., Liang, T. J., & Chen, J. F. (2001). Novel maximum-power-point-tracking controller for photovoltaic energy conversion system. *IEEE Transactions on Industrial Electronics*, *48*(3). https://doi.org/10.1109/41.925586

Lal, V. N., & Singh, S. N. (2017). Control and performance analysis of a single-stage utility-scale grid-connected PV system. *IEEE Systems Journal*, *11*(3). https://doi.org/10.1109/JSYST.2015.2408055

Lamzouri, F. E., Boufounas, E. M., & El Amrani, A. (2018). A robust backstepping sliding mode control for MPPT based photovoltaic system with a DC-DC boost converter. *2018 International Conference on Control, Automation and Diagnosis, ICCAD 2018*. https://doi.org/10.1109/CADIAG.2018.8751449

Lee, J., & Kim, Y. (2022). Comparative Estimation of Electrical Characteristics of a Photovoltaic Module Using Regression and Artificial Neural Network Models. *Electronics (Switzerland)*, *11*(24). https://doi.org/10.3390/electronics11244228

Li, C., Cao, C., Cao, Y., Kuang, Y., Zeng, L., & Fang, B. (2014a). A review of islanding detection methods for microgrid. In *Renewable and Sustainable Energy Reviews* (Vol. 35). https://doi.org/10.1016/j.rser.2014.04.026

Li, X. (2019). A review on energy management, operation control and application methods for grid battery energy storage systems. In *CSEE Journal of Power and Energy Systems: Vol. PP* (Issue 99). https://doi.org/10.17775/CSEEJPES.2019.00160

Li, X., & Wang, S. (2021a). Energy management and operational control methods for grid battery energy storage systems. *CSEE Journal of Power and Energy Systems*, *7*(5). https://doi.org/10.17775/CSEEJPES.2019.00160

Li, X., & Wang, S. (2021b). Energy management and operational control methods for grid battery energy storage systems. *CSEE Journal of Power and Energy Systems*, *7*(5). https://doi.org/10.17775/CSEEJPES.2019.00160

Liu, F., Duan, S., Liu, F., Liu, B., & Kang, Y. (2008). A variable step size INC MPPT method for PV systems. *IEEE Transactions on Industrial Electronics*, *55*(7). https://doi.org/10.1109/TIE.2008.920550

Luna, A. C., Diaz, N. L., Graells, M., Vasquez, J. C., & Guerrero, J. M. (2017). Mixed-integer-linear-programming-based energy management system for hybrid PV-wind-battery microgrids: Modeling, design, and experimental verification. *IEEE Transactions on Power Electronics*, *32*(4). https://doi.org/10.1109/TPEL.2016.2581021

Mahmood, H., & Jiang, J. (2018a). Autonomous coordination of multiple PV/Battery hybrid units in islanded microgrids. *IEEE Transactions on Smart Grid*, *9*(6), 6359–6368. https://doi.org/10.1109/TSG.2017.2709550

Mahmood, H., & Jiang, J. (2018b). Autonomous coordination of multiple PV/Battery hybrid units in islanded microgrids. *IEEE Transactions on Smart Grid*, *9*(6), 6359–6368. https://doi.org/10.1109/TSG.2017.2709550

Mahmood, H., Michaelson, D., & Jiang, J. (2014a). A power management strategy for PV/battery hybrid systems in Islanded microgrids. *IEEE Journal of Emerging and Selected Topics in Power Electronics*, *2*(4). https://doi.org/10.1109/JESTPE.2014.2334051

Mahmood, H., Michaelson, D., & Jiang, J. (2014b). A power management strategy for PV/battery hybrid systems in Islanded microgrids. *IEEE Journal of Emerging and Selected Topics in Power Electronics*, *2*(4), 870–882. https://doi.org/10.1109/JESTPE.2014.2334051

Manickam, C., Raman, G. R., Raman, G. P., Ganesan, S. I., & Nagamani, C. (2016). A Hybrid Algorithm for Tracking of GMPP Based on P&O and PSO with Reduced Power Oscillation in String Inverters. *IEEE Transactions on Industrial Electronics*, *63*(10). https://doi.org/10.1109/TIE.2016.2590382

Meng, X., Liu, J., & Liu, Z. (2019). A Generalized Droop Control for Grid-Supporting Inverter Based on Comparison between Traditional Droop Control and Virtual Synchronous Generator Control. *IEEE Transactions on Power Electronics*, *34*(6). https://doi.org/10.1109/TPEL.2018.2868722

Meng, Z., Shao, W., Tang, J., & Zhou, H. (2018). Sliding-mode control based on index control law for MPPT in photovoltaic systems. *CES Transactions on Electrical Machines and Systems*, *2*(3), 303–311. https://doi.org/10.30941/CESTEMS.2018.00038

Merabet, A., Tawfique Ahmed, K., Ibrahim, H., Beguenane, R., & Ghias, A. M. Y. M. (2017). Energy Management and Control System for Laboratory Scale Microgrid Based Wind-PV-Battery. *IEEE Transactions on Sustainable Energy*, *8*(1). https://doi.org/10.1109/TSTE.2016.2587828

Mir, M., Kamyab, M., Lariche, J., Bemani, A., & Baghban, A. (2018). *Petroleum Science and Technology Applying ANFIS-PSO algorithm as a novel accurate approach for prediction of gas density Applying ANFIS-PSO algorithm as a novel accurate approach for prediction of gas density*. https://doi.org/10.1080/10916466.2018.1446176

Mirhosseini, M., Pou, J., & Agelidis, V. G. (2015). Single- and Two-Stage Inverter-Based Grid-Connected Photovoltaic Power Plants With Ride-Through Capability Under Grid Faults. *IEEE Transactions on Sustainable Energy*, *6*(3). https://doi.org/10.1109/TSTE.2014.2347044

Mishra, S., Pullaguram, D., Buragappu, S. A., & Ramasubramanian, D. (2016). Single-phase synchronverter for a gridconnected roof top photovoltaic system. *IET Renewable Power Generation*, *10*(8). https://doi.org/10.1049/iet-rpg.2015.0224

Mishra, S., Rajashekaran, S., Mohan, P. K., Lokesh, S. M., Ganiga, H. J., Dash, S. K., & Roccotelli, M. (2023). Implementation of an ADALINE-Based Adaptive Control Strategy for an LCLC-PV-DSTATCOM in Distribution System for Power Quality Improvement. *Energies*, *16*(1). https://doi.org/10.3390/en16010323

Mohamed, A. A. S., El-Sayed, A., Metwally, H., & Selem, S. I. (2020). Grid integration of a PV system supporting an EV charging station using Salp Swarm Optimization. *Solar Energy*, *205*. https://doi.org/10.1016/j.solener.2020.05.013

Mohan, N. (2003). Power Electronics Converters, Applications and Design 3rd. In *John Wiley & Sons*.

Mondal, A., & Illindala, M. S. (2018). Improved Frequency Regulation in an Islanded Mixed Source Microgrid Through Coordinated Operation of DERs and Smart Loads. *IEEE Transactions on Industry Applications*, *54*(1), 112–120. https://doi.org/10.1109/TIA.2017.2761825

Morstyn, T., Momayyezan, M., Hredzak, B., & Agelidis, V. G. (2016). Distributed Control for State-of-Charge Balancing Between the Modules of a Reconfigurable Battery Energy Storage System. *IEEE Transactions on Power Electronics*, *31*(11). https://doi.org/10.1109/TPEL.2015.2513777

Neto, P. B. L., Saavedra, O. R., & De Souza Ribeiro, L. A. (2018). A Dual-Battery Storage Bank Configuration for Isolated Microgrids Based on Renewable Sources. *IEEE Transactions on Sustainable Energy*, *9*(4). https://doi.org/10.1109/TSTE.2018.2800689

Oliver, J. S., David, P. W., Balachandran, P. K., & Mihet-Popa, L. (2022). Analysis of Grid-Interactive PV-Fed BLDC Pump Using Optimized MPPT in DC–DC Converters. *Sustainability (Switzerland)*, *14*(12). https://doi.org/10.3390/su14127205

Ota, J. I. Y., Sato, T., & Akagi, H. (2016). Enhancement of performance, availability, and flexibility of a battery energy storage system based on a modular multilevel cascaded converter (MMCC-SSBC). *IEEE Transactions on Power Electronics*, *31*(4). https://doi.org/10.1109/TPEL.2015.2450757

Oviedo, E., Vazquez, N., & Femat, R. (2018a). Synchronization Technique of Grid-Connected Power Converters Based on a Limit Cycle Oscillator. *IEEE Transactions on Industrial Electronics*, *65*(1). https://doi.org/10.1109/TIE.2017.2703655

Oviedo, E., Vazquez, N., & Femat, R. (2018b). Synchronization Technique of Grid-Connected Power Converters Based on a Limit Cycle Oscillator. *IEEE Transactions on Industrial Electronics*, *65*(1), 709–717. https://doi.org/10.1109/TIE.2017.2703655

Pan, C. T., Cheng, M. C., Lai, C. M., & Chen, P. Y. (2015a). Current-ripple-free module integrated converter with more precise maximum power tracking control for PV energy harvesting. *IEEE Transactions on Industry Applications*, *51*(1). https://doi.org/10.1109/TIA.2014.2326076

Pan, C. T., Cheng, M. C., Lai, C. M., & Chen, P. Y. (2015b). Current-ripple-free module integrated converter with more precise maximum power tracking control for PV energy harvesting. *IEEE*

Transactions on Industry Applications, *51*(1), 271–278. https://doi.org/10.1109/TIA.2014.2326076

Philip, J., Jain, C., Kant, K., Singh, B., Mishra, S., Chandra, A., & Al-Haddad, K. (2016a). Control and Implementation of a Standalone Solar Photovoltaic Hybrid System. *IEEE Transactions on Industry Applications*, *52*(4), 3472–3479. https://doi.org/10.1109/TIA.2016.2553639

Pogaku, N., Prodanović, M., & Green, T. C. (2007). Modeling, analysis and testing of autonomous operation of an inverter-based microgrid. *IEEE Transactions on Power Electronics*, *22*(2). https://doi.org/10.1109/TPEL.2006.890003

Priyadarshi, N., Padmanaban, S., Holm-Nielsen, J. B., Blaabjerg, F., & Bhaskar, M. S. (2020). An Experimental Estimation of Hybrid ANFIS-PSO-Based MPPT for PV Grid Integration under Fluctuating Sun Irradiance. *IEEE Systems Journal*, *14*(1), 1218–1229. https://doi.org/10.1109/JSYST.2019.2949083

Priyadarshi, N., Padmanaban, S., Kiran Maroti, P., & Sharma, A. (2019). An Extensive Practical Investigation of FPSO-Based MPPT for Grid Integrated PV System under Variable Operating Conditions with Anti-Islanding Protection. *IEEE Systems Journal*, *13*(2). https://doi.org/10.1109/JSYST.2018.2817584

Pulcherio, M., Illindala, M. S., Choi, J., & Yedavalli, R. K. (2018). Robust Microgrid Clustering in a Distribution System with Inverter-Based DERs. *IEEE Transactions on Industry Applications*, *54*(5). https://doi.org/10.1109/TIA.2018.2853039

Rajeev, M., & Agarwal, V. (2020). Low Voltage Ride-Through Capability of a Novel Grid Connected Inverter Suitable for Transformer-Less Solar PV-Grid Interface. *IEEE Transactions on Industry Applications*, *56*(3). https://doi.org/10.1109/TIA.2020.2979134

Ramezani, M., Li, S., & Golestan, S. (2017). Analysis and controller design for stand-alone VSIs in synchronous reference frame. *IET Power Electronics*, *10*(9). https://doi.org/10.1049/iet-pel.2016.0883

Ramos-Paja, C. A., Bastidas-Rodriguez, J. D., & Saavedra-Montes, A. J. (2022). Sliding-Mode Control of a Photovoltaic System Based on a Flyback Converter for Microinverter Applications. *Applied Sciences (Switzerland)*, *12*(3). https://doi.org/10.3390/app12031399

Rezkallah, M., Hamadi, A., Chandra, A., & Singh, B. (2018). Design and Implementation of Active Power Control with Improved P&O Method for Wind-PV-Battery-Based Standalone Generation System. *IEEE Transactions on Industrial Electronics*, *65*(7). https://doi.org/10.1109/TIE.2017.2777404

Rocabert, J., Luna, A., Blaabjerg, F., & Rodríguez, P. (2012). Control of power converters in AC microgrids. *IEEE Transactions on Power Electronics*, *27*(11), 4734–4749. https://doi.org/10.1109/TPEL.2012.2199334

Saad, W., Sellami, A., & Garcia, G. (2018). Terminal sliding mode control-based MPPT for a photovoltaic system with uncertainties. *International Journal of Modelling, Identification and Control*, *29*(2). https://doi.org/10.1504/IJMIC.2018.090478

Safa, A., Berkouk, E. M., Messlem, Y., Chedjara, Z., & Gouichiche, A. (2018). A Pseudo Open Loop Synchronization technique for heavily distorted grid voltage. *Electric Power Systems Research*, *158*. https://doi.org/10.1016/j.epsr.2018.01.014

Safari, A., & Mekhilef, S. (2011). Simulation and hardware implementation of incremental conductance MPPT with direct control method using cuk converter. *IEEE Transactions on Industrial Electronics*, *58*(4). https://doi.org/10.1109/TIE.2010.2048834

Sangwongwanich, A., Yang, Y., & Blaabjerg, F. (2016). High-performance constant power generation in grid-connected PV systems. *IEEE Transactions on Power Electronics*, *31*(3). https://doi.org/10.1109/TPEL.2015.2465151

Sangwongwanich, A., Yang, Y., Blaabjerg, F., & Sera, D. (2017). Delta Power Control Strategy for Multistring Grid-Connected PV Inverters. *IEEE Transactions on Industry Applications*, *53*(4). https://doi.org/10.1109/TIA.2017.2681044

Sarvi, M., & Azadian, A. (2022). A comprehensive review and classified comparison of MPPT algorithms in PV systems. In *Energy Systems* (Vol. 13, Issue 2). https://doi.org/10.1007/s12667-021-00427-x

Saxena, N., Hussain, I., Singh, B., & Vyas, A. L. (2017). Solar PV interfaced to multifunctional VSC with a battery support. *2016 IEEE 7th Power India International Conference, PIICON 2016*. https://doi.org/10.1109/POWERI.2016.8077415

Saxena, N., Hussain, I., Singh, B., & Vyas, A. L. (2018). Implementation of a Grid-Integrated PV-Battery System for Residential and Electrical Vehicle Applications. *IEEE Transactions on Industrial Electronics*, *65*(8). https://doi.org/10.1109/TIE.2017.2739712

Saxena, N., Singh, B., & Vyas, A. L. (2017a). Integration of solar photovoltaic with battery to single-phase grid. *IET Generation, Transmission and Distribution*, *11*(8). https://doi.org/10.1049/iet-gtd.2016.1455

Saxena, N., Singh, B., & Vyas, A. L. (2017b). Single-phase solar PV system with battery and exchange of power in grid-connected and standalone modes. *IET Renewable Power Generation*, *11*(2). https://doi.org/10.1049/iet-rpg.2016.0143

Sera, D., Mathe, L., Kerekes, T., Spataru, S. V., & Teodorescu, R. (2013). On the perturb-and-observe and incremental conductance mppt methods for PV systems. *IEEE Journal of Photovoltaics*, *3*(3). https://doi.org/10.1109/JPHOTOV.2013.2261118

Sera, D., Teodorescu, R., & Rodriguez, P. (2007). PV panel model based on datasheet values. *IEEE International Symposium on Industrial Electronics*. https://doi.org/10.1109/ISIE.2007.4374981

Sharma, P., Duttagupta, S. P., & Agarwal, V. (2014). A novel approach for maximum power tracking from curved thin-film solar photovoltaic arrays under changing environmental conditions. *IEEE Transactions on Industry Applications*, *50*(6). https://doi.org/10.1109/TIA.2014.2322136

Shen, J., & Khaligh, A. (2015). A supervisory energy management control strategy in a battery/ultracapacitor hybrid energy storage system. *IEEE Transactions on Transportation Electrification*, *1*(3). https://doi.org/10.1109/TTE.2015.2464690

Shi, Y., Li, R., Xue, Y., & Li, H. (2016a). High-frequency-link-based grid-tied PV system with small DC-link capacitor and low-frequency ripple-free maximum power point tracking. *IEEE Transactions on Power Electronics*, *31*(1). https://doi.org/10.1109/TPEL.2015.2411858

Shi, Y., Li, R., Xue, Y., & Li, H. (2016b). High-frequency-link-based grid-tied PV system with small DC-link capacitor and low-frequency ripple-free maximum power point tracking. *IEEE Transactions on Power Electronics*, *31*(1), 328–339. https://doi.org/10.1109/TPEL.2015.2411858

Singh, B., & Arya, S. R. (2013). Adaptive theory-based improved linear sinusoidal tracer control algorithm for DSTATCOM. *IEEE Transactions on Power Electronics*, *28*(8). https://doi.org/10.1109/TPEL.2012.2228884

Singh, B., Jayaprakash, P., Kumar, S., & Kothari, D. P. (2011). Implementation of neural-network-controlled three-leg VSC and a transformer as three-phase four-wire dstatcom. *IEEE Transactions on Industry Applications*, *47*(4). https://doi.org/10.1109/TIA.2011.2153811

Singh, Y., Singh, B., & Mishra, S. (2018). PV-battery based single phase microgrid with grid synchronization and de-synchronization capabilities. *2018 IEEMA Engineer Infinite Conference, ETechNxT 2018*. https://doi.org/10.1109/ETECHNXT.2018.8385382

Slotine, J. J. E. (1984). Sliding controller design for non-linear systems. *International Journal of Control*, *40*(2). https://doi.org/10.1080/00207178408933284

Srivastava, S., Lata, C., Lohan, P., & Mosobi, R. W. (2022). Comparative Analysis of Particle Swarm Optimization and Artificial Neural Network Based MPPT with Variable Irradiance and Load. *International Journal of Electrical and Electronics Research*, *10*(3). https://doi.org/10.37391/ijeer.100309

Subudhi, B., & Pradhan, R. (2013b). A comparative study on maximum power point tracking techniques for photovoltaic power systems. *IEEE Transactions on Sustainable Energy*, *4*(1), 89–98. https://doi.org/10.1109/TSTE.2012.2202294

Sun, K., Zhang, L., Xing, Y., & Guerrero, J. M. (2011). A distributed control strategy based on DC bus signaling for modular photovoltaic generation systems with battery energy storage. *IEEE Transactions on Power Electronics*, *26*(10). https://doi.org/10.1109/TPEL.2011.2127488

Sundareswaran, K., Vigneshkumar, V., Sankar, P., Simon, S. P., Srinivasa Rao Nayak, P., & Palani, S. (2016). Development of an Improved P&O Algorithm Assisted Through a Colony of Foraging Ants for MPPT in PV System. *IEEE Transactions on Industrial Informatics*, *12*(1). https://doi.org/10.1109/TII.2015.2502428

Tang, Z., Yang, Y., & Blaabjerg, F. (2022). Power electronics: The enabling technology for renewable energy integration. *CSEE Journal of Power and Energy Systems*, *8*(1). https://doi.org/10.17775/CSEEJPES.2021.02850

Tareen, W. U. K., Aamir, M., Mekhilef, S., Nakaoka, M., Seyedmahmoudian, M., Horan, B., Memon, M. A., & Baig, N. A. (2018). Mitigation of power quality issues due to high penetration of renewable energy sources in electric grid systems using three-phase APF/STATCOM technologies: A review. In *Energies* (Vol. 11, Issue 6). https://doi.org/10.3390/en11061491

Taufik, Oi, A., Anwari, M., & Taufik, M. (2009). Modeling and simulation of photovoltaic water pumping system. *Proceedings - 2009 3rd Asia International Conference on Modelling and Simulation, AMS 2009*, 497–502. https://doi.org/10.1109/AMS.2009.85

Tayab, U. B., Roslan, M. A. Bin, Hwai, L. J., & Kashif, M. (2017). A review of droop control techniques for microgrid. In *Renewable and Sustainable Energy Reviews* (Vol. 76). https://doi.org/10.1016/j.rser.2017.03.028

Teng, J. H., Luan, S. W., Lee, D. J., & Huang, Y. Q. (2013). Optimal charging/discharging scheduling of battery storage systems for distribution systems interconnected with sizeable PV generation systems. *IEEE Transactions on Power Systems*, *28*(2). https://doi.org/10.1109/TPWRS.2012.2230276

Teodorescu, R., Liserre, M., & Rodríguez, P. (2010). Grid Converters for Photovoltaic and Wind Power Systems. In *Grid Converters for Photovoltaic and Wind Power Systems*. https://doi.org/10.1002/9780470667057

Thale, S. S., & Agarwal, V. (2016). Controller Area Network Assisted Grid Synchronization of a Microgrid With Renewable Energy Sources and Storage. *IEEE Transactions on Smart Grid*, *7*(3). https://doi.org/10.1109/TSG.2015.2453157

Thang, T. V., Ahmed, A., Kim, C. I., & Park, J. H. (2015). Flexible System Architecture of Stand-Alone PV Power Generation with Energy Storage Device. *IEEE Transactions on Energy Conversion*, *30*(4). https://doi.org/10.1109/TEC.2015.2429145

Thirugnanam, K., Kerk, S. K., Yuen, C., Liu, N., & Zhang, M. (2018). Energy Management for Renewable Microgrid in Reducing Diesel Generators Usage with Multiple Types of Battery. *IEEE Transactions on Industrial Electronics*, *65*(8). https://doi.org/10.1109/TIE.2018.2795585

Torreglosa, J. P., García, P., Fernández, L. M., & Jurado, F. (2015). Energy dispatching based on predictive controller of an off-grid wind turbine/photovoltaic/hydrogen/battery hybrid system. *Renewable Energy*, *74*. https://doi.org/10.1016/j.renene.2014.08.010

Tremblay, O., & Dessaint, L. A. (2009). Experimental validation of a battery dynamic model for EV applications. *World Electric Vehicle Journal*, *3*(2). https://doi.org/10.3390/wevj3020289

Tsai, H., Tu, C., & Su, Y. (2008). Development of Generalized Photovoltaic Model Using MATLAB / SIMULINK. *Proceedings of the World Congress on Engineering and Computer Science 2008 WCECS 2008, October 22 - 24, 2008, San Francisco, USA*.

Vahedi, H., Labbé, P. A., & Al-Haddad, K. (2016). Sensor-Less Five-Level Packed U-Cell (PUC5) Inverter Operating in Stand-Alone and Grid-Connected Modes. *IEEE Transactions on Industrial Informatics*, *12*(1). https://doi.org/10.1109/TII.2015.2491260

Verma, A. K., & Singh, B. (2018). Harmonics and Reactive Current Detection of a Grid-Interfaced PV Generation in a Distribution System. *IEEE Transactions on Industry Applications*, *54*(5). https://doi.org/10.1109/TIA.2018.2830752

Villalva, M. G., Gazoli, J. R., & Filho, E. R. (2009). Comprehensive approach to modeling and simulation of photovoltaic arrays. *IEEE Transactions on Power Electronics*, *24*(5). https://doi.org/10.1109/TPEL.2009.2013862

Wang, F., Zhu, T., Zhuo, F., & Yi, H. (2018). An improved submodule differential power processing-based PV system with flexible multi-MPPT control. *IEEE Journal of Emerging and Selected Topics in Power Electronics*, *6*(1), 94–102. https://doi.org/10.1109/JESTPE.2017.2719919

Windarko, N. A., Tjahjono, A., Anggriawan, D. O., & Purnomo, M. H. (2016). Maximum power point tracking of photovoltaic system using adaptive modified firefly algorithm. *Proceedings - 2015 International Electronics Symposium: Emerging Technology in Electronic and Information, IES 2015*. https://doi.org/10.1109/ELECSYM.2015.7380809

Wu, L., Zhao, Z., & Liu, J. (2007). A single-stage three-phase grid-connected photovoltaic system with modified MPPT method and reactive power compensation. *IEEE Transactions on Energy Conversion*, *22*(4). https://doi.org/10.1109/TEC.2007.895461

Xiao, B., Hang, L., Mei, J., Riley, C., Tolbert, L. M., & Ozpineci, B. (2015). Modular Cascaded H-Bridge Multilevel PV Inverter with Distributed MPPT for Grid-Connected Applications. *IEEE Transactions on Industry Applications*, *51*(2). https://doi.org/10.1109/TIA.2014.2354396

Yi, Z., Dong, W., & Etemadi, A. H. (2018). A unified control and power management scheme for PV-Battery-based hybrid microgrids for both grid-connected and islanded modes. *IEEE Transactions on Smart Grid*, *9*(6). https://doi.org/10.1109/TSG.2017.2700332

Younus, S. A. M., Nardello, M., Tosato, P., & Brunelli, D. (2017). Power controlling, monitoring and routing center enabled by a DC-transformer. *Energies*, *10*(3). https://doi.org/10.3390/en10030403

Zeng, Z., & Shao, W. (2017). Reconnection of micro-grid from islanded mode to grid-connected mode used sliding Goertzel transform based filter. *IET Renewable Power Generation*, *11*(7). https://doi.org/10.1049/iet-rpg.2016.0932

Zhang, L., Sun, K., Li, Y. W., Lu, X., & Zhao, J. (2018). A Distributed Power Control of Series-Connected Module-Integrated Inverters for PV Grid-Tied Applications. *IEEE Transactions on Power Electronics*, *33*(9). https://doi.org/10.1109/TPEL.2017.2769487

Zhu, H., Zhang, D., Zhang, B., & Zhou, Z. (2015). A Nonisolated Three-Port DC-DC Converter and Three-Domain Control Method for PV-Battery Power Systems. *IEEE Transactions on Industrial Electronics*, *62*(8), 4937–4947. https://doi.org/10.1109/TIE.2015.2393831

Zia, M. F., Nasir, M., Elbouchikhi, E., Benbouzid, M., Vasquez, J. C., & Guerrero, J. M. (2022). Energy management system for a hybrid PV-Wind-Tidal-Battery-based islanded DC microgrid: Modeling and experimental validation. *Renewable and Sustainable Energy Reviews*, *159*. https://doi.org/10.1016/j.rser.2022.112093

APPENDIX

Appendix : PV System Parameters and BES System Parameters

PV System Parameters:

PV Boost Converter Parameters

- L = 1 mH,
- R = 0.0050 **Ω**
- C_{in} = 200 **μ**F
- C_{dc} = 66.7 mF,

Filter Parameters

- L= 91.6 **μ**H,
- R=345.6 **μ Ω**
- Qc = 500 kvar

BES System Parameters:

Filter Parameters

- L_1 = 6.9833 **μ**H,
- R_1 = 2.6326 **μ Ω**
- L_2 = 7.7592 **μ**H,
- R_2 = 2.9252 **μ Ω**
- Qc = 500 kvar

- **The PSO-ANFIS parameters**: No. of iteration = 100, No. of population = 25, Inertia Weight (w)=1, Personal Learning Coefficient (c1) = 1, Global Learning Coefficient (c2) = 2;
- **The PSO-ANN parameters:** No. of iteration = 100, No. of population = 100, Inertia Weight (w)=1, Personal Learning Coefficient (c1) = 1.5, Global Learning Coefficient (c2) = 2;
- **SMC parameters:** Inertia Weight (w)=0.1, Personal Learning Coefficient (c1) = 1.2, Global Learning Coefficient (c2) = 1.2, *k=200*

BIO-DATA

Mr. Siddaraj is a part-time research scholar in the Department of Electrical & Electronics Engineering, National Institute of Technology Karnataka (NITK), Surathkal, Mangalore, INDIA. He obtained a bachelor's degree in electrical and electronics Engineering from SDM College of Engineering and Technology, Dharwad, VTU Belgaum, in the year 2008 with First Class. He holds master's degree in Power and Energy Systems from NITK, Surathkal in the year 2011. After his master's degree, he is working as an Assistant Professor in the Department of Electrical and Electronics Engineering, MIT, Manipal. He has 11 years of teaching experience. His fields of interest are Power and Energy systems.

Address:

Mr. Siddaraj
Assistant Professor,
Department of Electrical & Electronics Engineering,
Manipal Institute of Tech. Manipal,
Udupi, Karnataka-576104, INDIA.
Phone: +91-9743060741
Email: usiddaraj@gmail.com